Friends of the Pleistocene, Pacific Northwest Cell Field Trip
September 17-20, 2015

Late Pleistocene to Modern Geomorphic and Biotic History of the Olympic Peninsula, Washington

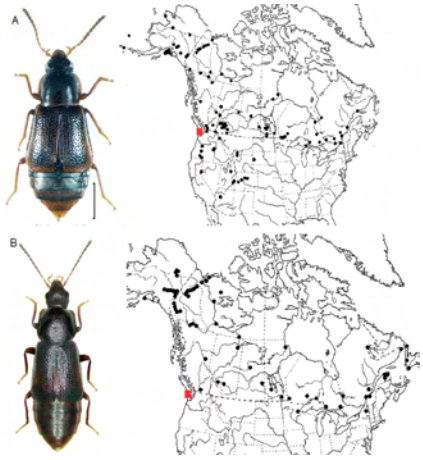

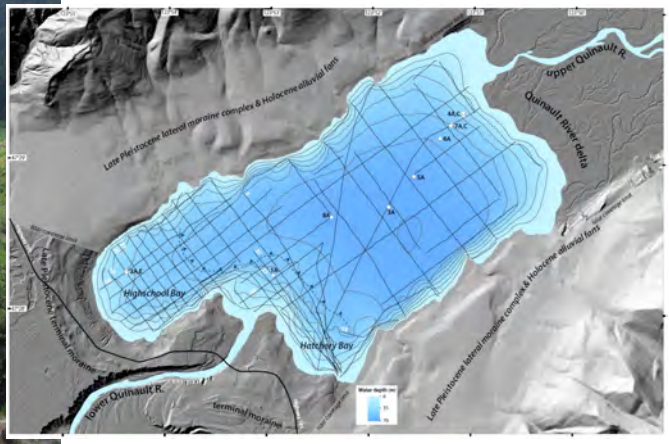

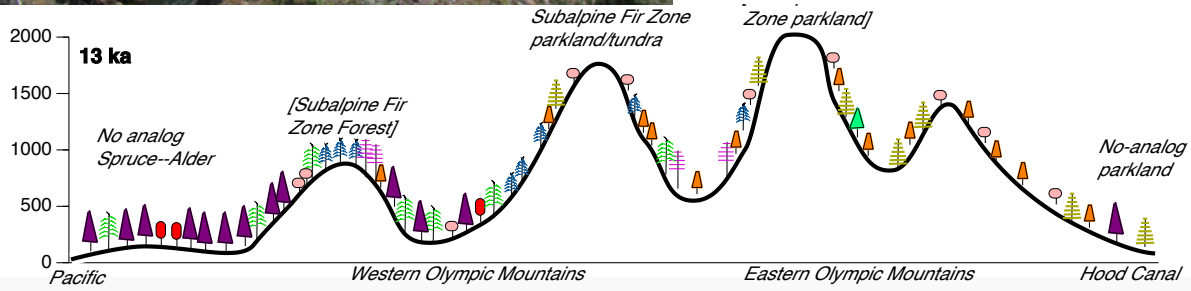

GLENN THACKRAY, Idaho State University
DAN GAVIN, University of Oregon,
ANDY RITCHIE, U.S. Geological Survey and National Park Service
KARL WEGMANN, North Carolina State University
ALLAN ASHWORTH, North Dakota State University
LISA ELY, Central Washington University

Friends of the Pleistocene, Pacific Northwest Cell Field trip, September 17-20, 2015

Late Pleistocene to Modern Geomorphic and Biotic History of the Olympic Peninsula, Washington

Introduction and Organization of the Field Guide

Welcome to the 2015 Friends of the Pleistocene Pacific Northwest Cell field trip. The FOP is a great organization, dating back to the 1920s when, legend has it, a group of Quaternary scientists gathered in New England to look at outcrops and argue about scientific ideas. The FOP has always truly been a non-organization, and it has persisted partly for that reason. There is no real organization, no membership, no offices, no officers, … just a series of field trips spanning the decades in each of several regions of the country. The FOP persists through a community enthusiasm for Quaternary science, geomorphology and related fields, an interest among scientists and the interested public in examining field evidence and arguing about it, and a tendency to have a really good time. Thank you for joining this and other FOP trips and keeping the tradition alive!

This field trip will cover a variety of scientific topics, by visiting research sites on the western and northern Olympic Peninsula. We will visit sites that reveal evidence of earthquake history, glaciation, paleoecology, river recovery following very recent dam removal, and many other aspects of the Quaternary and modern processes of the region.

This field guide is an informal compilation of work by the several leaders and the multiple projects that we will discuss. Much of the work is in progress, and all of it builds on a wealth of previous work in the region. As such, the field guide organization presents a bit of a challenge. The guide is mainly organized by the sequence of stops that we will visit, organized as a roadlog. There are roadlogs between stops that provide directions, and, in some cases, a bit of observation along the way. You will find inconsistencies in the styles and formatting, but we have mainly focused on getting the necessary directions and science into the guide. In cases where there are several supporting figures or additional text that amplify the science to be discussed, we have placed that material at the end of the sequential roadlog so that it does not confuse the roadlog itself.

On Saturday night, we will choose the trip for next year's PNW FOP, from the offerings put forth by the potential leaders. As we go through this trip, we encourage those of you working in the region (the PNW is used loosely here, and sometimes includes Idaho and other states) to consider potential trips, and we also encourage arm twisting, cajoling, and other means of persuasion. For the PNW FOP to thrive, an annual gathering is essential.

Thanks again for joining the FOP event, and let's go enjoy some of the best Pleistoscenery and Holoscenery the region has to offer.

Roadlog and description of field trip stops

Thursday, 9/17

Gather in the evening at Falls Creek Campground, Quinault Lake, South Shore Road. There are no specific "official" plans for the evening.

Friday, 9/18

Meet at 9 AM, Quinault Lake USFS ranger station (officially: Pacific Ranger District-Quinault). The ranger station is on the South Shore Road, very close to Falls Creek campground, and there should be ample parking.

Stop 1 (Wegmann/Thackray) Quinault Lake ranger station. Trip overview, glacial geomorphology and setting of Quinault Lake, Quinault geomorphology background, lacustrine records, and geomorphic response to earthquakes. (1.5 hours, leave by 10:30).

See appended text and figures by Thackray entitled: "**Glaciation of the Western Olympic Peninsula"**

See appended text and figures by Wegmann entitled: **Lacustrine paleoseismology above the Cascadia Subduction Zone from Lake Quinault: Initial Results - FOP Field Trip Stop 1**

Lake Quinault, located at the foot of the Olympic Mountains in western Washington (Fig. 1), formed above the Last Glacial maximum terminal moraine of the Quinault valley glacier (Thackray, 1996, 2001; Gavin and Brubaker, 2015). The lake is particularly well suited to serve as a lacustrine-terrestrial paleoseismologic archive for northern Cascadia because of both its location above the subduction interface and proximity to crustal faults with late Pleistocene-to-Holocene surface ruptures (Fig. 1). The 15-km^2 lake is situated about 30 km inland from the Pacific Ocean and has steep sides and a flat bottom with a maximum depth of 73 m. Upstream of the lake, the Quinault River originates at about 2250 m as it drains the rugged central core of the Olympic Mountains within Olympic National Park. The 600 km^2 landslide-prone catchment is the major source of water and sediment to the lake. The discharge of both water and sediment from the upper Quinault River is highly seasonal, with most of the annual flow occurring in the winter months between November and February (U.S. Geological Survey, 2015). The lake outlet is a single channel cut through the moraine and is referred to as the lower Quinault River.

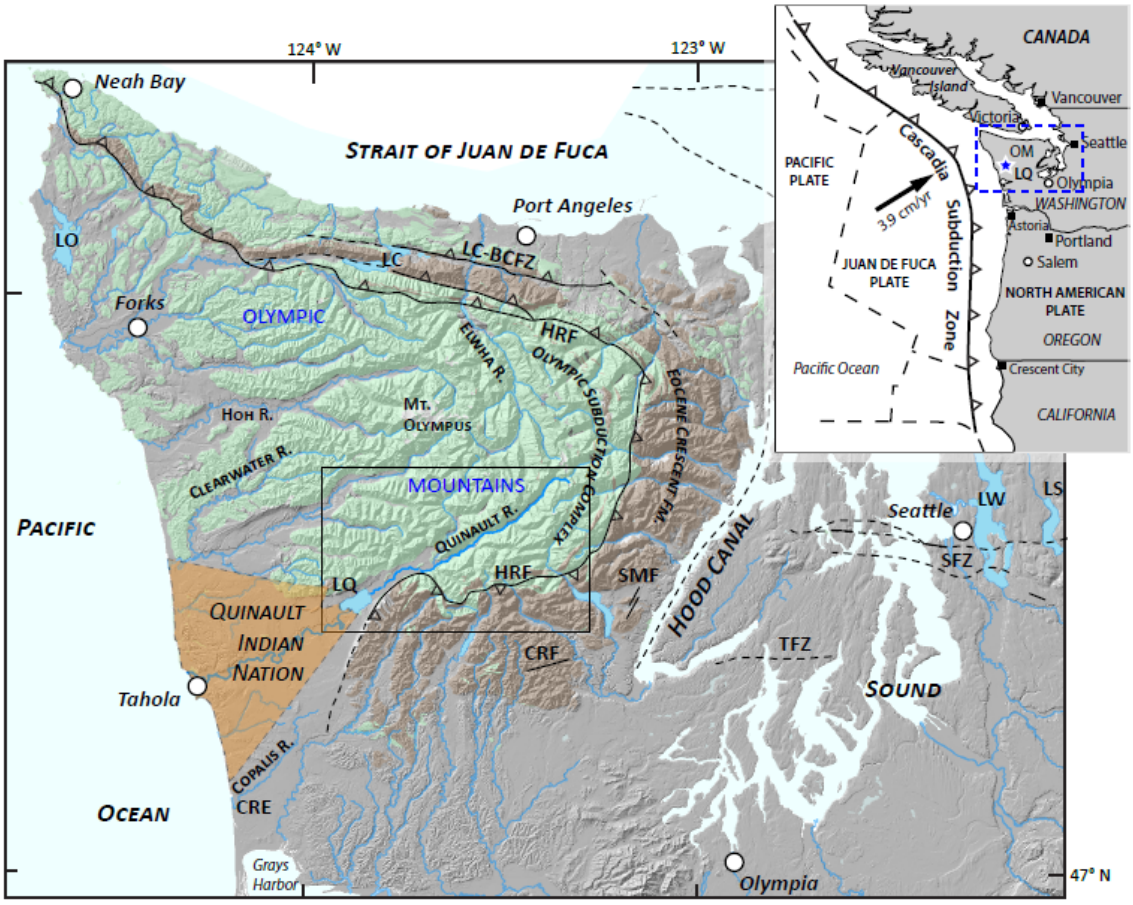

Directions to next stop

When departing Quinault Lake, it is essential that we carpool into as few vehicles as possible, for reasons of parking, safety and logistics. The road to Yahoo Lake (Stop 3) is a bit rough, but passable for 2WD vehicles.

Two maps are included below for the route to Stop 2.

Head southwest on 93400/S Shore Rd toward US 101 N

1.3 mi Slight right turn onto Route 38560/9

1.1 mi Turn right onto US-101 N. For the next 24 miles, we will be driving across the moraine-outwash terrace sequence of the Quinault and Queets valleys. The moraines are broad, low-relief features that merge gradually with the associated downvalley outwash terraces (See Fig. 5).

23.9 mi. Turn left onto 4700 Rd. This is a gravel road with a turnoff on a broad curve of Hwy 101. There has never been a sign for the road, but it is marked by a low (1 m) green electrical box. Note 1: this will be a left turn for our many vehicles across the southbound lanes. Please turn carefully! The lead cars will drive down road 4700 and wait before proceeding. Note 2 for future users of this guide: The trip enters Quinault Indian Nation lands, and permission from the Quinault offices

in Taholah is required to enter this area and visit the Stop 2 exposures

0.5 mi Bear left to stay on the main gravel road, which parallels the N-S coastline about 1 km inland from the seacliff.

1.8 mi Park alongside road, and an on old logging road to left. Please don't drive down the hill, as turning around gets difficult. The bridge across Whale Creek has been out for many years, so there is very little traffic. There are several driveways on the right (west) side of the road, which we should be careful not to block.

Walk down hill on road toward former bridge over the north fork of Whale Creek. Follow the track trail along the right (north) bank of Whale Creek to the beach, cross driftwood field, and walk north along the seacliffs. Walk north approximately 200 m to the first exposures lying parallel the coast.

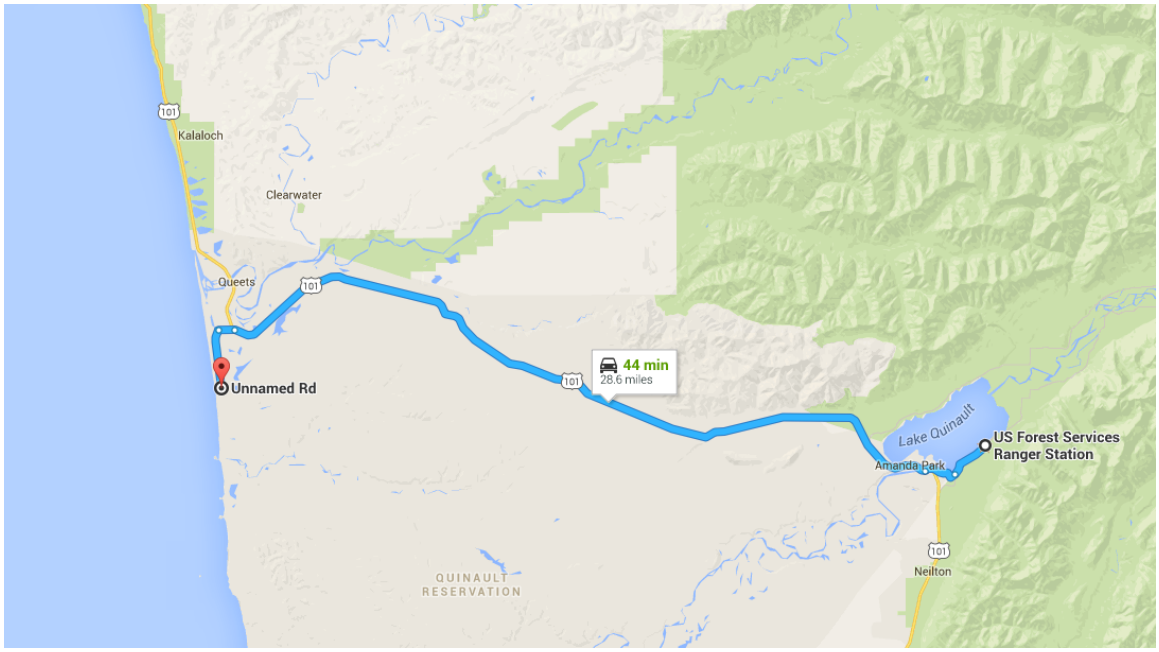

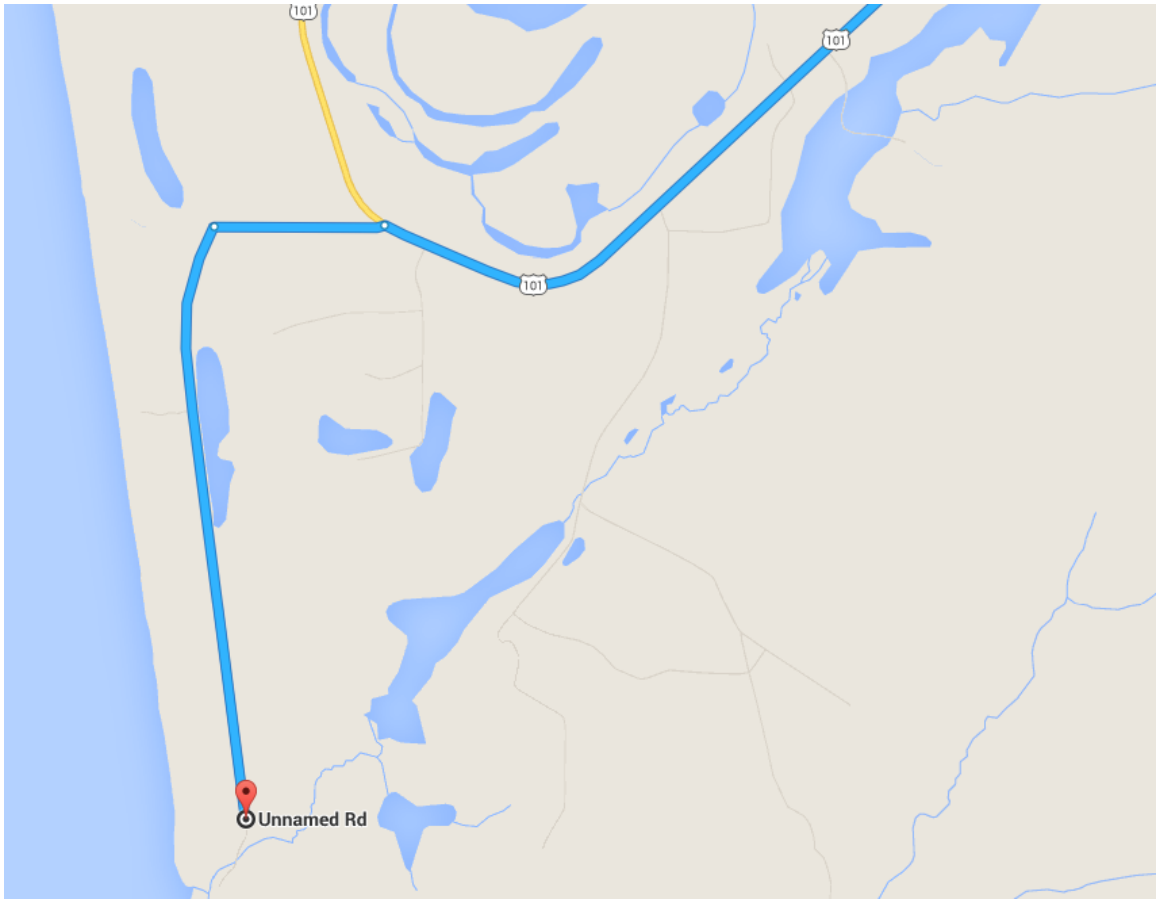

STOP 2: GLACIAL - INTERGLACIAL STRATIGRAPHY, GEOCHRONOLOGY AND DEFORMATION, WHALE CREEK AREA. The purpose of this stop is to observe strata and deformational features on the south limb of the Kalaloch syncline and to discuss the evolution of geochronology for the sequence.

The stratigraphic sequence in this area (Figures 8 and 9 of Thackray, this volume) is typical of the stratigraphy near the mouths of the Queets and Hoh rivers. In both areas, the coastal sequence fills a 1.5-km-wide zone seaward of a paleoshoreline that separates older and younger outwash surfaces, and here the seacliffs truncate an MIS 4/3 outwash sequence.

The seacliffs cut the broad coastal terrace that correlates upvalley with Lyman Rapids end moraines (Thackray, 1996; Marshall, 2013). Radiocarbon dates from seacliffs north of this exposure and from a bog at Moses Prairie (3 km northeast), support the IS 4 interpretation, as does an OSL age on outwash gravel from a gravel pit near Highway 101 south of Queets.

A prominent last-interglacial wave-cut surface in both areas separates older and younger glacial-fluvial sequences. The sequence is broadly

deformed by the Kalaloch syncline (Fig. 8), and fine-grained sediments fill the coastal zone between the outwash fans of the Hoh and Queets rivers (see Stop 6 description and Thackray, 1996, 1998)

The wave-cut surface here is an angular unconformity, while at the mouth of the Hoh River, the underlying sequence is less deformed but is marked by a boulder lag. Here, the wave-cut surface has an apparent dip of approximately 3˚ north in this immediate area. Strata underlying the wave-cut surface have an apparent dip of 11˚ north. The wave-cut surface descends to beach level a short distance north of this first exposure. Horizontally bedded beach deposits overlie the wave-cut surface, and form the base of the exposed sequence north of that location.

The younger sequence at this first exposure north of Whale Creek consists of 6.3 m of outwash and 6.3 m of fine-grained sediments. The latter consist of interbedded fine sand and silt, fining generally upward to silt with peat interbeds. A pebble-gravel bed cuts that fining upward sequence. To the north, the outwash bodies thicken to dominate the sequence, and fine-grained, organic-bearing sediments are found locally at the base of the sequence and in discontinuous interbeds within the outwash. Pollen spectra from this fine-grained sequence indicate cooling climatic conditions, from stable, mild conditions (at base) to cold-climate conditions represented by an alpine assemblage at the top (Florer, 1972).

Radiocarbon and luminescence dates constrain the age of the sequence here and at various locations in the 30 km north to the Hoh River mouth. At this location, chronologic data from radiocarbon thermoluminescence (TL; Thackray, 1998), and from OSL (unpublished data) reveal both the promises and pitfalls of dating the sequence.

Early TL dates of 261,000 $\pm$ 50,000 yr BP (mud below wave-cut surface), 273,000 $\pm$ 31,000 yr BP (beach sand above wave-cut surface), and 238,000 $\pm$ 31,000 (mud atop channel fill truncating beach sediments) suggested the wave-cut surface formed during IS 7, but these dates did not fit with the known stratigraphy and radiocarbon chronology, and were disregarded (see Thackray, 1998).

More recently, we have applied OSL techniques to the sequence (Marshall, 2013). The beach sands overlying the wave-cut platform produced an age of 93.0+12.1 ka, suggesting that the marine incursion dates to MIS 5a or 5c. Below the wave-cut surface, a sand lens in tilted gravel beds dates to 156.3+22.6 ka. Approximately 1-2 km north of this site, the overlying outwash yielded an age of 38.6+8.0 ka. This date does correlate with a well-constrained radiocarbon and OSL age for the Hoh Oxbow advances, but wood from interbeds high in the sequence yielded older, mostly infinite, ages. This relationship calls the OSL date into question. A gravel pit in the coastal terrace near US 101 south of Queets yielded an age of 83.5$\pm$11.6 ka, which correlates with the broad chronological and geomorphological framework.

A general pattern of apparent OSL reliability has emerged from all three major valleys (Hoh, Queets, Quinault) in the area. Inland exposures in the major valleys have yielded OSL chronologies that a) are internally

consistent, without stratigraphic or geomorphic reversals (see Figs. 4, 5, 6, 7; Wyshnytzky et al., 2015; Wyshnytzky, 2013, Marshall, 2013, Staley, 2013), and b) correlate with the extensive radiocarbon chronology (Thackray, 1996, 1998, 2001, and unpublished data). In coastal exposures, OSL dating has thus far proven to be problematic. OSL dates are locally stratigraphically reversed with other OSL dates and with radiocarbon. IRSL dates appear more reliable in some cases. In general, OSL and IRSL dates on the interglacial beach sands appear more reliable than on the interbeds in outwash. These patterns lead us the hypothesis, yet untested, that the inland rock units yield quartz that develops and retains a reliable OSL signal, while exposures nearer the coast produce poor quality quartz. Aside from being of different ages, the units in the two parts of the system differ in the depth to which they were carried in the accretionary wedge, and in the unique contribution of an active volcanic source to the coastal sequence (see Stewart and Brandon, 2004). It is plausible that either factor affects the suitability of the quartz for OSL dating.

As noted, the interglacial beach sands yield a more internally consistent OSL chronology. Several ages fall within MIS 5a and 5c and indicate that the wave-cut platform and beach sands originated during those highstands, rather than during MIS 5e as inferred by Thackray (1996, 1998).

Transit time to next stop: 1:15. Arrive Yahoo Lake ca. 2:00. There are some rough spots on the road, but we are told that 2WD cars can make it to Yahoo Lake.

Retrace route to cars and thence back to US101.
Turn right (southeast) on US101.

3.4 mi	Turn left onto Hoh Mainline (the sign may say “Hoh-Clearwater Road” and/or “Olympic Corrections Facility”
0.9 mi	Continue onto Clearwater Rd
7.5 mi	Continue onto Hoh Mainline
4.8 mi	Continue onto C-1010
0.4 mi	Continue onto Clear Water Rd/Hoh Mainline
0.1 mi	Turn right onto C-3000
9.5 mi	Turn left to stay on C-3000

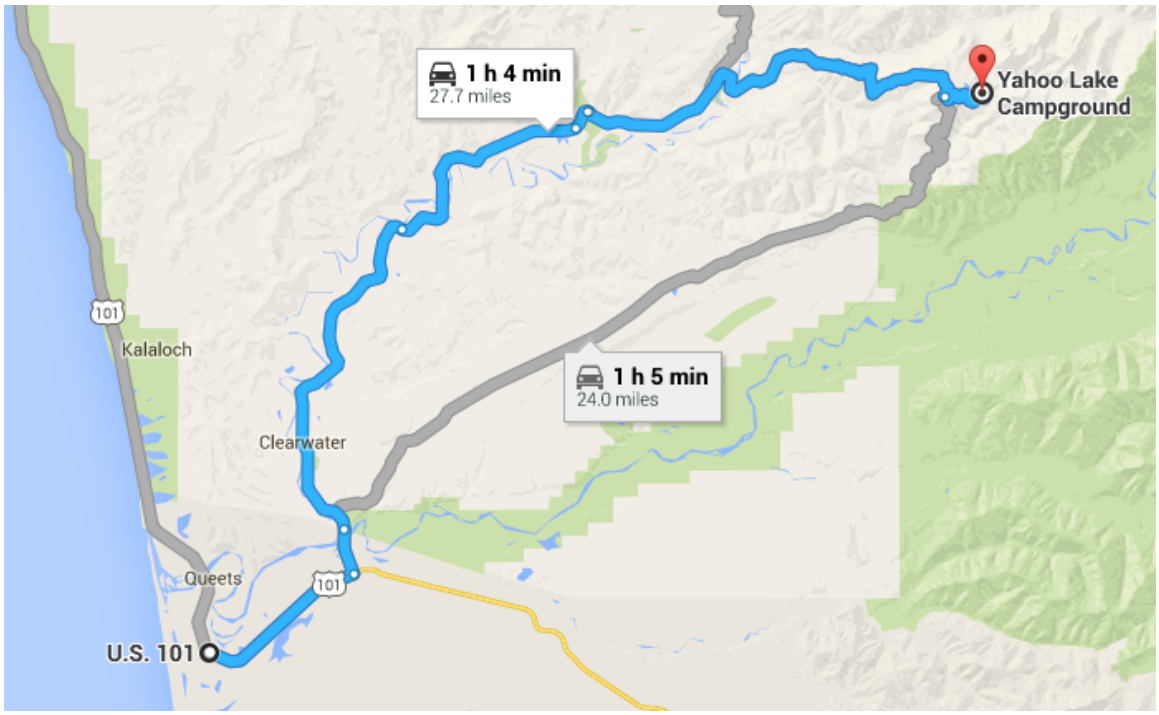

Stop 3 Yahoo Lake paleolimnology and paleoecology. (Dan Gavin). See Appendix Figures for Stop 3.

We will hike the perimeter of Yahoo Lake (ca. 0.6 miles). We will see the typical composition in old-growth western hemlock/western redcedar/Pacific silver fir forest, occurring at the lower elevation limit of the Pacific silver zone. This area has highly variable spring snowpack and thus the vegetation ecotone is particularly sensitive to a changing climate. We will discuss the paleo-records from the lake (Dan Gavin) and the vegetation modeling of postglacial period (Christoph Schworer).

Yahoo Lake is a 17.8-m-deep, 3.7-ha cirque lake located at 717 m asl on a ridge above Stequaleho Creek and 5.5 km north of the Queets River. The lake has a watershed of only 9.6 ha and no inflowing streams. The site is located at the lower limits of the Pacific silver fir zone. The forests are composed on western hemlock, western redcedar, Pacific silver fir, and minor amounts of Douglas-fir and Sitka spruce. The record from this site was published in Gavin et al. (2013).

The indistinctly laminated sediments at this site contain abundant conifer needle macrofossils and a high-resolution charcoal stratigraphy. In conjunction with preexisting climate records, we are able to reconstruct the vegetation response to climate and fire at landscape (‘‘landscape’’ here refers to the pollen source area of several square kilometers) and local (stand-level sources for macrofossils) scales.

The pollen diagram agrees well with the generalized post-glacial climate changes in the Pacific Northwest: A cold and wet Late-glacial and a cold/dry Younger Dryas (up to 11.6 ka), a warm and dry early Holocene, which transitions into a cool and wet late Holocene. This site also reveals many centennial-scale features that are poorly resolved at other sites. A hiatus in the warm/dry early Holocene, from 11 to 10 ka, is marked by

decreased fire and increased Sitka spruce. Many abrupt local vegetation changes (seen in macrofossils) occur after large fires and lag the regional vegetation changes (seen in pollen) by several centuries (see 13.6 and 11.2 ka, for example). The late Holocene is marked by some fire periods that are difficult to explain using paleoclimate proxies.

Given that the early Holocene had a summer temperature of about 4°C warmer than present, this period may provide the simplest analog for the anticipated changes on the Olympic Peninsula. The size of the recent Paradise Fire on the Queets River is certainly consistent with this interpretation; documenting forest composition in the natural succession following the Paradise Fire may provide further evidence of a shift to early Holocene forest composition.

(ca. 2.5 hours total) Scheduled departure 4:30 pm.

Transit time to next stop: 40 minutes, arrive ca. 5:15 pm.

Retrace route to Hoh-Clearwater/Hoh Mainline Road.

Stop 4. Clearwater River terraces (Karl Wegmann).

See appended text and figures by Karl Wegmann entitled “

The purpose of this stop is to introduce the concept of a strath, the terrace deposit, and some of the relative and numeric criteria in establishing strath age. Detailed discussions of these topics can be found in Wegmann (1999), Pazzaglia and Brandon (2001), and Wegmann and Pazzaglia (2002, and 2009) (Figures 1 & 2). Terraces are well preserved in the Clearwater drainage (Figue 1). There are two major flights of terraces: a higher, outer, older sequence that is underlain by thick alluvial-fill deposits, and a lower, inner, younger sequence underlain by thin alluvial deposits (Figs. 2 & 5). The terrace exposed here at the Grouse Bridge is a fine example of the lower, inner, younger sequence, and it contains all of the stratigraphic characteristics important to distinguishing and using terraces in tectonic interpretations (Figs. 2 & 3). The lower terraces like the one exposed here are composed of a basal, coarse-grained, 1–3-m-thick axial channel, sandy gravel facies, and overlying fi ne-grained 1–3-m-thick sandy silt overbank facies. The sandy gravel facies locally preserve sedimentary structures consistent with lateral accretion processes, as might be expected for point and transverse bars, which can be seen in the adjacent modern channel. So by analogy, we take the coarse-grained facies of the terrace deposit to represent the bedload being transported when the terrace strath was cut. In contrast, the fine-grained facies represent vertical accretion atop the floodplain, presumably related to deposition during floods. (continued in appended text and figures.)

(45 minutes; leave by 6:00; return to campground and lodging, or, if time permits, proceed to Stop 5)

Return to US 101 via Hoh-Clearwater/Hoh Mainline Rd. Turn left (east) onto Hwy101

southbound.

13.7 Near mile marker 133, turn right (south) onto the partially paved 9100 road near the Crane Creek Forest Products sign. Note that this forest access road appears to be open to the public, though Quinault Indian Nation permission is required to access this area.
0.4 mi Continue onto BIA Rd 9100
2.2 mi Turn right at BIA Rd 9112
0.8 mi Continue onto BIA Rd 9410
1.0 mi Turn left into gravel pit.

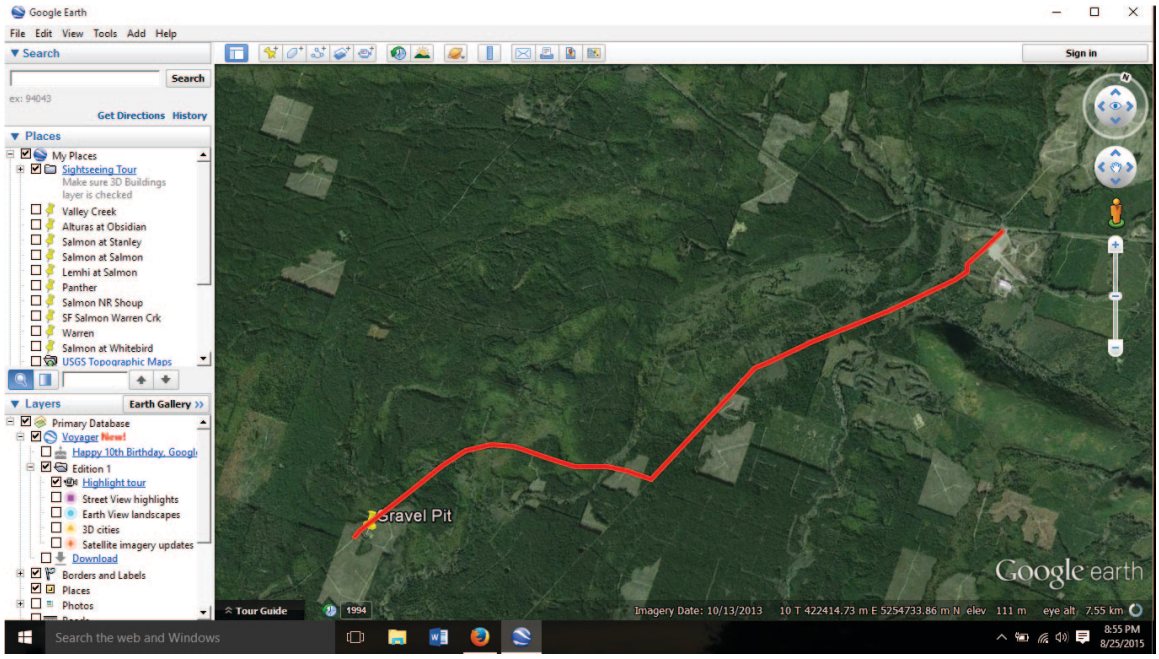

Stop 5 OPTIONAL (Thackray). Gravel pit south of Hwy 101, about 15 km west of Quinault Lake.

STOP 5: GLACIAL GEOMORPHOLOGY, STRATIGRAPHY, AND GEOCHRONOLOGY IN THE QUINAULT VALLEY. The purpose of this stop is to observe shallow stratigraphy in the Quinault valley glacial sequence and discuss sediment analysis and OSL dating strategy for glacial deposits.

The following description and results are from Staley (2013, ISU M.S. thesis).

A shallow gravel pit cuts into the surface of Qo3 outwash and diamict of its associated moraine (UTM 10T 419158, 5253940). The northern end of the gravel pit exposes 0.5-1 meters of compact, matrix supported, cobbly to pebbly, light brown diamict stratigraphically above stratified, poorly sorted, intermixed clast-to-matrix-supported pebbly-cobbly (Fig 5-1A below). Diamict clasts are mostly sub-rounded and are mixed blocky/elongate/slab shaped in a medium to fine-grained sand and silt matrix (Fig. 5-1B). The diamict is compact, but the matrix easily breaks into blocks and thickens west to east from 0.5 m to 1 m. The diamict clasts were measured for clast orientation and plotted using Orient Software (Vollmer, 2012). B-axis orientation yields a maximum eigenvalue (average trend and plunge of b-axis) 203.09, 1.59 (Fig. 5-2). The orientation shows a moderate trend of the b-axis perpendicular to inferred paleo ice-flow. The underlying upper gravel contains mostly blocky to elongate, sub-rounded to rounded, cobbly to pebbly clasts in a medium to fine-grained matrix (Fig. 5-1 C).

At the south end of the gravel pit, a 10 m exposure of the diamict and gravel was sampled for luminescence in a sand lens in the bottom 0.5 m of the gravel (Fig. 5-3 A). The outwash is gray-brown stratified, matrix-supported pebbly to cobbly gravel with interbedded sand lenses. Clasts are sub-rounded to rounded, mixed blocky/elongate/slab shape pebbles and uncommon cobbles, with a coarse to medium-grained matrix (Fig 5-3B). Open work channel deposits, 5-15 cm thick, contain well-rounded pebbles. A 30 cm thick sand bed lies stratigraphically above the outwash and pinches out to the east. Approximately 1.5 m of diamict lies above the sand bed and displays similar characteristics to the diamict exposed in the northern section of the gravel pit. Luminescence sample USU 1839 was extracted from a 23 cm thick, medium-to fine-grained sand lens 0.5 m from the bottom of exposure, yielding a preliminary age of 56.5 ± 10.1 ka. An OSL age of 50.4 ± 8.8 ka was obtained from slightly distal outwash in a gravel pit closer to US101. Together, these ages indicate an early MIS 3 age for this prominent glacial advance.

The diamict is associated with the Qm3 moraine and the gravel is associated with the Qo3 outwash, inferred to have been deposited during the advancing stage of the ice. The diamict displays a wide variety of roundness and a mix of blocky/elongate/slab shaped clasts, typical for a thin moraine deposit that incorporated large amounts of outwash deposits into the moraine. The outwash is dominantly sub-rounded and blocky in nature, suggesting close proximity to the advancing ice during deposition.

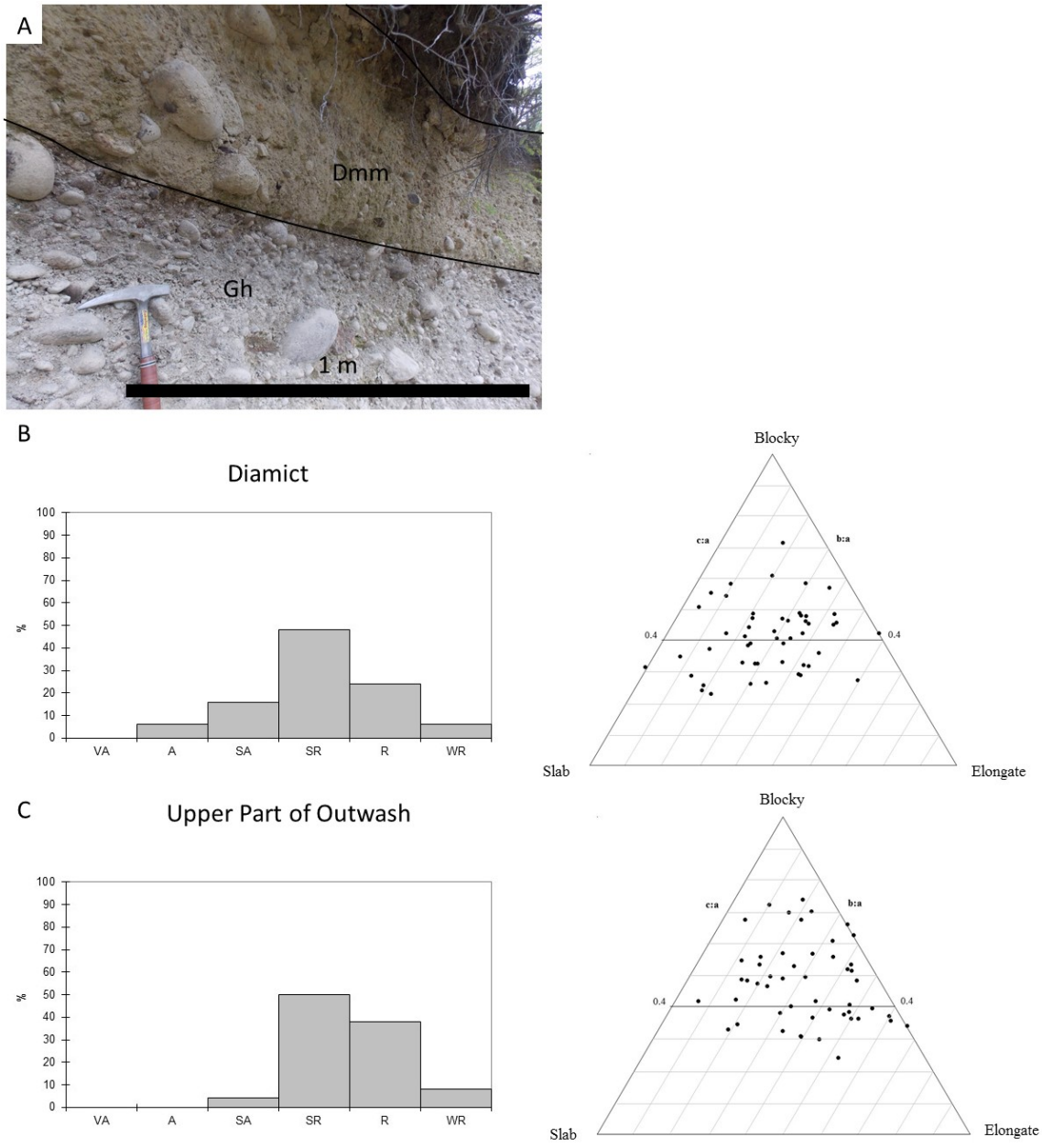

Figure 5-1 Quin_10 gravel pit. A) Exposure of diamict above upper outwash unit. B) Location of luminescence sample USU 1839 in lower outwash. C) Roundness and clast shape diagrams for upper part of outwash unit.

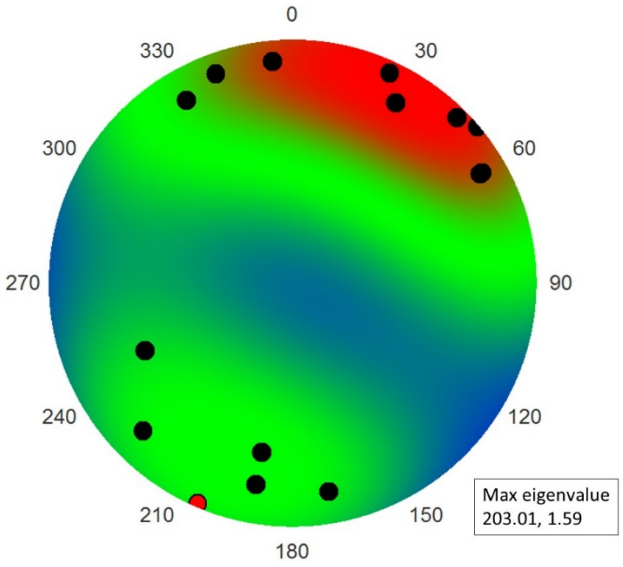

Figure 5-2. Spherical projection of the b-axis orientation of diamict clasts. Maximum eigenvalue is 203.01, 1.59 (red dot).

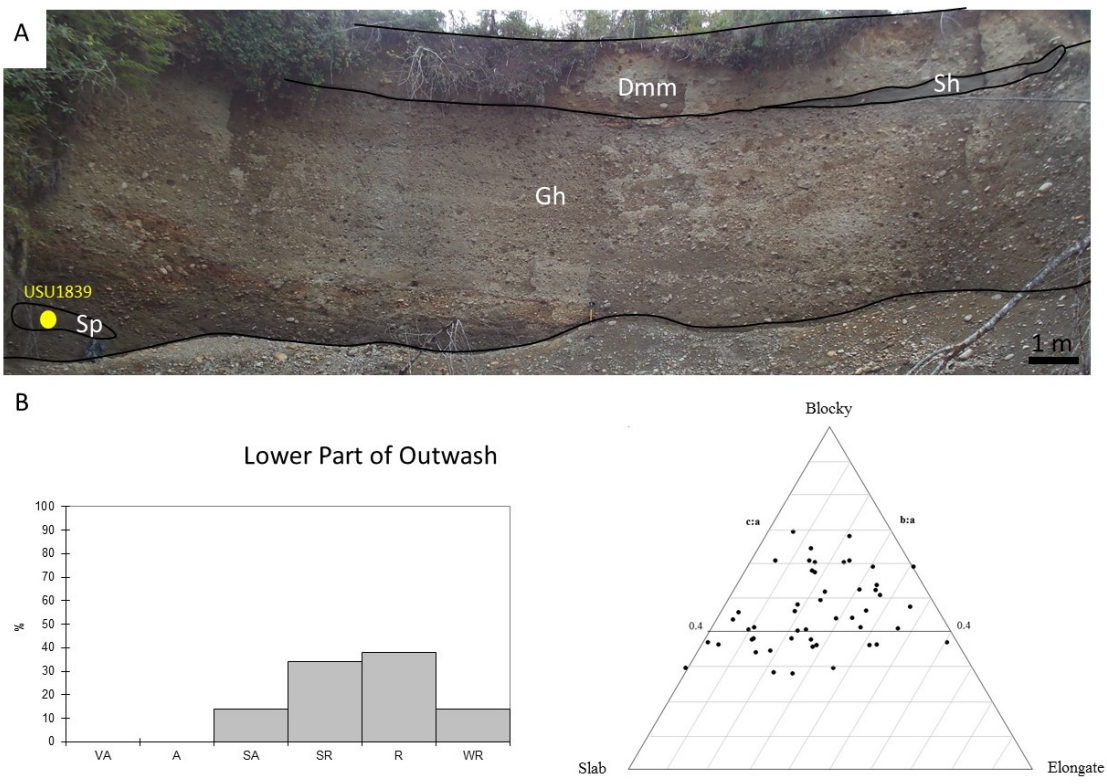

5-1 Quin_10 gravel pit. A) USU 1839 sample (56.5 ± 10.1ka) extracted from outwash in lower portion of gravel pit. B) Roundness and clast shape diagrams for lower part of outwash unit.

Return to US101, turn right, and return to Quinault Lake/Falls Creek Campground for night.

Saturday, 9/19: pack up and meet at Quinault ranger station (same as Friday) for northward migration. Transit time to stop 6: 40 minutes, arrive 9:40.

Return to Hwy 101 and turn right (north).

33.5 Turn left into Kalaloch Campground. Park in the day-use area straight ahead. If we have too many cars, we may need to park the last few on a gravel road to the right (east) of US101, about 0.1 mi south toward the lodge.

From the west edge of the parking area, walk down the short beach trail onto the lovely, wide beach and head north toward Browns Point, the prominent headland about 1.5 miles away. That is our desination.

Note that this stop should only be done around low tide. The beach is very flat, the rising tide covers ground quickly, and the beach logs can roll and become deadly. Heed the "beach logs kill" signs.

Stop 6. **KALALOCH-BROWNS POINT SEACLIFFS (Allan Ashworth and Glenn Thackray). The purpose of this stop is to discuss beetle paleoecology, pollen paleoecology of Heusser (1972), and interglacial-glacial stratigraphy.** (2 hours, including 3 mile RT walk on beach; low tide 10:30 on 9.18.15). Bathrooms at/near parking area.

Stratigraphy of the Kalaloch Area (see also appended text/figures by Thackray)

The coastal terrace surface in this area is only about 4.5 m above the high sea-level datum, approximately 25 m lower than the terraces lying near the mouths of the Hoh and Queets rivers. The Kalaloch area lies in the axial zone of the Kalaloch syncline, a broad, NNE-trending low-amplitude fold evidenced by deformed strata and the morphology of the coastal terrace (Fig. 8; Baldwin, 1939; Thackray, 1996 and 1998). The coastal terrace can be seen to rise to the north and south from this location, a function of both the folding and the thinning of outwash gravels away from the Queets River mouth.

The stratigraphic sequence in the Kalaloch area is dominated by silt, peat, and minor gravel beds. The gravel beds are locally derived, containing pebbles of lithologies endemic to the Kalaloch Creek basin. A body of gravel outwash, likely of early Wisconsin age (stage 4) and Queets River origin, dips below beach level a short distance south of Kalaloch, reappears above beach level approximately 400 m north of the campground beach access trail, and rises to the north before pinching out.

Exposure is mediocre to nonexistent for approximately 1.5 km north of the beach trail, to the Brown's Point area, making stratigraphic relationships difficult to discern. In the Brown's Point area, however, a 32-m thick section is sometimes

exposed by large slope failures, and slope failures also open ephemeral exposures between Kalaloch and Browns Point.

At and near Browns Point, parallel-bedded interglacial sand and gravel beach deposits lie at the base of the sequence and fill erosional topography in pholad clam-bored bedrock. The beach deposits are up to 5 m thick. These sands yielded an OSL age of 77.6 $\pm$ 15.3 ka and an IRSL age of 73.94 $\pm$ 16.9 ka, suggesting correlation to the MIS 5a sea level highstand. On the north side of Browns Point, sands at a similar elevation yielded an OSL age of 104.0 $\pm$ 17.2 ka and an IRSL age of 77.9 $\pm$ 15.2 ka. At face value, these latter results are ambiguous, and suggest correlation with either MIS 5c or 5a highstands. The rest of the section is dominated by silt and peat beds with minor, locally-derived gravel. Heusser (1972) described the pollen of this sequence and obtained a series of radiocarbon dates. The radiocarbon dates range from 16,700 years near the top of the sequence to 42,700 years, 11m above the beach deposits. Heusser discerned several stadial and interstadial events in the pollen spectra, largely on the basis of arboreal to non-arboreal pollen ratios. Western hemlock, Sitka spruce, and lodgepole pine were the dominant tree pollen species, except for a period of mountain hemlock dominance during the period of 22,000 to 18,000 years before present.

North of Brown's Point, a similar sequence stretches north to Beach Trail 4 and beyond. Minor Hoh valley outwash gravels extend as far south as Beach Trail 4, and dominate the sequence northward to the Hoh River. The wave-cut surface and beach sediments rise progressively higher above beach level on the north limb of the Kalaloch syncline (Fig. 8).

Beetle Paleoecology of the Kalaloch Section (Allan Ashworth)

Cong and Ashworth (1996) provided an interpretation of the middle to late Wisconsin (MIS 3-2) fossil beetle assemblages from the Kalaloch section. Fossil information for the Kalaloch section and an age model for the site (20,500 – 47,500 cal yr BP) are now available online at the Neotoma Database (http://apps.neotomadb.org/explorer/ - search Dataset/insect and select location). In addition to the paleoecological interpretation, Cong (1997) reported the discovery in the fossil assemblages of a species of a blind trechine ground beetle. Blind beetles are usually associated with caves but this highly unusual specimen had to associated with bedrock fissures beneath deep leaf litter.

The Kalaloch section was divided into two assemblage zones – the lower one (KA1, 44-52 cal ka BP), represented by thicker peat beds, contained several scolytid taxa.

Scolytids are bark borers and indicated the presence at the site of forested habitats. Based mostly on the occurrence of taxa which inhabit the region today, supplemented by a few northern species, the middle Wisconsinan coastal climate was estimated to have had a mean July temperature about -1°C lower than today. The discontinuous distribution within this zone, however, of more cold-adapted taxa, such as *Olophrum boreale* (Fig. 1) could lead to a different interpretation – a climate which oscillated between warmer phases with mean July temperatures similar to those of today, and colder phases with mean July temperature at least 2°C colder than today.

The upper zone (KA2, 31-20 cal ka BP) is represented by thinner peat beds interbedded with gravels. The assemblage is different than that of zone KA1 in that it contains a higher percentage of more cold-adapted taxa and a noticeable absence of beetles associated with trees, especially scolytids. *O. boreale* (Fig. 1) is well represented as well as the sub-alpine and alpine chrysomelid *Asiorestia pallida* and carabid *Bembidion rusticum.* Based on the presence of colder-adapted species the mean July temperature was estimated to be 2-3°C colder than today.

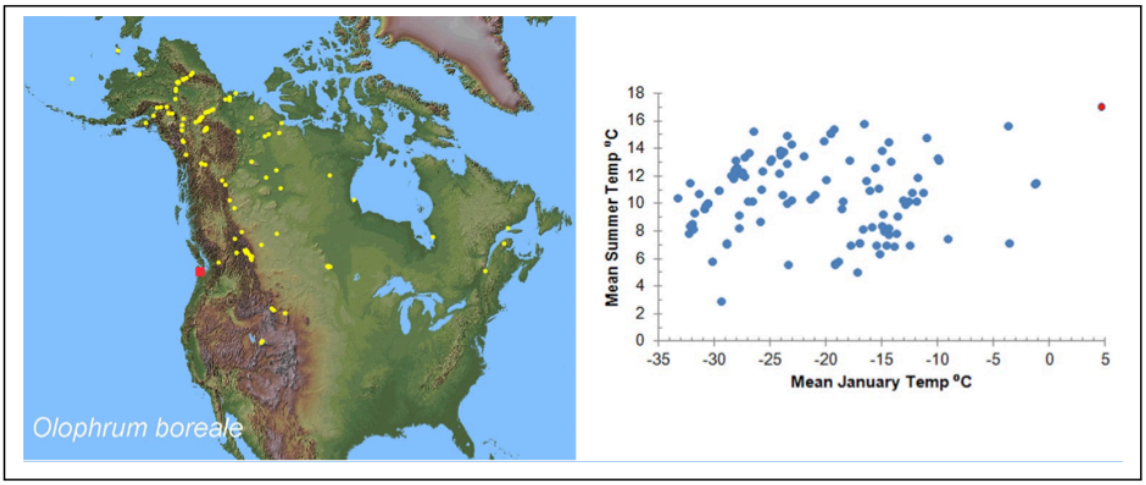

Fig. 1. Modern distribution of *Olophrum boreale* and associated temperature graph. The red square marks the position of the Kalaloch section (Modified from Ashworth and Nelson, 2013)

Return to parking area.

Travel time to next stop: 1 hour; arrive 12:45.

Return to Kalaloch Campground and proceed north on US Hwy 101, crossing the bedrock spur of Brown's Point. Note that the following roadlog section is in cumulative miles, rather than intervals, and points out several interesting locations where we will not plan to stop.

2.7 Beach Trail 4. The base of this beach trail exposes typical sandstone bedrock of the area, as well as a beautiful example of an angular unconformity between bedrock and overlying beach sand.

6.5 Destruction Island viewpoint. The seacliffs below this viewpoint, partially visible from above, expose one of the most varied stratigraphic sections along this portion of the coast. Basal gravels (MIS 6) are truncated by the prominent wave-cut surface and overlying beach sediments. The beach sediments grade upward into interglacial paleosols and peat. Outwash of the Lyman Rapids (MIS 4?) and Hoh Oxbow 2 units (MIS 3) comprise the bulk of the section above the interglacial sediments.

6.9 Ruby Beach parking lot. The road leaves the coast and turns inland, crossing Cedar Creek. North of Ruby Beach, Lyman Rapids outwash dominates. As the road climbs out of Cedar Creek and onto a high outwash terrace, the Lyman Rapids A moraine sequence lies a short distance inland. The geochronology on sediments of this ice limit is equivocal but suggests a possible MIS 5b age.

13.2 A short distance past the Hoh Humm Ranch, a gravel road on the right leads to a large gravel pit (private land owned by Rayonier) from which we have obtained OSL ages on two outwash units, dating to 61.24±13.65 ka and 84.54±16.66 ka. The younger date is near the outwash surface, which correlates with the Lyman Rapids B moraine a short distance upvalley. We provisionally correlate the lower outwash unit, which is separated from the upper unit by a thin diamict unit and yielded the older date, with the Lyman Rapids A ice limit downvalley. These results indicate that the two earlier Lyman Rapids advances occurred during MIS 5(?) and 4.

20.9 Turn right onto the Hoh-Clearwater Road and reset odometer.

Please note that we may be unable to reach Stop 7 on the South Fork Hoh River, as there is bridge work on the only viable route in. If that is the case, we may substitute a stop a short drive along the Hoh-Clearwater Road.

0.0 Reset odometer at the turn onto the Hoh-Clearwater Road. The road climbs a bedrock high, capped by a moraine that represents the Hoh Oxbow 2 glacial limit, dated to 30-34 cal yr BP with radiocarbon (Thackray, 2001). OSL dates on recessional outwash in dead-ice features a short distance upvalley of the moraine are 39.0 ± 7.5 ka and 32.3 ± 7.6 ka. These dates and the one obtained a short distance upvalley at the Winfield pits, correlate with the radiocarbon chronology and indicate a late MIS3 age for this portion of the glacial sequence. **1.5**

1.5 Winfield gravel pits, exposing Hoh Oxbow 3 outwash, dated with OSL to 40.7 ± 6.4 ka. **1.5**

3.0 Dead-ice moraine on right. Heusser (1974) obtained a 14,480 ± 600 14C yr BP radiocarbon date on peat from a bog on the moraine, as well as a 15,600 ± 240 yr 14C BP date from a bog lying 0.9 mi northwest. **2.0**

5.0 Eocene-Oligocene bedrock on right (Tabor and Cady, 1978), Hoh Oxbow 3 lateral moraine to left. **1.8**

6.8 Turn left at signed intersection, toward South Fork Hoh Campground. Heusser (1974) reported an 18,800 ± 800 14C yr BP radiocarbon date on peat from a bog 1.6 miles north. **2.4**

9.2 Just past DNR Timberlands sign, turn right toward Owl Creek (*this is an easy turn to miss!*). **0.2**

9.4 Owl Creek bridge. Rumor has it that the dents in the railing were created by boulders carried by a debris flow. Yikes. **0.1**

9.5 Turn left toward South Fork Campground. **2.8**

12.3 Iron Maiden Creek. In the late 1980's, debris flows originating at a logging road high in this drainage swept past this point and into the Hoh River valley. Concern

for salmon spawning grounds prompted mitigation measures, including debris retention structures upstream that were removed by subsequent debris flows in the mid-1990's. **2.2**

14.5 Turn left toward South Fork Campground. **0.1**

14.6 Dirt road on left leads to spectacular viewpoint for the exposure. This is on the west side of the South Fork (river left). Park along main road, in campground, etc., and walk 0.2 miles down dirt road to river.

STOP 7. Twin Creeks MIS 2 glacial sequence near confluence of South Fork Hoh and Hoh Rivers. The purpose of this stop is to observe the well-exposed Twin Creeks drift and discuss the record of valley glaciation in the Olympic Mountains.
Note 1: Bridge construction on the main Hoh south-side road may preclude this stop.

Note 2: If the South Fork Hoh is accessible…. this exposure can be accessed via a similar road on the east side of the bridge (river right), or by following the logging roads to the top of the terrace and descending the closed, terrace-edge logging road. Either access route can be rather treacherous, with the latter providing the best access to the entire exposure.

The stratigraphy of the Hoh valley forms the foundation of the glacial chronology developed for the western Olympic Peninsula by Thackray (1996, 2001, 2008; Marshall, 2013; Wyshnytzky, 2013; Wyshnyntzky et al., 2015). Several moraine-terrace sequences mark the Hoh valley (Fig. 4) and associated stratigraphic exposures reveal the processes and chronology of glacial advance and retreat and provide detailed chronology (Fig. 6, 7 in appended material by Thackray). This South Fork Hoh exposure (Figure 1a below) is one of many that reveal the style of stratigraphic evolution during the main MIS 2 advances of the South Fork glacier, as well as important chronologic data.

Following deposition of the Hoh Oxbow drift, the Hoh glacier retreated well upvalley, separating into two lobes at the confluence of the Hoh River and its South Fork. The two glaciers then readvanced to deposit the Twin Creeks drift. The inferred maximum-phase Twin Creeks end moraine in the main valley lies about 2.5 km north of this exposure, adjacent the confluence area. Its South Fork counterpart lies about 3 km upvalley from this exposure, with a later-phase moraine about 2 km further upvalley (Thackray, 2001; Wyshnytzky, 2013).

The stratigraphic sequence exposed here records events prior to and during the Twin Creeks 1 advance (Thackray, 2001). Three meters of grey, clast-rich diamict form the base of the exposure. Three meters of clay- and silt-rich lacustrine sediment overlie the till. Dropstones are common in the bottom meter. The lacustrine sediments yielded several wood samples, three closely correlating dates around 23.0 cal ka, and an OSL age of 20.1 $\pm$ 3.7 ka (preliminary age shown as 19.2 in Figure 1a below).

Delta sediments overlie the lacustrine beds. Sand interbeds near the base produced an OSL age of 20.5 $\pm$ 5.2 ka. The delta sediments are overlain by about 25 m of outwash. A fine-grained organic-bearing interbed near the middle of the unit yielded radiocarbon ages of 18.8 and 19.4 ka, and produced the fossil beetles discussed below. The coarse outwash near the top of the exposure forms a prominent terrace that can be

traced upvalley to the end moraine. The terrace merges with main-valley terraces in the confluence area.

The stratigraphy and geochronology of this outcrop and several others in the South Fork Hoh (Fig. 1a and 1b below; Wyshnytzky, 2013; Thackray, 2001) confirm that the MIS 2 glacier descending the South Fork Hoh valley was restricted in extent in comparison to MIS 5(?)-3 advances, which terminated several tens of kilometers downvalley.

A major slope failure changed this exposure considerably and diverted the river several tens of meters toward the left bank in 2004, and further erosion will likely continue to alter the specific strata exposed.

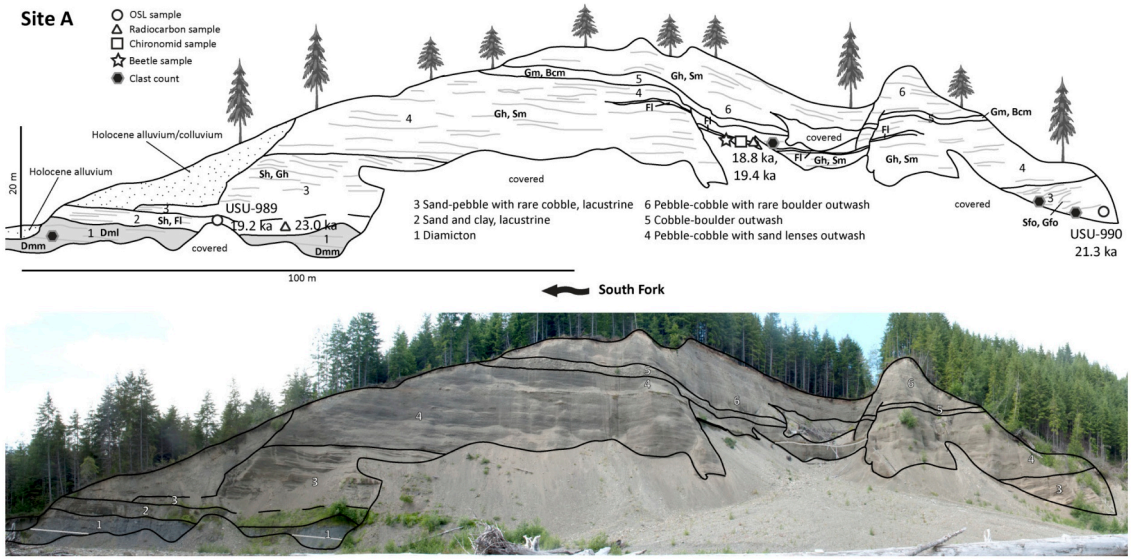

Stop 5, Figure 1a. Stratigraphy and geochronology of a prominent exposure, South Fork Hoh River near the South Fork Campground.

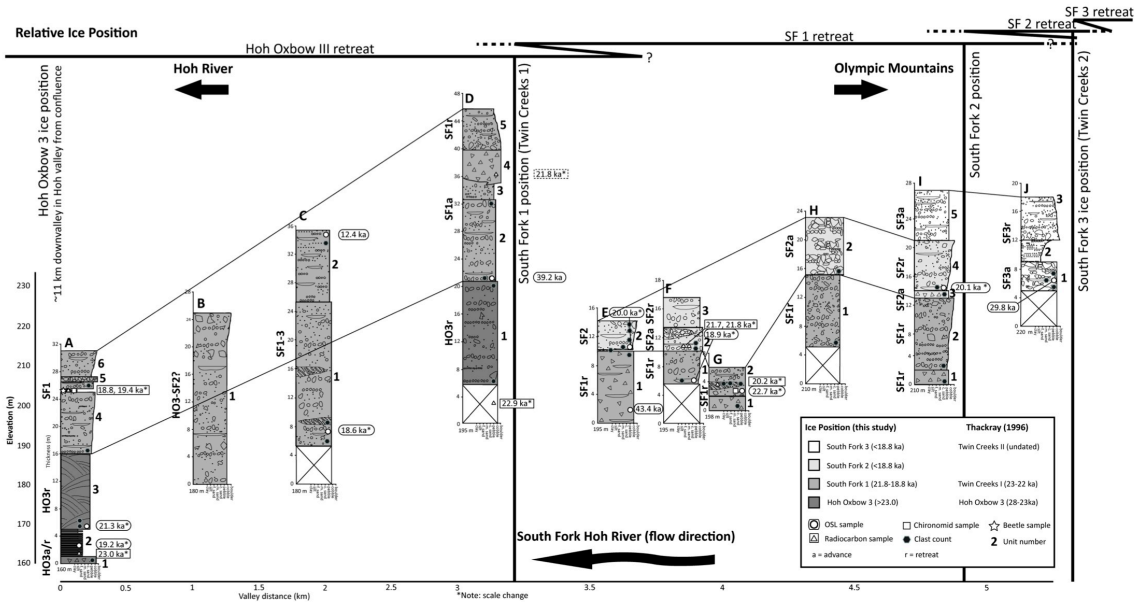

Stop 5 Figure 1b. Glacial stratigraphy and geochronology of the South Fork Hoh River valley.

Beetles of the South Fork Hoh River section

The Hoh River fossil beetle assemblage consists of about 500 disarticulated skeletal pieces. The chitin is well-preserved and was not weathered before burial. The assemblage consists of a limited number of taxa. The assemblage contains several water beetle taxa, both dytiscids and hydrophilids, indicating that the depositional environment was a shallow lake. There are no taxa associated with trees in the assemblage but there are several specimens of Apioninae, which are associated with grass meadows.

The most abundant taxon in the assemblage is the omaliine staphylinid *Olophrum consimile* (Fig. 2a) a species which is circumpolar and in North America occurs throughout the cold temperate and boreal zones. It lives in mosses and vegetation in bogs frequently on the margins of lakes. This species, together with a very closely related species *O. cascadense*, occurs within the Pacific Northwest but only at higher elevations within the Cascades (1400m in northern Washington State to 1981- 2500m in Oregon). The assemblage also contains a related species *O. rotundicolle* which does not occur in Washington State. The closest location it occurs today is in southern British Columbia at an elevation of 1800m (Fig. 2b).

Other identified species within the assemblage include the ground beetles *Elaphrus clairvillei* and *Patrobus stygicus*. Both of these taxa occur on wet peaty substrates adjacent to lakes amongst vegetation of mosses, sedges and other mesic-loving plants. Both occur throughout the cold temperate and boreal zones in North America. *E. clairvillei* (Fig. 3) occurs in Washington State but *P. stygicus* has not been recorded. The fossil beetle assemblage indicates that the climate was colder and drier than the present day. Using a conservative lapse rate (0.5° C/100m) argument for *Olophrum consimile*, which has been recorded in northern Washington State at 1400 m elevation, the climate

could have been 6.5°C cooler than the present. A more complete analysis of the climate distribution for *O. consimile* would likely result in this estimate being lowered.

The lake and bog were likely developed in an abandoned channel. Whether or not gravel continued to be deposited in different parts of the Hoh valley at the time the lake was active is uncertain.

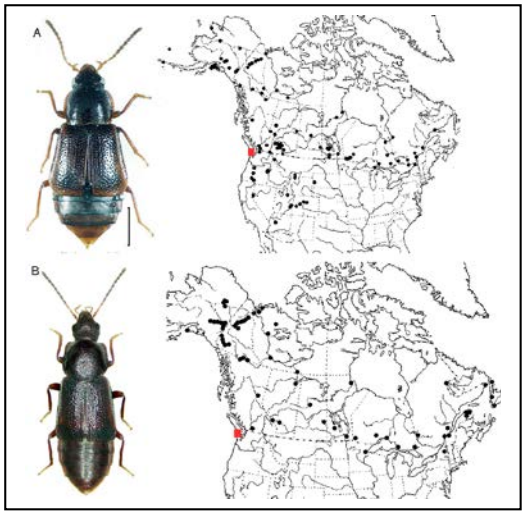

Fig. 2. The Omaliine staphylinids *Olophrum consimile* (A) and O. *rotundicolle* (B). Both are represented by heads, pronota and elytra. On the modern distribution maps (Campbell 1983) the location of Kalaloch is shown by the red square

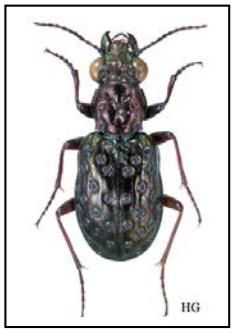

Fig. 3. *Elaphrus clairvillei* represented by elytra

References

Ashworth, A.C. and Nelson, R.E., 2014, The paleoenvironment of the Olympia beds based on fossilbeetlesfrom Discovery Park, Seattle, Washington, U.S.A. *Quaternary International* 341:243-254.

Campbell, J.M., 1983, A revision of the North American Omaliinae (Coleoptera:Staphylinidae). The genus *Olophrum* Erichson. The Canadian Entomologist 115: 577-622.

Cong, S. and Ashworth, A.C., 1996, Palaeoenvironmental interpretation of Middle and

late Wisconsinan fossil coleopteran assemblages from western Olympic Peninsula, Washington, USA. Journal of quaternary Science, 11 (5): 345-356.

Cong, S., 1997, Fossils of an undescribed blind trechine (Coleoptera, Carabidae) from near Kalaloch, Olympic peninsula, Washington. Coleopterists Bulletin 51(3):208-211.

Return to cars. Pit toilets available at campground. Leave 2:45. Transit time to next stop 2:00 (actual drive time 1:40). Groceries and gas can be obtained in Forks. We will reconvene at Stop 8 at Crescent Lake.

Return to US 101
0.0 Turn right (north) on US101 toward Forks and Port Angeles. As you pass through Forks beware of vampires, and also note that a short distance north of town the road passes the MIS 2 ice limit of the Juan de Fuca lobe of the Cordilleran ice sheet. The topography becomes more subdued north of here, and Canadian granite clasts appear in roadcuts of glacial sediment.

52.0 Turn left toward Crescent Lake Lodge and Barnes Point. We will park in the Crescent Lake Lodge parking lot and walk to the beach.

Stop 8. Evidence for Post-glacial Surface Rupture on the Lake Creek—Boundary Creek Fault from Chirp Seismic Investigations at Lake Crescent

See extended text and figures by Karl Wegmann, appended at the end of the field guide.
(1 hour)

Improving the estimates of sizes, recurrence intervals, and effects of late Quaternary earthquakes in the Puget Sound region is one of the priority research topics for the Pacific Northwest hazards community. Herein we present preliminary evidence supporting the hypothesis that the Lake Creek – Boundary Creek Fault (LCBCF) has experienced multiple post-glacial rupture events at Lake Crescent, Washington (Figure 1). One or more of these events is likely to have triggered rock avalanches, drainage reorganization, and isolation of aquatic species. The LCBCF is an east-west trending oblique slip fault on the northern flank of the Olympic Peninsula near the town of Port Angeles. The LCBCF is one of a number of steeply-dipping crustal faults in the Puget Sound region recognized primarily in the past decade or so as exhibiting evidence for latest Pleistocene - Holocene surface rupture based on the evaluation of high-resolution lidar-derived digital elevation models (Haugerud, 2002; Polenz et al., 2004; Schasse et al., 2004) and subsequent fault trenching investigations (Nelson et al., 2007). The LCBCF is one of several fault zones in the Puget Sound region accommodating north-south contraction and clockwise rotation of the western Washington portion of the Cascadia forearc (e.g., Wells et al., 1998).

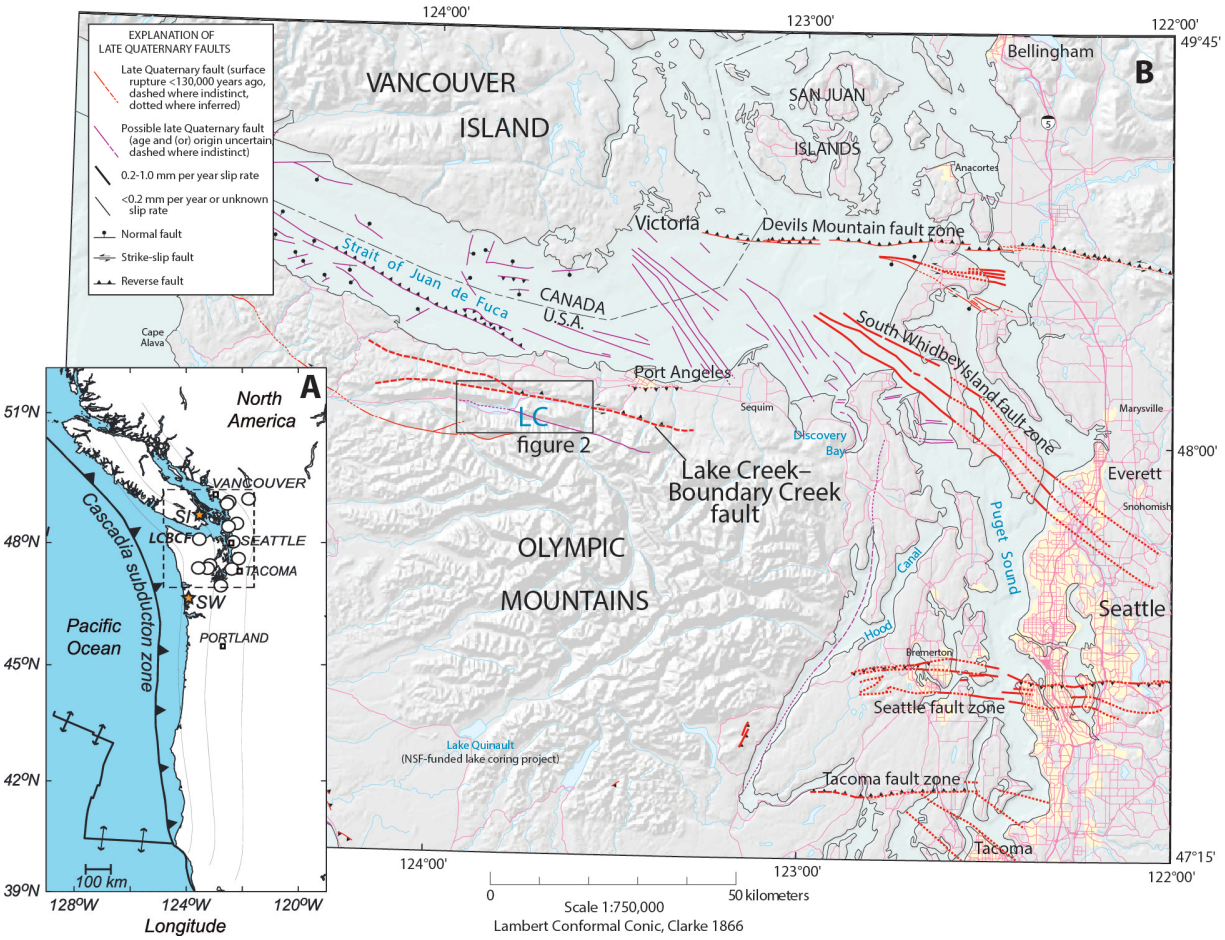

Stop 8 - Figure 1. Active tectonics of the Cascadia margin. **A**. Map of the Cascadia subduction zone showing locations of known late Holocene upper plate earthquakes (open circles), modified from Sherrod & Gomberg (2014). Dashed rectangle shows location of enlarged map. **B**. Map of the Olympic Peninsula and Puget Sound region in northwest Washington State showing known and possible late Quaternary faults from Lidke et al. (2003) and Blakely et al. (2004). Study area along the Lake Creek-Boundary Creek fault in the vicinity of Lake Crescent outlined by rectangle. Figure modified from Nelson et al. (2007).

Stop 9 (optional, if time allows): Landslide separating Lake Crescent and Lake Sutherland.

By 6:30 : Depart for camp at Crescent Beach RV Park. FOP gathering and decisions for next year's trip.

Sunday 9/20. Pack up and depart Crescent Beach RV Park.

Meet and carpool at Laird's Corner Park and Ride, junction of Hwy 112 and Hwy 101.

Transit time to Stop 10: total 8.8 miles, 25 min.

Depart Laird's Corner Park and Ride. Turn right (west) on Hwy 101.

3.3 mi: Turn left on Olympic Hot Springs Road toward Olympic National Park and Elwha Valley.

2 mi (5.3 cumulative miles from start at Laird's Corner Park): Olympic National Park Entrance and fee station. Pause to consolidate vehicles to enter park.

0.7 mi (6.0 mi.): Note large log jams in Elwha River channel on right. This portion of the river saw an influx of sediment and large woody debris during the removal of the upstream Glines Canyon Dam in 2012-14.

1.6 mi (7.6 mi): Cross Altair Bridge over Elwha River. We will return here for Stop 11.

1.2 mi. (8.8 mi): STOP 10, Glines Canyon Dam Site. Pull into parking lot on left side of road. Additional vehicles park along gravel road to the left, just past the parking lot.

STOP 10: Glines Canyon Dam removal, sediment transport from the former Lake Mills Reservoir, and overview of the Elwha River Restoration Project. 40-60 min.

Compiled by: Lisa Ely and **Bryon Free**, Dept. of Geological Sciences, Central Washington University; and **Andy Ritchie**, U.S. National Park Service

The removal of the two dams on the Elwha River (Fig. 1) was the largest dam removal project in history. The dam removal process began in 2011. The downstream Elwha Dam (constructed in 1913) was fully removed by September 2012, and the Glines Canyon Dam at this field trip stop (constructed in 1927) was removed by August 2014. The two dam removals were undertaken to restore natural fish passage and habitat to the river. The dams collectively impounded 21 million m^3 of sediment, 16 million m^3 of which was stored in the reservoir behind the Glines Canyon Dam at this site (Warrick et al., 2015). The dams were lowered incrementally to allow the river to rework the sediment within the reservoir and maximize the sediment transport downstream (Fig. 2; Randle et al., 2015). Lowering the dams in stages minimized the hazards associated with dam removal, reduced the cost of removing the sediment, and allowed the sediment releases to be scheduled to avoid spawning seasons and other downstream impacts (Duda et al., 2011; Magirl et al., 2011).

The Glines Canyon Dam sat at the head of a 2-km-long, narrow bedrock canyon, and remnants of the former dam are visible from this overlook (Fig. 3). The water in the reservoir was incrementally lowered from 2011-2012, allowing the river delta to prograde across the reservoir basin toward the dam. At this site, sand and gravel deltaic sediments overlie fine-grained lakebed sediments deposited in the former reservoir (Fig. 4). Cut

stumps of the pre-dam old-growth forest reemerged as the lake was lowered; some are still capped with lacustrine sediments. Large logs and stumps strewn across the terraces cut into the delta sediments accumulated in the reservoir over the life of the dam and have recently been reworked by the river. Ongoing research on the Elwha River by University of Washington Ph.D. student Vivian Leung demonstrates that the large woody debris creates channel complexity that enhances the erosion and removal of the reservoir sediment (Leung and Montgomery, 2010).

In October, 2012, the reservoir was completely drained and the coarser sand and gravel fluvial sediments began to be released downstream. Within the first 2 years of dam removal, 37% of the sediment had flushed out of the reservoir (Randle et al., 2015). Terraces of the prograded delta remain along the margins of the reservoir basin, marking some of the baselevel stages as the dam was lowered. These are rapidly revegetating through natural processes and revegetation projects, which increases the stability of the new river banks. The two largest discharges since the inception of the dam removal in December, 2014 and February, 2015 mobilized a significant amount of sediment within the reservoir, creating the most recent evidence of fluvial erosion and deposition visible from the dam overlook. The amount of future erosion will depend on the growth rate of bank-stabilizing vegetation and the timing of additional large discharge events.

(see additional figures and references appended at end of field guide)

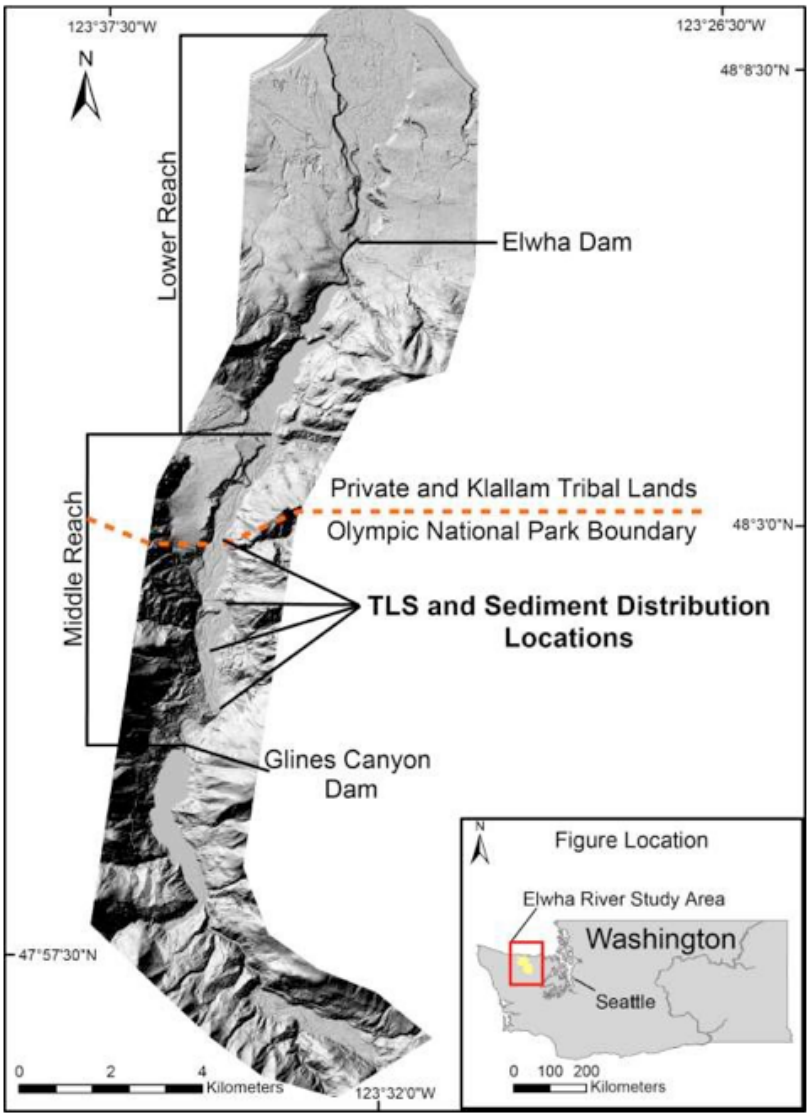

Elwha Figure 1. Elwha Restoration Project Map, northwestern Washington State on the Olympic Peninsula. Base map is the 2012 aerial LiDAR provided by the USGS. From B. Free (2015).

1.2 mi. STOP 11, Altair Bridge over Elwha River. (Transit time from Stop 10, 10 min.) Retrace route from Stop 10 back down Olympic Hot Springs Rd. 1.2 mi to Stop 11. Park in the entrance to the closed, former Altair Campground on left (north) side of road just before the bridge. Additional vehicles can park on right shoulder of road before the bridge and left shoulder of road just after the bridge.

STOP 11: Altair Bridge over the Elwha River. Effects of the Glines Canyon Dam removal on the river channel geomorphology, sediment transport, and large woody debris. 30-60 min.

The Altair Bridge site is the farthest upstream of four study sites between the two dams on the Elwha River that were monitored for the effects of the dam removal on the channel before, during and after the dam removal process from 2012-2015 (Figs. 1 and 5).

Changes in the river channel were quantified through annual repeat Terrestrial LiDAR (TLS), bimonthly sediment distribution surveys, and periodic large woody debris (LWD) mapping (Fig. 2). The results form the basis of a Central Washington University Masters thesis by Bryon Free (2015). The data presented for this field trip stop are from his MS thesis. This study, along with numerous others that are part of the Elwha River Restoration Project, provides empirical data to support models of sediment transport and channel response for future dam removal projects.

Although ~90% of the sediment released from the two dams from September 2011-September 2013) reached the coast (Warrick et al., 2015), the retention of the additional sediment and large woody debris resulted in substantial channel changes that continue to date. The complexity and particular geomorphic characteristics of each site were major factors in the deposition and accumulation of the new influx of woody debris and sediment from the dam removal. The Altair Bridge site lies at the first expansion of the Elwha River channel below the dam site as it exits the 2-km Glines Canyon. Prior to the initial release of coarse sediment from the dam in October 2012, this site consisted of four armored and incised channels separated by heavily vegetated, established islands (Fig. 6), which have now partially coalesced (Fig. 7). Except for a single log jam and a few scattered logs, the copious woody debris visible from the bridge has accumulated since the inception of the dam removal.

The initial sediment pulse filled the riffles and pools throughout the entire middle reach of the river within the first few months (East et al, 2015). Within the 300-meter Altair reach, sediment deposition greatly outpaced erosion in the first year, with a minimum net accumulation of 5000 m^3 above the low-flow water surface (Fig. 7). In contrast, net erosion and deposition were approximately equal in the second year (Fig. 7), partly due to a 9-month hiatus in the dam removal that limited the influx of new sediment (Fig. 2). As the initial sediment wave dissipated and the river continued to transport sediment from the reservoir, the timing of the sediment deposition and erosion was increasingly dictated by the discharge of the river (Figs. 8 and 9). As the individual pieces of woody debris coalesced into log jams, it influenced the sediment deposition by armoring the banks of channels, creating low-velocity pools, and directing the flow of water and sediment (Fig. 10). Over the past 3 years, the combined deposition of sediment and woody debris blocked the right-hand channel and caused a dominant channel to form on the left. This channel has migrated 20-30 m to the west, and eroded entire campsites from the former Altair campground. Overall, at the four study sites, the preexisting geomorphology influenced the capture and retention of sediment and large woody debris to a large degree, which affected subsequent channel changes in a continuing feedback process.

(see additional figures appended at the end of the field guide)

Continue to retrace route from Stop 11 north on Olympic Hot Springs Rd.

Return to Laird's Corner and the parked cars.

This marks the end of the organized trip, but if you have time and have never been to Hurricane Ridge, this is a great time to do so. The high vantage point at Hurricane Ridge provides a spectacular view into the rugged core of the Olympic Mountains, the glaciers surrounding Mt. Olympus and other high peaks, and the upper Elwha Valley.

Thanks to all of you for joining us on this FOP extravaganza. Hope to see you for the 2016 Pacific Northwest FOP gathering, focusing on the _____ (please, somebody, fill in the blank)!

Lacustrine paleoseismology above the Cascadia Subduction Zone from Lake Quinault: Initial Results - FOP Field Trip Stop 1

Compiled by Karl Wegmann, Elana Leithold, DelWayne Bohnenstiehl & Steven Smith
Dept. of Marine, Earth, and Atmospheric Sciences, North Carolina State University

Excerpted from Leithold et al., in review, Journal of Sedimentology.

In recent years, studies in tectonically active regions have demonstrated the utility of lakes as recorders of paleoseismic activity. Glacially-formed lakes such as those in the Swiss, Italian, and New Zealand Alps and the Andes of southern Chile have been shown to be particularly sensitive to subaqueous mass wasting during large earthquakes (Siegenthaler et al., 1987; Chapron et al., 1999, 2007; Moernaut et al., 2007; Schnellmann et al., 2005, 2006; Simonneau et al., 2013; Strasser et al., 2013; Hilbe and Anselmetti, 2014; Van Daele et al., 2015; Kremer et al., 2015), and to also serve as efficient traps for sediment derived from subaerial mass wasting in mountainous catchments (Chapron et al., 2007, Howarth et al., 2012). In these environments, characterized by steep lateral slopes and relatively high rates of sediment accumulation, subaqueous slides, mass flow deposits, and turbidites preserved in lacustrine sedimentary records have been attributed to historical earthquakes and used to reconstruct regional paleoseismic histories.

Over the past decades, abundant evidence for the occurrence of great ($M \geq 8$) earthquakes at the Cascadia subduction zone (CSZ) has been amassed. The Holocene earthquake history of the CSZ megathrust has been reconstructed based upon stratigraphic studies of tsunami deposits overlying rapidly subsided coastal lowland soils and within low-lying coastal lakes and lagoons, from mass flow "seismite" deposits preserved in the deep fiords of western Vancouver Island, and from margin-parallel studies of offshore marine turbidites (e.g., Atwater, 1987; Adams, 1990; Atwater and Hemphill-Hailley, 1997; Kelsey et al., 2005; Williams et al., 2005; Nelson et al., 2006; Blais-Stevens et al., 2011; Goldfinger, 2011; Goldfinger et al., 2012; Enkin et al., 2013). These and other studies also further address questions about seismic magnitudes, recurrence intervals, event clustering, and fault segmentation along the Cascadia margin. These paleoseismic reconstructions, perhaps the most complete records for any active margin, have not only informed research questions centering on subduction zone processes, but coupled with the specter of devastating loss of life and infrastructure during recent events around the globe (e.g., Sumatra-Andaman 2004, Chile, 2010, Japan, 2011), they have captured the attention of both governmental planning agencies and the public.

Landward of the coastal zone, however, very little is known about the ***terrestrial upland*** response to great subduction earthquakes or other large earthquakes in Cascadia. Based on research in other areas of the world (e.g., Keefer, 1984, 2002; Dadson et al., 2004; Meunier et al., 2008; Yanites et al., 2010; Hovius et al., 2011; Tang et al., 2011), in regions with large topographic relief, earthquake-triggered landslides are likely to be one of the most significant hazards faced during and in the immediate aftermath of future events. Furthermore, the Earth surface process response is likely to have decadal-scale

impacts on sediment supply to fluvial networks and coastal margins (e.g., Hovius et al., 2011), with implications for both fresh and salt-water ecosystems. Over millennial time scales, moreover, mass wasting associated with large earthquakes has likely played a fundamental role in modulating the flux of terrigenous sediments to the marine environment and to the evolution of topography above Cascadia and other subaerial forearc subduction margins. The apparent mismatch between tectonic addition of mass and landslide-derived erosion resulting, for example, from the 2008 M 7.9 Wenchuan earthquake (Parker et al., 2011), highlights the need for a much greater understanding of the role of large earthquakes in setting regional erosion rates and long-term patterns of orogen evolution (e.g., Parker et al., 2011).

Lake Quinault, located at the foot of the Olympic Mountains in western Washington (Fig. 1), formed above the Last Glacial maximum terminal moraine of the Quinault valley glacier (Thackray, 1996, 2001; Gavin and Brubaker, 2015). The lake is particularly well suited to serve as a lacustrine-terrestrial paleoseismologic archive for northern Cascadia because of both its location above the subduction interface and proximity to crustal faults with late Pleistocene-to-Holocene surface ruptures (Fig. 1). The 15-km^2 lake is situated about 30 km inland from the Pacific Ocean and has steep sides and a flat bottom with a maximum depth of 73 m. Upstream of the lake, the Quinault River originates at about 2250 m as it drains the rugged central core of the Olympic Mountains within Olympic National Park. The 600 km^2 landslide-prone catchment is the major source of water and sediment to the lake. The discharge of both water and sediment from the upper Quinault River is highly seasonal, with most of the annual flow occurring in the winter months between November and February (U.S. Geological Survey, 2015). The lake outlet is a single channel cut through the moraine and is referred to as the lower Quinault River.

Lake Quinault Seismic Stratigraphy

The seismic reflection survey revealed abundant indicators of shallow gas, similar to those that have been documented in other lacustrine and marine settings (e.g. Loseth et al., 2009, Cukur et al., 2013). Over most of the lake, Chirp profiles show acoustic blanking indicating absorption of the seismic signal in gas-charged sediments. Near the base of the distal, southwestern slopes of the lake adjacent to the moraine, however, acoustic penetration increases abruptly, extending to ~15-20 m depth beneath the lake bed (Figure 2). Two distinct, superposed seismic facies can be delineated in profiles from this area and are in abrupt contact with one another (Fig. 3). ***Seismic Facies A*** extends from the present-day lake floor to about 3 m depth. ***Seismic Facies B*** extends to the limit of acoustic penetration.

Seismic Facies A is characterized by medium to high amplitude, parallel and continuous reflectors. The acoustic layers of this facies indicate even draping of previous bathymetry. The very similar pattern of reflections observed in Seismic Facies A across the entire southwestern side of the lake indicates a uniform stratigraphy (Fig. 4). In only one limited area along trackline 27 does Seismic Facies A contain intercalated lens-shaped sediment bodies with chaotic to transparent seismic character that indicates mass wasting deposits (Fig. 5).

Seismic Facies B, in contrast, is characterized by weaker, parallel and more discontinuous reflectors. Narrow vertical to sub-vertical zones of acoustic turbidity are abundant in this facies and resemble gas chimneys documented in other locations (e.g., Hovland and Judd, 1988; Cathles, et al. 2010; Cukur, 2013; Fig.3). In Lake Quinault, the lower ends of the gas chimneys can be traced to 15-20 m depth beneath the lake floor, where acoustic energy is attenuated and beyond which seismic stratigraphy cannot be resolved. Most of the chimneys extend upward and terminate at the base of Seismic Facies A; although some cut across it to reach the sediment-water interface. In several places, active venting of gas to the water column was observed during the seismic survey (Fig. 6).

Seismic Facies B shows evidence for mass wasting, including two relatively large, lobate slides originating from the subaqueous lake slopes, with volumes of roughly 6 x 10^6 m^3 and 1 x 10^6 m^3. In High School Bay (Fig. 2), trackline 16 imaged a longitudinal profile along the flank of the larger of these slides (Fig. 7), while tracklines 19, 20, and 21 are transverse sections across the depositional lobe of the same slide that show progressively lower slide-body relief with distance from the shore towards the center of the lake (Fig.8). The detachment surface at the base of the slide appears to lie around 12 m below the sediment-water interface. Strata above this surface are cut by listric normal faults, indicating extension and lateral spreading during sliding (Fig. 7). In the transverse profiles this level marks a transition from flat to convex-upward reflectors (Fig.8). The continuity of acoustic layering in internal parts of the slide indicates basinward movement of a relatively coherent block of sediment. Flanking the slide deposit, however, is an acoustically chaotic – to – transparent lens of sediment up to 4 m thick. It is likely that this body is a mass flow deposit that has undergone a higher degree of disintegration than the large slide and has ponded in the confined area adjacent to the slide body. The draping of the slide and adjacent mass flow deposit by the relatively undisturbed strata of Seismic Facies A indicates that movement occurred just prior to accumulation of that facies. In several places, however, Seismic Facies A shows flexure above the listric faults within the slide, suggesting small-scale, ongoing movement (Fig.7). In a few places the faults extend to the lake bed.

Discussion & Initial Conclusions

The present study is the first to examine the long-term sedimentary record of Lake Quinault, including the potential impacts of past earthquakes on the lake and its catchment. Chirp seismic profiles provide the broadest spatial and temporal overview of the lake's stratigraphy, but they are unfortunately limited to its distal side by gas blanking of the acoustic signal. Gas blanking is commonly observed near sites of fluvial sediment input to lakes where rates of organic carbon burial are high (e.g. Chapron et al., 2004; Duck and Herbert, 2006; Cukur et al., 2013), and the fact that seismic stratigraphy is only apparent on the distal side of Lake Quinault may similarly reflect that phenomenon. On many of the Lake Quinault chirp profiles, however, the abrupt transition from acoustic blanking to acoustic penetration depths of 15 m or more coincides with evidence for fracturing and faulting, suggesting that deformation may have facilitated localized degassing of the lake bed. Disturbance of sediments during an event sometime between 1450-1650 cal yr BP apparently allowed gas to escape from sediments on the slopes, as revealed by common gas chimneys in the seismic profiles. Given the widespread

distribution of evidence for this disturbance in separated coves across the entire SW side of the lake, a large earthquake is the most likely trigger. The chirp profiles indicate that comparable disturbance on these slopes has not occurred since and has been rare in the past. Based on estimated rates of sediment accumulation for the lower part of core 2, for example, the age of the earlier prominent mass wasting deposit buried about 6 m beneath the lake surface in Hatchery Bay (Fig. 9) is thousands of years older.

The lack of significant disruption of sediments on the SW side of Lake Quinault in the past 1450-1650 years is surprising given its location in a region where large earthquakes are known to occur on the subduction interface at roughly 500 year frequency. These events have been shown to have caused co-seismic subsidence and tsunami deposition at nearby coastal lowlands in AD 1700 (250 cal yr BP), 700-1100 cal yr BP, and c. 1350 cal yr BP (Atwater and Hemphill-Haley, 1997; Nelson et al., 2006). What was the nature of the 1450-1650 cal yr BP event and why did it cause widespread mass wasting on the SW margin of Lake Quinault when subsequent regional subduction zone earthquakes apparently did not? One possibility is that the deformation event at Lake Quinault was not related to an earthquake generated at the subduction interface but instead was triggered on a nearby, upper crustal fault. The Canyon River fault, 30 km SE from Lake Quinault, is estimated to have produced a surface-rupturing earthquake of magnitude 6.8 to 7.5, and charcoal from an offset buried soil horizon recovered in a fault scarp trench across the this fault returned a calibrated limiting maximum rupture age of 1830-1600 cal yr BP (Walsh and Logan, 2007a, b). It is possible that seismic ground accelerations at Lake Quinault were greater during this shallow, local hypocenter event than during subduction earthquakes whose predicted down-dip limit lies >40 km to the west of the lake.

An alternative possibility is that the mass wasting event ca. 1450-1650 cal yr BP was in fact triggered by a great subduction earthquake during which shaking was particularly strong at Lake Quinault and/or site conditions rendered the sediments on the lake's SW margin particularly prone to failure during this event. Evidence for a Cascadia earthquake around 1600 cal yr BP recognized at the Copalis River estuary (the "S" event; Atwater 1992, Atwater and Hemphill-Haley, 1997) has been correlated to coastal, fjord, and deep sea sites across the entire Cascadia margin (Goldfinger et al., 2012, Enkin et al., 2013). Nelson et al. (2006) summarized evidence for coastal subsidence and tsunamis during this event at eight coastal sites from British Columbia to northern California, suggesting rupture over much of the plate boundary and generation of a magnitude 9 earthquake. They noted that the highest tsunamis recorded in the past 2000 years at Bradley Lake, Oregon and Lagoon Creek, northern California occurred around this time. They also noted that the ca. 1600 cal yr BP earthquake followed the longest interseismic interval (800-1130 yr) of the past 5000 years (Atwater and Hemphill-Haley, 1997; Goldfinger et al., 2012). In Effingham Inlet in British Columbia, where an 11,000-year-long record includes twenty-one "seismite" layers generated by earthquake-triggered mass wasting on steep fjord walls, the roughly 1600 cal yr BP E4 layer is the thickest seismite deposited in the past 3000 years, exclusive of one attributed to the M7.2, 1946 AD crustal earthquake centered 60 km from the inlet (Enkin et al., 2013). Enkin et al. (2013) noted that the thickness of such layers in Effingham Inlet might reflect a variety of

factors, including the magnitude and quality of seismically induced ground shaking, and the volume of sediment built up in the local environment between shaking events. In Lake Quinault, it is possible that the long period of apparent seismic quiescence along the Cascadia subduction interface prior to the ca. 1600 cal yr BP event allowed the accumulation of not only a relatively thick layer of undisturbed sediment, but also of interstitial biogenic gas on the lake's SW slopes, making them especially prone to failure.

Evidence for the impacts of other earthquakes at Lake Quinault is less certain, in part because the seismic reflection survey was unable to image the stratigraphy of a large portion of the lake. Although we have no direct evidence for slope failures on the more proximal lake margins, the sandy turbidite and mass flow deposit at sites 3 and 5 are interpreted as recording a delta-front failure that was unique in the past 500 years. Although delta front failures can occur in lakes in the absence of earthquakes (e.g., Girardclos et al., 2007), the timing of this event brackets that of the well-documented AD 1700 Cascadia megathrust event (Satake et al., 1996; Yamaguchi et al., 1997; Jacoby et al., 1997), and as such seems to be more than fortuitous.

There is independent evidence, moreover, of the impact of this earthquake on the upper Quinault River catchment. Limited radiocarbon dating of alluvial deposits 10 to 20 km up valley from the lake is suggestive of forced sediment aggradation in the valley bottom around AD 1700. The deposits of a 5-m high alluvial terrace are exposed in a cut bank of the Quinault River across from the Graves Creek confluence where buried conifer tree stumps in growth position are observable as they erode out of the terrace riser (Fig. 10). This "event terrace" is a mappable landform that exists on both sides of the Quinault River for at least one km downstream from the Graves Creek confluence. The presence of numerous buried trees in growth position that are now exposed in a cut bank of the river argues for a relatively short period of rapid sediment accumulation. The valley topography upstream from this event terrace is suggestive of a large valley-blocking landslide, which is coincident with the only prominent convexity (increase in stream gradient) in the longitudinal profile of the Quinault River from the Pacific Ocean to the top of the catchment. A possible spillway channel across the landslide deposit is observable in the field and on the 1:24,000-scale topographic map as a now dry, amphitheater-headed valley (Fig 10). The outermost growth ring beneath bark from one of the buried tree stumps in the event terrace deposit returned an age of 219 ± 27 ^{14}C ybp, which when calibrated (1760 ± 90 calAD) brackets the AD 1700 subduction zone earthquake. Dendrochronology on both the buried stumps as well as the living trees growing on the tread of the event terrace is needed to narrow the range provided by the radiocarbon age determination for this terrace.

Valley-bottom geomorphic mapping by the U.S. Bureau of Reclamation (Bounty et al. 2005) identified three prominent mid-to-late Holocene alluvial terrace surfaces between Lake Quinault and the confluence of the North Fork and Quinault Rivers. Their intermediate level terrace returned an age from detrital conifer charcoal of 1560 ± 40 ^{14}C ybp (1460 ± 50 calBP), which overlaps with the timing of paleoseismic sediment disruption in Lake Quinault and the Cascadia Subduction Zone "S" event of Atwater and Hemphill-Haley (1997). Similarly, the lowest (youngest) terraces identified by Bounty et

al. (2005) was dated by detrital *Populus* charcoal to 270 ± 40 ^{14}C ybp (1610 ± 90 calAD), which is slightly older than the AD 1700 subduction zone earthquake, but that would be expected for charcoal present in the fluvial system at the time of the earthquake. Collectively, these fluvial deposits and associated geochronology are suggestive, although not definitive, of intervals of forced aggradation in the Quinault River system, perhaps in response to short-lived (years to decades) increases in hillslope sediment delivery to the fluvial system via earthquake-triggered mass wasting in the catchment.

Transitioning back to the lake, a number of observations from the cores are consistent with the hypothesis that the delta-slope failure occurred in response to an event c. 1700 AD that also impacted the fluvial system. Evidence for a temporary reduction in rates of sediment accumulation on the prodelta slope and in the lake center immediately after the event may indicate initial stemming of river discharge and reduced fluvial sediment transport by impoundment behind landslide or large tributary debris flow dams. Based on average accumulation rates, the bioturbated interval in core 3 that overlies the thick turbidite/mass flow deposit and the correlative fine-grained, thinly bedded interval in core 7 (Fig. 11) are estimated to record a few decades of sediment accumulation at most. In both cores, flood layers are increasingly common above these intervals (e.g., Fig. 12), suggesting a return to more typical conditions, and perhaps step-wise delta progradation after this pause. Age-depth models for both cores 7 and 2 (Fig. 13) indicate that accumulation rates increased sometime after about 200-300 cal yr BP, but the data do not allow us to say whether this occurred in response to the 1700 AD earthquake or was perhaps related to later, anthropogenic impacts within the catchment above the lake. The floodplain of the upper Quinault River, between the lake and the confluence of the main stem with the North Fork Quinault River, was logged in the early 1900's, and the source for large woody debris was reduced. These activities may have led to increased bank erosion (Bountry et al., 2005) and could account for some or all of the increased sediment accumulation rates observed in the lake during the past century. On the other hand, increased accumulation rates in the past ca. 300 years may at least partially reflect drainage of impoundments and flushing of sediment delivered from hillslopes to the fluvial network by earthquake-triggered landslides. Future acquisition of additional radiocarbon dates from both aggradational Holocene river terraces in the catchment and lake sediment cores paired with the acquisition of ^{10}Be/^{26}Al ratios recovered from sandy intervals below and above the putative AD 1700 event layer in Core 7 will help in testing these hypotheses.

Subtle features of the 5000-year long record from the distal side of the lake suggest the possibility that not only the AD 1700 (250 calBP), but also earlier earthquakes have modulated sediment supply and delta progradation in Lake Quinault. It is evident that relatively few turbidity currents have been strong enough to carry enough sediment to the distal side of the lake to generate graded layers in excess of a few centimeters thickness. The putative AD 1997 flood layer (RI = 33 years), for example, thins from a maximum of 18 cm at site 3 to only 3 cm at site 2 (Fig. 14). The 5 to 7 cm-thick layers that that are preserved at greater depth in the lakebed at sites 1 and 2, which accumulated when the river delta was farther to the east than its present location, must represent events that generated substantially higher sediment concentrations than the 1997 event. The

clustering of these thicker beds into groups of 4 to 5 layers that generally thin and fine upward is intriguing, as is their apparent relationship to levels of overall stepwise coarsening observed in the distal (western) cores. The fine clay drapes that are best developed on the lowermost and thickest bed in each cluster indicate that the individual beds were not the products of pulsation of one turbidity current. Instead, the slow settling velocity of this fine material requires that each bed was deposited during a separate event followed by a period of quiescence. These characteristics suggest that each cluster represents a protracted response of the sedimentary system to an episode of sediment input, perhaps triggered by widespread landsliding in the upper Quinault River catchment, where seismic energy may have been amplified by mountainous topography in the months to years following the event (e.g., Meunier et al., 2008; Buech et al., 2010; Marc et al., 2015). Observations made in the aftermath of recent earthquakes in mountainous regions of Taiwan and China indicate that impacted fluvial systems may show decadal responses as sediment introduced by mass wasting to the channel network is mobilized and flushed from the system during periods of high flow (e.g. Dadson et al., 2004; Hovius et al., 2011, Wang et al., 2015) and clusters of turbidites in other lakes have similarly been interpreted to record the post-earthquake response of catchments (Chapron et al., 2007; Howarth et al., 2012). Aside from the turbidite cluster that coincides with the top of Seismic Facies B, presently available data from Lake Quinault do not allow us to ascertain whether or not pulsed sediment supply evinced by clusters of turbidites at other levels in cores 1 and 2 were the result earthquakes, or alternatively of large atmospheric-driven river discharge events. The timing of their deposition, at around 250, 700, 1550, and 2600 cal yr BP, however, does seem consistent with the ages of great Cascadia subduction earthquakes inferred from other sites; suggesting a causal link (Fig. 15). Future studies at Lake Quinault, aimed at bathymetric mapping and dating mass wasting features along the lake margins and at sampling a longer stratigraphic record from the lake's center, may serve to test this hypothesis.

References:

Adams, J., 1990, Paleoseismicity of the Cascadia subduction zone: Evidence from turbidites off the Oregon-Washington margin: Tectonics, v. 9, p. 569-583.

Atwater, B.F., 1987, Evidence for great Holocene earthquakes along the outer coast of Washington State: Science 236, 942-944.

Atwater, B. F., and Moore, A. L., 1992, A tsunami about 1000 years ago in Puget Sound, Washington: Science, v. 258, no. 5088, p. 1614-1617.

Atwater, B.F., and Hemphill-Haley, E., 1997, Recurrence intervals for great earthquakes of the past 3500 years in northeastern Willapa Bay, Washington: U.S. Geological Survey Professional Paper 1576, 108 p.

Blaauw, M., and Christen, J., 2011, Flexible paleoclimate age-depth models using an autoregressive gamma process: Bayesian Analysis 6, 457-474.

Blais-Stevens, A., Rogers, G.C., and Clague, J.J., 2011, A revised earthquake chronology for the last 4,000 years inferred from varve-bounded debris-flow deposits beneath an inlet near Victoria, British Columbia: Bulletin of the Seismological Society of America, v. 101, p. 1-12.

Bountry, J.A., Randle, T.J., Piety, L.A., Lyon, E.W., Jr., Abbe, T., Barton, C., Ward, G., Fetherston, K., Armstrong, B. and Gilbertson, L. (2005) Geomorphic Investigation of Quinault River, Washington: 18 Km Reach of Quinault River Upstream from Lake Quinault, pp. 175. U.S. Department of the Interior, Bureau of Reclamation, Denver.

Buech, F., Davies, T.R., and Pettinga, J.R., 2010, The Little Red Hill seismic experimental study: topographic effects on ground motion at a bedrock-dominated mountain edifice: Bulletin of the Seismological Society of America 100, 2219-2229.

Cathles, L.M., Su, Z., and Chen, D., 2010, The physics of gas chimney and pockmark formation, with implications for the assessment of seafloor hazards and gas sequestration: Marine and Petroleum Geology 27, 82-91.

Chapron, E., Beck, C., Pourchet, M., and Deconink, J.F., 1999, 1822 earthquake-triggered homogenite in Lake Le Bourget (NW Alps): Terra Nova 11, 86-92

Chapron, E., Van Rensbergen, P., De Batist, M., Beck, C., and Henriet, J.P., 2004, Fluid-escape features as a precursor of a large sublacustrine sediment slide in Lake Le Bourget, NW Alps, France: Terra Nova 16, 305-311.

Chapron, E., Juvigne, E., Muslow, S., Ariztegui, A., Magand, O., Bertrand, S., Pino, M., and Chapron, O., 2007, Recent clastic sedimentation processes in Lake Puyehue (Chilean Lake District, 40.5oS): Sedimentary Geology 201, 365-385.

Cukur, D., Krastel, S., Tomonaga, Y., Cagatay, N.M., Meydan, A.F., and the PaleoVan Science Team, 2013, Seismic evidence of shallow gas from Lake Van, eastern Turkey: Marine and Petroleum Geology 48, 341-352.

Dadson, S.J., Hovius, N., Chen, H., Dade, W.B., Lin, J.-C., Hsu, M.-L., Lin, C.-W., Horng, M.-J., Chen, T.-C., and Milliman, J., 2004, Earthquake-triggered increase in sediment delivery from an active mountain belt: Geology, v. 32, p. 733-736.

DeMets, C., and Dixon, T., 1999, New kinematic models for Pacific-North America motion from 3 Ma to present: I, Evidence for steady motion and biases in the NUVEL-1A model: Geophysical Journal International, v. 101, p. 425-478.

Bottjer, D.J., and Droser, M.L., 1991, Ichnofabric and basin analysis: Palaios, v. 6, no. 3, p. 199-205.

Duck, R.W., and Herbert, R.A., 2006, High-resolution shallow seismic identification of gas escape features in the sediments of Loch Tay, Scotland: tectonic and microbiological associations: Sedimentology 53, 481-493.

Enkin, R.J., Dallimore, A., Baker, J., Southon, J.R., and Ivanochko, T., 2013, A new high-resolution radiocarbon Bayesian age model of the Holocene and Late Pleistocene from core MD02-2494 and others, Effingham Inlet, British Columbia, Canada; with an application to the paleoseismic event chronology of the Cascadia Subduction Zone1: Canadian Journal of Earth Sciences, v. 50, p. 746-760.

Gavin, D.G., and Brubaker, L.B., 2015, Late Pleistocene and Holocene Environmental Change on the Olympic Peninsula, Washington, Ecological Studies 222, Springer, Switzerland, 142 pp.

Girardclos, S., Schmidt, O.T., Sturm, M., Ariztegui, D., Pugin, A., and Anselmetti, F.S., 2007, The 1996 AD delta collapse and large turbidite in Lake Brienz: Marine Geology 231, 137-154.

Goldfinger, C., 2011, Submarine paleoseismology based on turbidite records: Annual Review of Marine Science 3, 35-66.

Goldfinger, C., Nelson, C.H., Morey, A., Johnson, J.E., Guterrrez-Pastor, J., et al., 2012, Turbidite event history: Methods and implications for Holocene paleoseismicity of the Cascadia Subduction Zone: USGS Professional Pape 1661-F, U.S. Geological Survey, Reston, 170 pp.

Hilbe, M., and Anselmetti, F.S., 2014, Signatures of slope failures and river-delta collapses in a perialpine lake (Lake Lucerne, Switzerland): Sedimentology 61, 1883-1907.

Hovius, N., Meunier, P., Lin, C.W., Hongey, C., Chen, Y.G., Dadson, S., Horng, M.J., and Lines, M., 2011, Prolonged seismically induced erosion and the mass balance of a large earthquake: Earth and Planetary Science Letters 304, 347-355.

Hovland, M., and Judd, A.G., 1988, Seabed Pockmarks and Seepages: Impacts of Geology, Biology, and the Marine Environment: Granham & Trotman Ltd., London, UK, 293 pp.

Howarth, J.D., Fitzsimons, S.J., Norris, R.J., and Jacobsen, G.E., 2012, Lake sediments record cycles of sediment flux driven by large earthquakes on the Alpine fault, New Zealand: Geology 40, 1091-1094.

Hua, Q, Barbetti, M., and Rakowski, A.Z., 2013, Atmospheric radiocarbon for the period 1950-2010: Radiocarbon 55, 2059-2072.

Jacoby, G.C., Bunker, D.E. and Benson, B.E. (1997) Tree-ring evidence for an AD 1700 Cascadia earthquake in Washington and northern Oregon. Geology, 25, 999-1002.

Keefer, D.K., 1984, Landslides caused by earthquakes: Geological Society of America Bulletin, v. 95, p. 406-421.

Keefer, D.K., 2002, Investigating landslides caused by earthquakes–a historical review: Surveys in geophysics, v. 23, p. 473-510.

Kelsey, H.M., Nelson, A.R., Hemphill-Haley, 2005, Tsunami history of an Oregon coastal lake reveals a 4600 yr record of great earthquakes on the Cascadia subduction zone: Geological Society of America Bulletin 117, 1009-1032.

Kremer, K., Hilbe, M., Simpson, G., Decrouy, L., Wildi, W., and Girardclos, S., 2015, Reconstructing 4000 years of mass movement and tsunami history in a deep peri-Alpine lake (Lake Geneva, France-Switzerland): Sedimentology.

Leithold, E.L., Wegmann, K.W., Bohnenstiehl, D.R., Smith, S.G., Noren, A., and O'Grady, R., submitted, Lacustrine paleoseismology above the Cascadia Subduction zone from Lake Quinault, Washington: Journal of Sedimentology.

Loseth, H., Gading, M., and Wensaas, L., 2009, Hydrocarbon leakage interpreted on seismic data: Marine and Petroleum Geology 26, 1304-1319.

Marc, O., Hovius, N., Meunier, P., Uchida, T., and Hayashi, S., 2015, Transient changes of landslide rates after earthquakes: Geology, doi:10.1130/G36961.1

Meunier, P., Hovius, N., and Haines, J.A., 2008, Topographic site effects and the location of earthquake induced landslides: Earth and Planetary Science Letters 275, 221-232.

Moernaut, J., De Baptist, M., Charlet, F., Heirman, K., Chapron, E., Pino, M., Brummer, R., and Urrutia, R., 2007, Giant earthquakes in South-Central Chile revealed by Holocene mass-wasting events in Lake Puyehue: Sedimentary Geology 195, 239-256.

Nelson, A.R., Kelsey, H.M., and Witter, R.C., 2006, Great earthquakes of variable magnitude at the Cascadia subduction zone: Quaternary Research, v. 65, p. 354-365.

Parker, R.N., Densmore, A.L., Rosser, N.J., de Michele, M., Li, Y., Huang, R., Whadcoat, S., and Petley, D.N., 2011, Mass wasting triggered by the 2008 Wenchuan earthquake is greater than orogenic growth: Nature Geosci, v. 4, p. 449-452.

Reimer, P.J., Bard, E., Bayliss, A., Beck, J.W., Blackwell, P.G., Bronk Ramsey, C., Buck, C.E., Cheng, H., Edwards, R.L., and Friedrich, M., 2013, IntCal13 and Marine13 radiocarbon age calibration curves 0-50,000 years cal BP: Radiocarbon, v. 55, p. 1869-1887.

Ritchie, A., and Bourgeois, J., 2010, Late Quaternary sediment source and deposition history of Lake Ozette, Report to Olympic National Park: Seattle, University of Washington - Department of Earth and Space Sciences, p. 103.

Satake, K., Shimzzaki, K., Tsuji, Y., and Ueda, K., 1996, Time and size of a giant earthquake in Cascadia inferred from Japanese tsunami records of January 1700: Nature 379: 246-249.

Schnellmann, M., Anselmetti, F.S., Gardini, D., and McKenzie, J., 2005, Mass movement-induced fold-and-thrust belt structures in unconsolidated sediments in Lake Lucerne (Switzerland): Sedimentology 52, 271-289.

Schnellman, M., Anselmetti, F.S., Giardini, D., and McKenzie, J.A., 2006, 15,000 years of mass-movement history in Lake Lucerne: Implications for seismic and tsunami hazards: Eclogae geol. Helv. 99, 409-428.

Siegenthaler, C., Finger, W., Kelts, K., and Wang, S., 1987, Earthquake and seiche deposits in Lake Lucerne, Switzerland: Ecologae Geologicae Helvetiae 8-, 241-260.

Simonneau, A., Chapron, E., Vanniere, B., Wirth, S.B., Gilli, A., Di Giovanni, C., Anselmetti, F.S., Desmet, M., and Magny, M., 2013, Mass movement and flood-induced deposits in Lake Ledro, southern Alps, Italy: implications for Holocene paleohydrology and natural hazards: Climate of the Past 9, 825-840.

Strasser, M., Monecke, K., Schnellman, M., and Anselmetti, F.S., 2013, Lake sediments as natural seismographs: A compiled record of Late Quaternary earthquakes in Central Switzerland and its implication for Alpine deformation: Sedimentology 60, 319-341.

Tabor, R.W., and Cady, W.M., 1978, The structure of the Olympic Mountains, Washington—Analysis of a subduction zone: U.S. Geological Survey Professional Paper 1033, 39 p.

Tang, C., Zhu, J., Qi, X., and Ding, J., 2011, Landslides induced by the Wenchuan earthquake and the subsequent strong rainfall event: A case study in the Beichuan area of China: Engineering Geology, v. 122, p. 22-33.

Thackray, G.D., 1996, Glaciation and neotectonic deformation on the western Olympic Peninsula, Washington, Ph.D. thesis, University of Washington, Seattle, 139 pp.

Thackray, G.D., 2001, Extensive early and middle Wisconsin glaciations in the western Olympic Peninsula, Washington, and the variability of Pacific moisture delivery to the northwestern United States: Quaternary Research 55, 257-270.

U.S. Geological Survey (2015) USGS 12039500 Quinault River at Quinault Lake, WA, 2015. U.S. Department of the Interior, http://waterdata.usgs.gov/wa/nwis/uv?site_no=12039500 [accessed 08/11/2015].

Van Daele, M., Moernaut, J., Doom, L., Boes, E., Fontijn, K., Heirman, K., Vandoorne, W., Hebbeln, D., Pino, M., Urrutia, R., Brummer, R., and De Batist, M., 2015, A comparison of the sedimentary records of the 1960 and 2010 great Chilean earthquakes in 17 lakes: Implications for quantitative lacustrine paleoseismology: Sedimentology 62, 1466-1496.

Walsh, T.J., and Logan, J.B., 2007a, Field data for a trench on the Canyon River fault, southeast Olympic Moutains, Washington: Washington Division of Geology and Earth Resources Open File Report 2007-1, 1 plate [accessed Jan. 4, 2012 at http://www.dnr.wa.gov/Publications/ger_ofr2007-1_canyon_river_fault_trench.pdf].

Walsh, T.J., and Logan, R.L., 2007b, Results of trenching the Canyon River fault, southeast Olympic Mountains, Washington: Geological Society of America Abstracts with Programs, v. 39, p. 60-61.

Wang, J., Jin, Z., Hilton, R.G., Zhang, F., Densmore, A.L., Li, Gen., and West, A.J., 2015, Controls on fluvial evacuation of sediment from earthquake-triggered landslides: Geology 43, 115-118.

Wegmann, K.W., Leithold, E.L., and Bohnenstiehl, D.R., 2014, How important is seismically-induced erosion above the Cascadia subduction zone? Insights from the stratigraphy of large lakes on the Olympic Peninsula, Washington State, *in* Gillespie, A., and Montgomery, D., eds., Proceedings of the 23rd Biennial Meeting of the American Quaternary Association, Volume 23: University of Washington, Seattle, WA, American Quaternary Union, p. 35-37.

Williams, H.F., Hutchinson, I., and Nelson, A.R., 2005, Multiple sources for late-Holocene tsunamis at Discovery Bay, Washington State, USA: The Holocene, v. 15, p. 60-73.

Yamaguchi, D.K., Atwater, B.F., Bunker, D.E., Benson, B.E., and Reid, M., 1997, Tree-ring dating the 1700 Cascadia earthquake: Nature 389, 922-923.

Yanites, B.J., Tucker, G.E., Mueller, K.J., and Chen, Y.-G., 2010, How rivers react to large earthquakes: Evidence from central Taiwan: Geology, v. 38, p. 639-642.

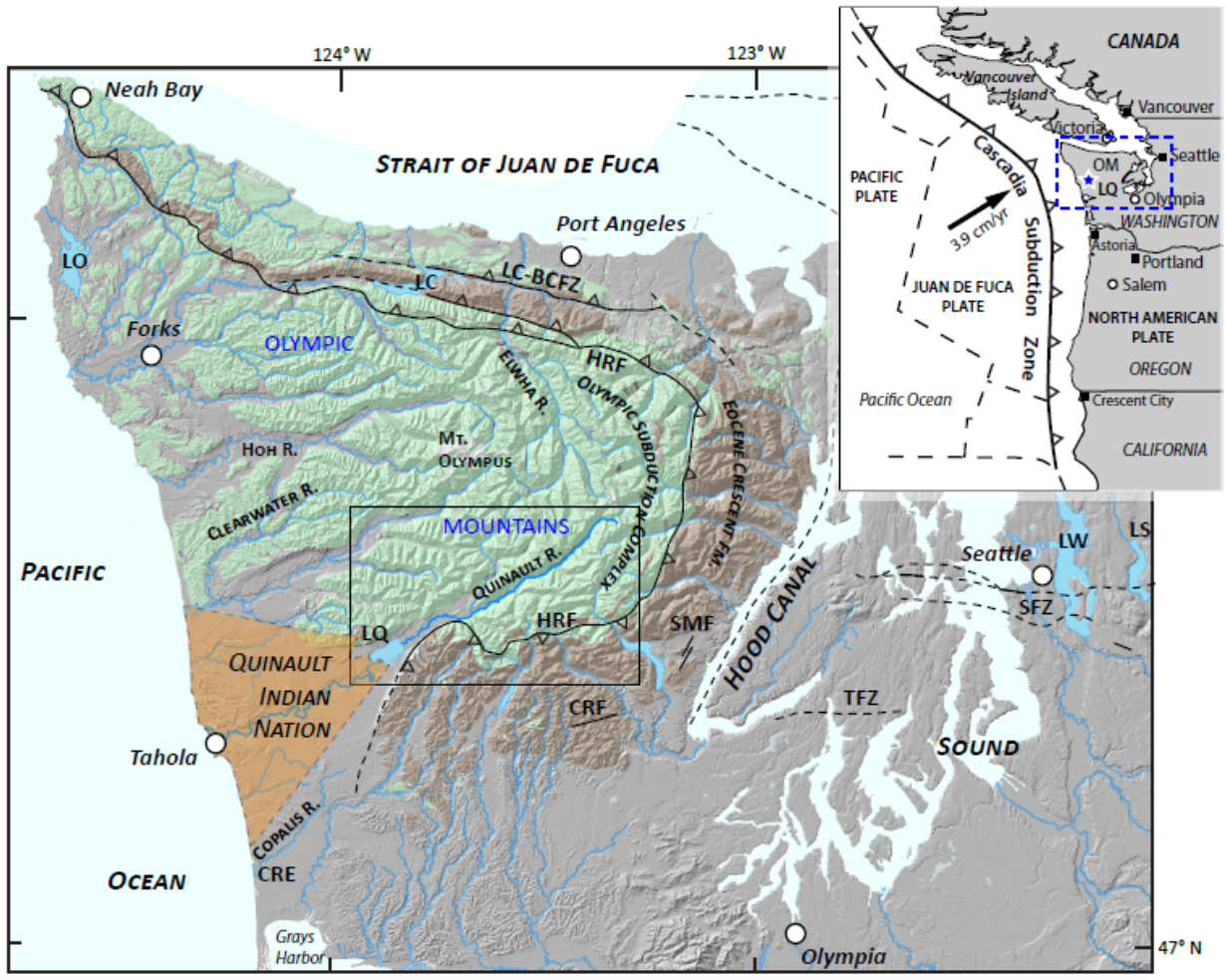

Stop 1 – Figure 1. Regional setting of Lake Quinault. ***Top Inset***: Simplified tectonic map of the Cascadia Subduction Zone, where the Juan de Fuca plate is diving beneath North America at the rate of 36 m/kyr (DeMets and Dixon, 1999). Much of this convergent plate motion is accommodated during great earthquakes, like the AD 1700 event. Lake Quinault (LQ) is located on the west side of the tectonically active Olympic Mountains. The area of the larger map is shown by the blue dashed line. ***Main map:*** Simplified tectonic and geologic map of the Olympic Peninsula. The Cascadia accretionary wedge is subaerially exposed within the Olympic Mountains as the Olympic subduction complex (OSC; Tabor and Cady, 1978). The Tertiary OSC is in thrust-fault contact with the overlying, and older volcanics of the Eocene Crescent Formation along the Hurricane Ridge Fault (HRF). 90% of the Lake Quinault catchment is underlain by the clastic sedimentary rocks of the OSC. The Seattle fault (SFZ), Tacoma fault (TFZ), Saddle Mountain fault(SMF), Canyon River fault (CRF), and Lake Creek – Boundary Creek fault (LCBCF) zones are identified. Coseismic landslides in Lakes Washington (LW) and Sammamish (LS) are attributed to both the SFZ and CSZ. Lakes Ozette (LO) and Crescent (LC) are other potential sources for lacustrine paleoseismic archives on the Olympic Peninsula (e.g., Ritchie and Bourgeois, 2010; Wegmann et al., 2014); Figure 2 area is marked by the box.

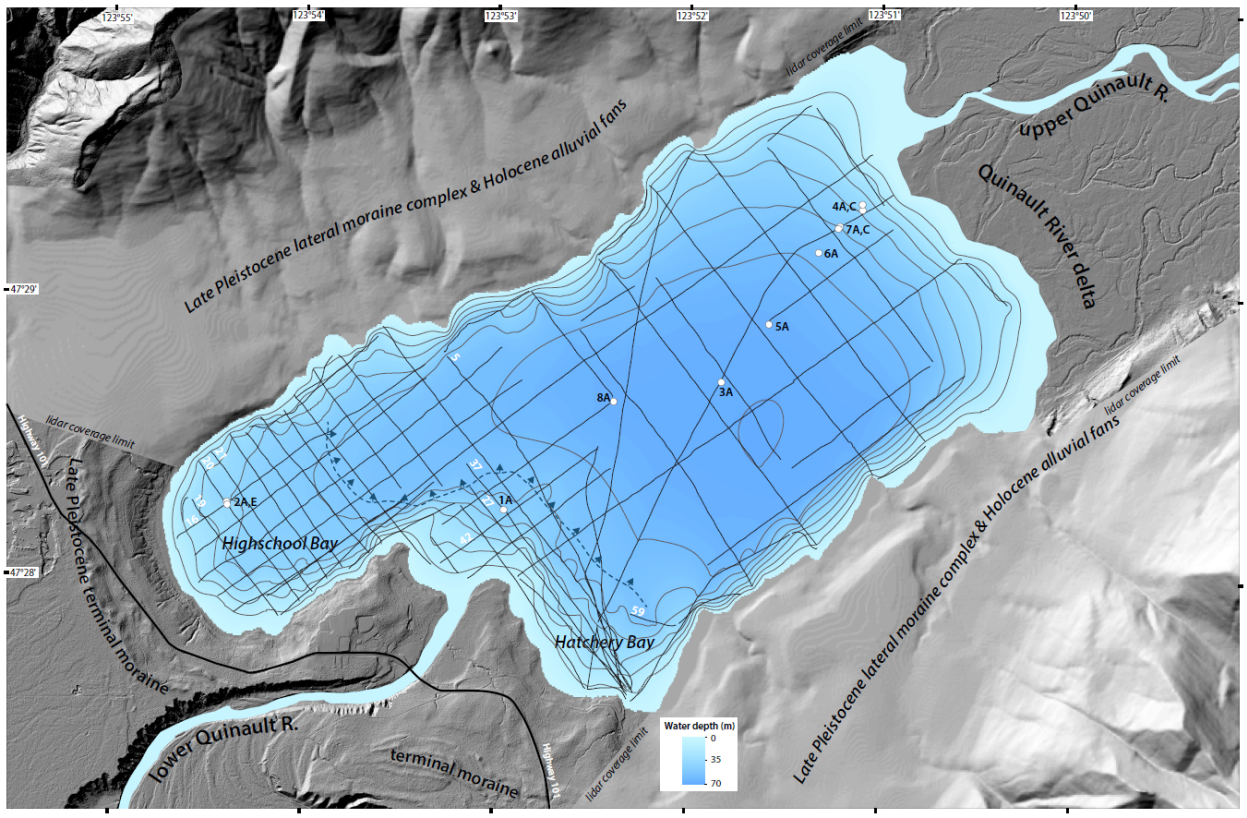

Stop 1 – Figure 2. Close-up map of Lake Quinault showing seismic tracklines, core locations, and contoured bathymetry (contour interval 10 m), along with locations discussed in the text. Also shown by the dashed lined is the approximate boundary between the area of the lake where there is acoustic penetration so that seismic stratigraphy is visible, and the area (toward which the arrows point) where there is gas blanking.

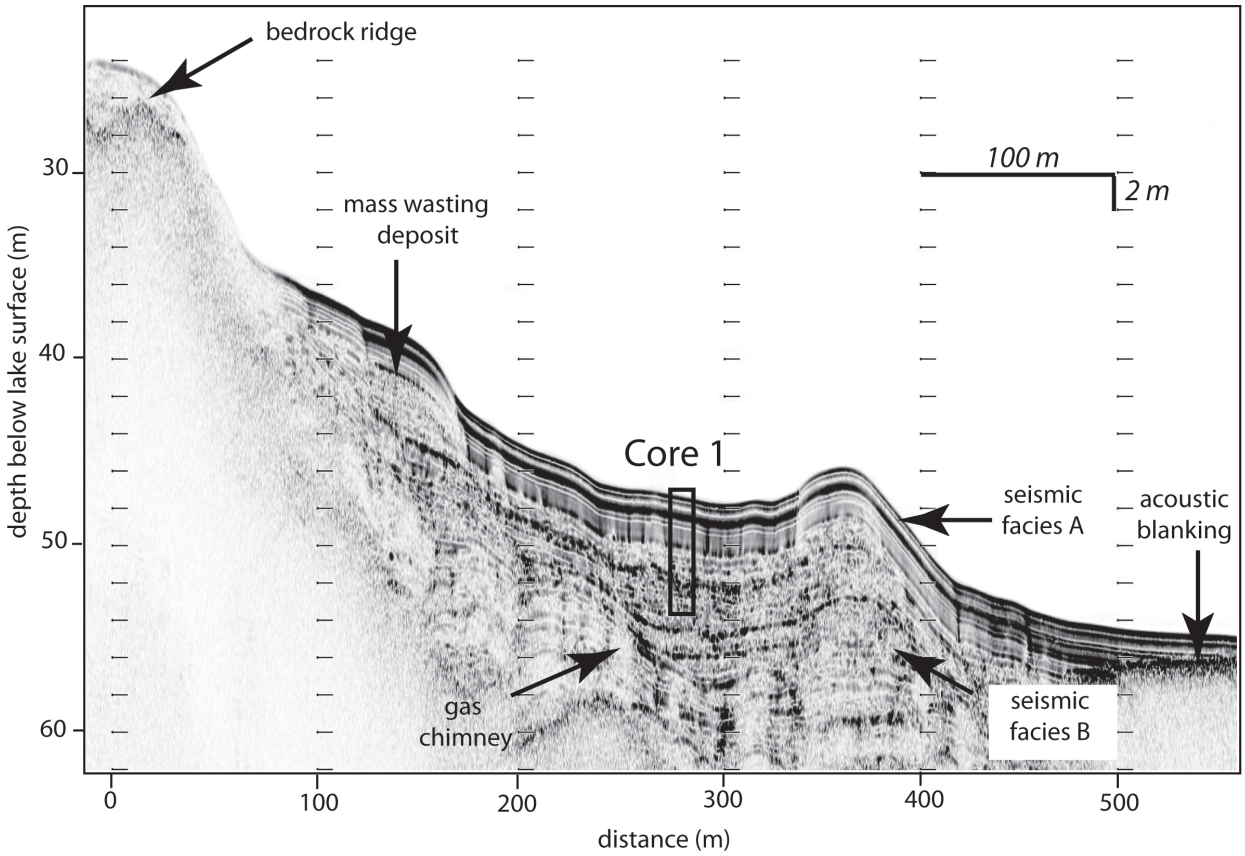

Stop 1 – Figure 3. Figure 3. Seismic profile along trackline 37, along which core 1 was collected, showing the abrupt contact between Seismic Facies A and B. Sediment depth was calculated for an acoustic velocity of 1500 m s^{-1}.

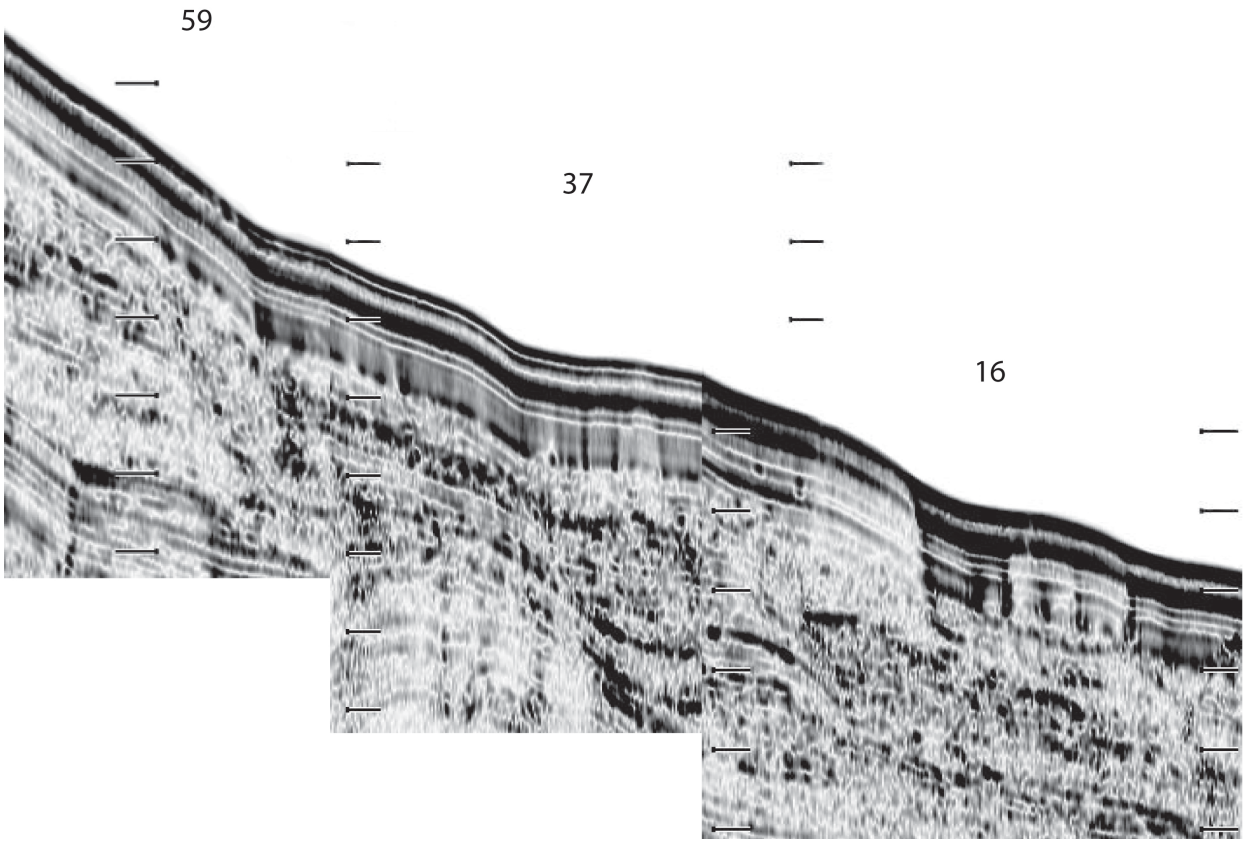

Stop 1 - Figure 4. Comparison of seismic stratigraphy at three locations along the western side of Lake Quinault, including spliced records from Hatchery Bay (trackline 59), near coring site 1 (trackline 37), and High School Bay (trackline 16). Reflectors in the acoustically well-stratified Seismic Facies A can be correlated amongst these sites, indicating uniform sediment accumulation. Tick marks denote 2 m vertical spacing in the water column and lake bed, assuming an acoustic velocity of 1500 m s^{-1}.

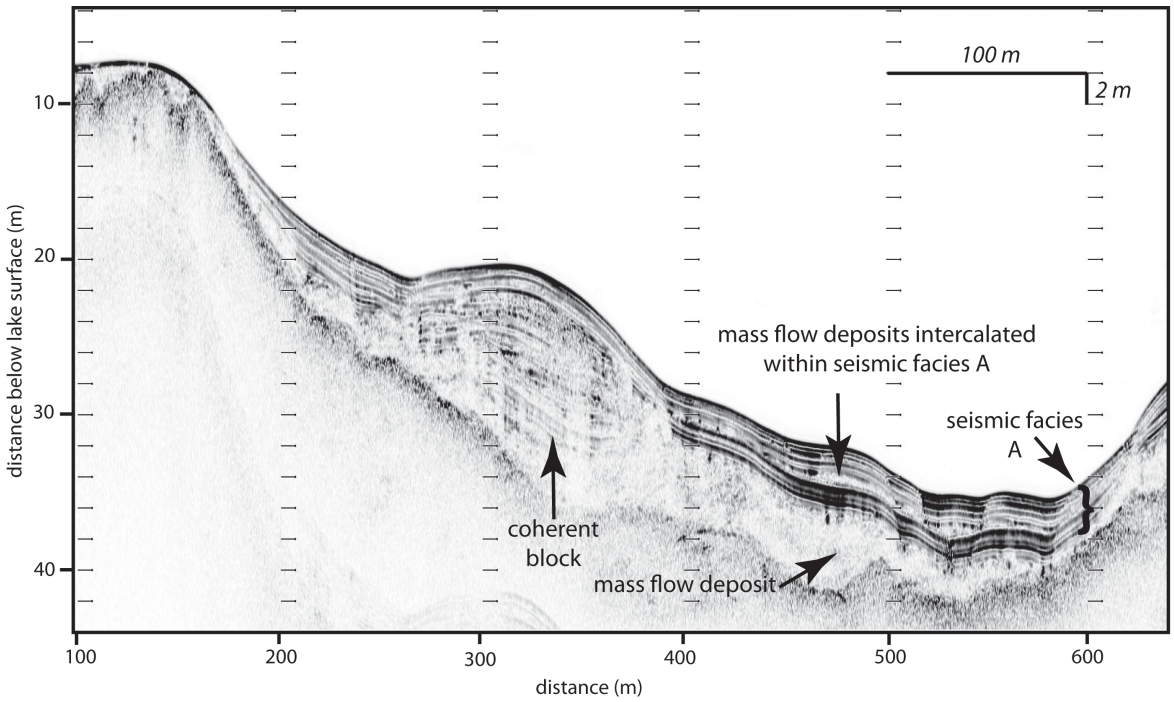

Stop 1 - Figure 5. Seismic profile along trackline 27 showing a large subaqueous slide and mass flow deposit in Hatchery Bay that is draped by the acoustically well-stratified Seismic Facies A. This profile shows a rare example of the intercalation of mass flow deposits within Seismic Facies A. Sediment depth was calculated for an acoustic velocity of 1500 m s^{-1}.

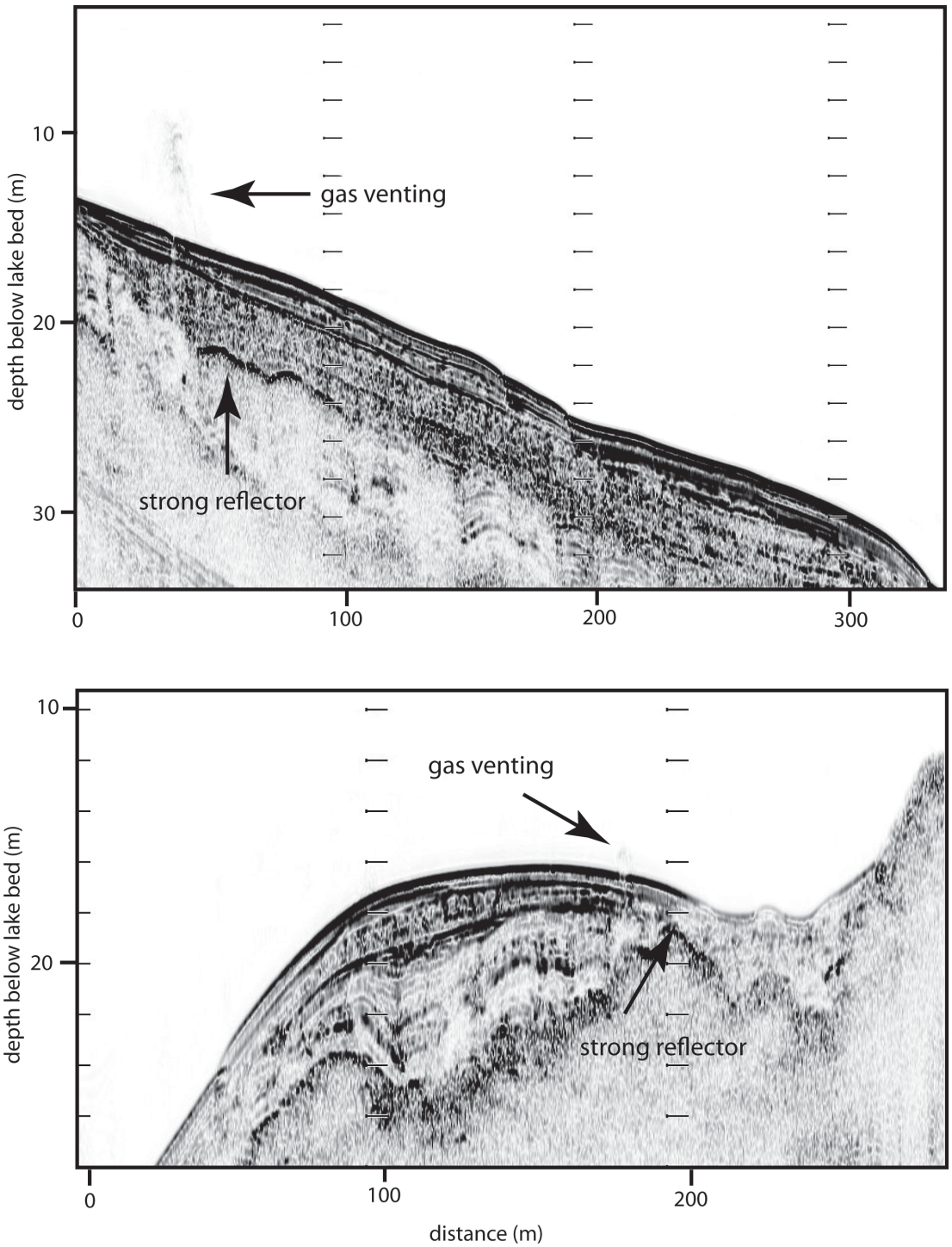

Stop 1 - Figure 6. Evidence from seismic tracklines 42 (upper) and 27 (lower) for ongoing venting of gas from Lake Quinault sediments. Note strong reflectors in the sediments beneath the vents indicating a marked contrast in acoustic impedance and suggesting the presence of free gas. Sediment depth was calculated for an acoustic velocity of 1500 m s^{-1}.

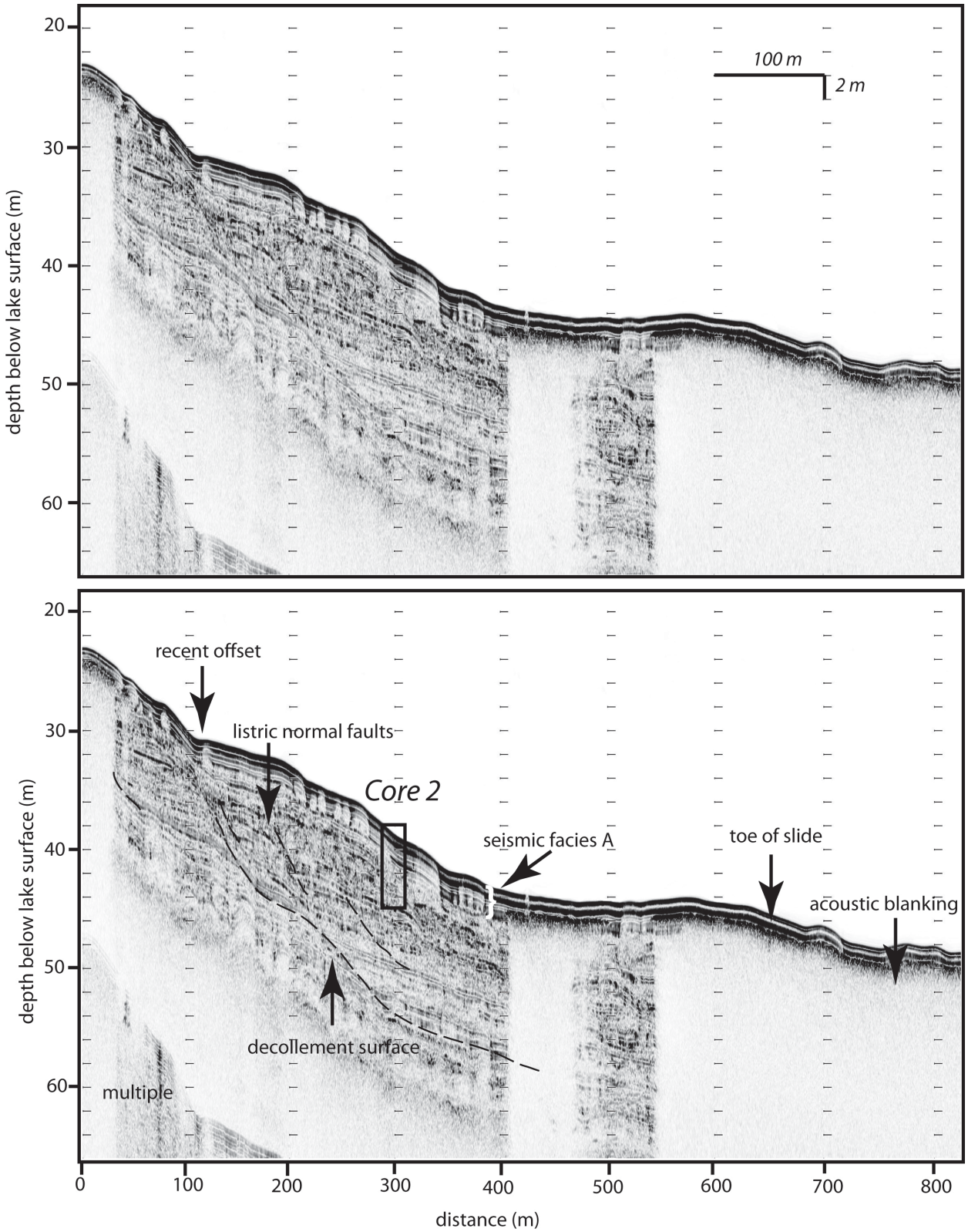

Stop 1 - Figure 7. Side and cross-sectional views of large slide in High School Bay, imaged along trackline 16. Sediment depth was calculated for an acoustic velocity of 1500 m sec^{-1}.

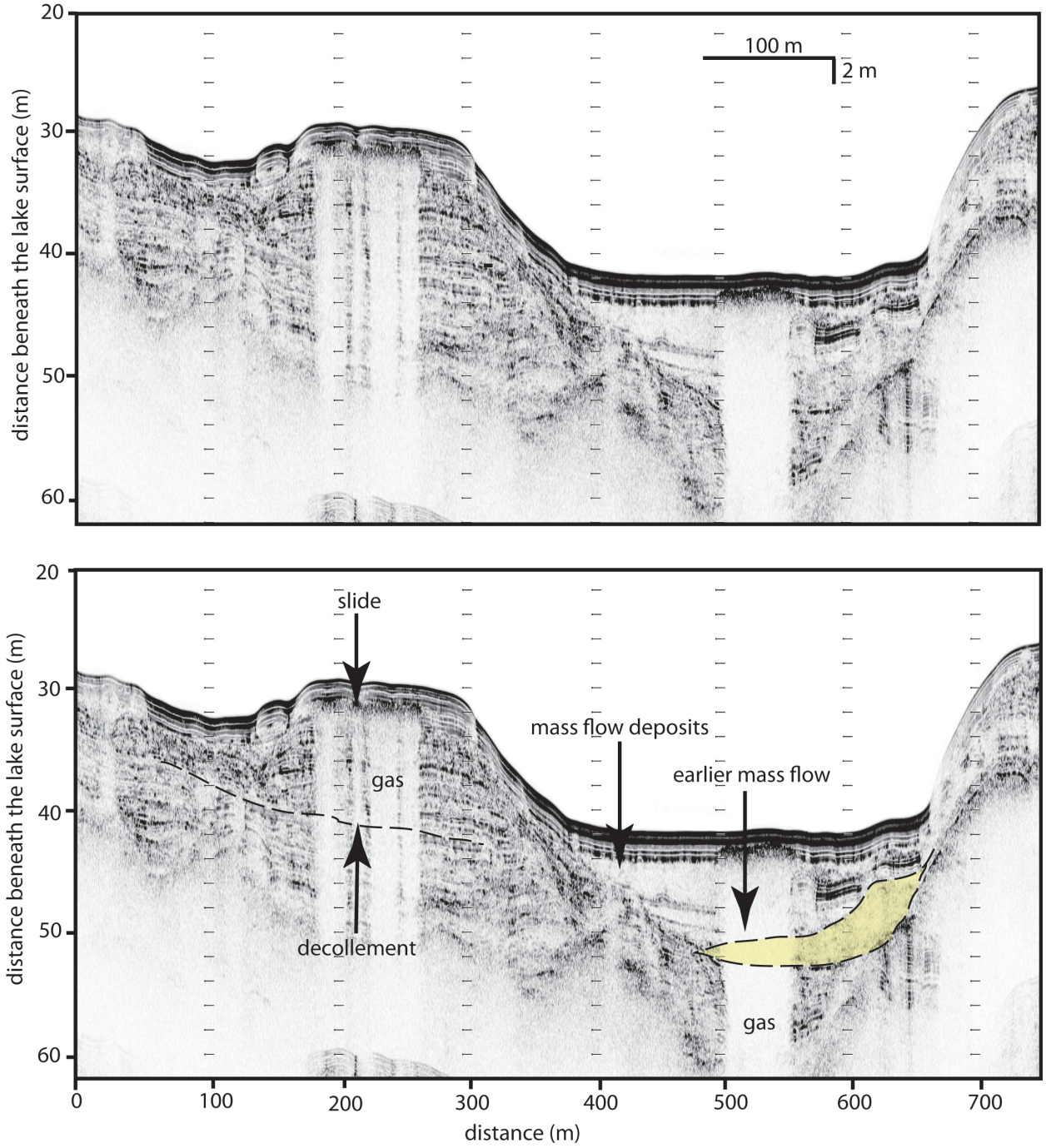

Stop 1 - Figure 8. Cross-sectional view of the slide and adjacent mass flow deposits in High School Bay, imaged along trackline 19. Sediment depth was calculated for an acoustic velocity of 1500 m sec^{-1}. An interpreted earlier mass flow deposit is denoted by the yellow shading.

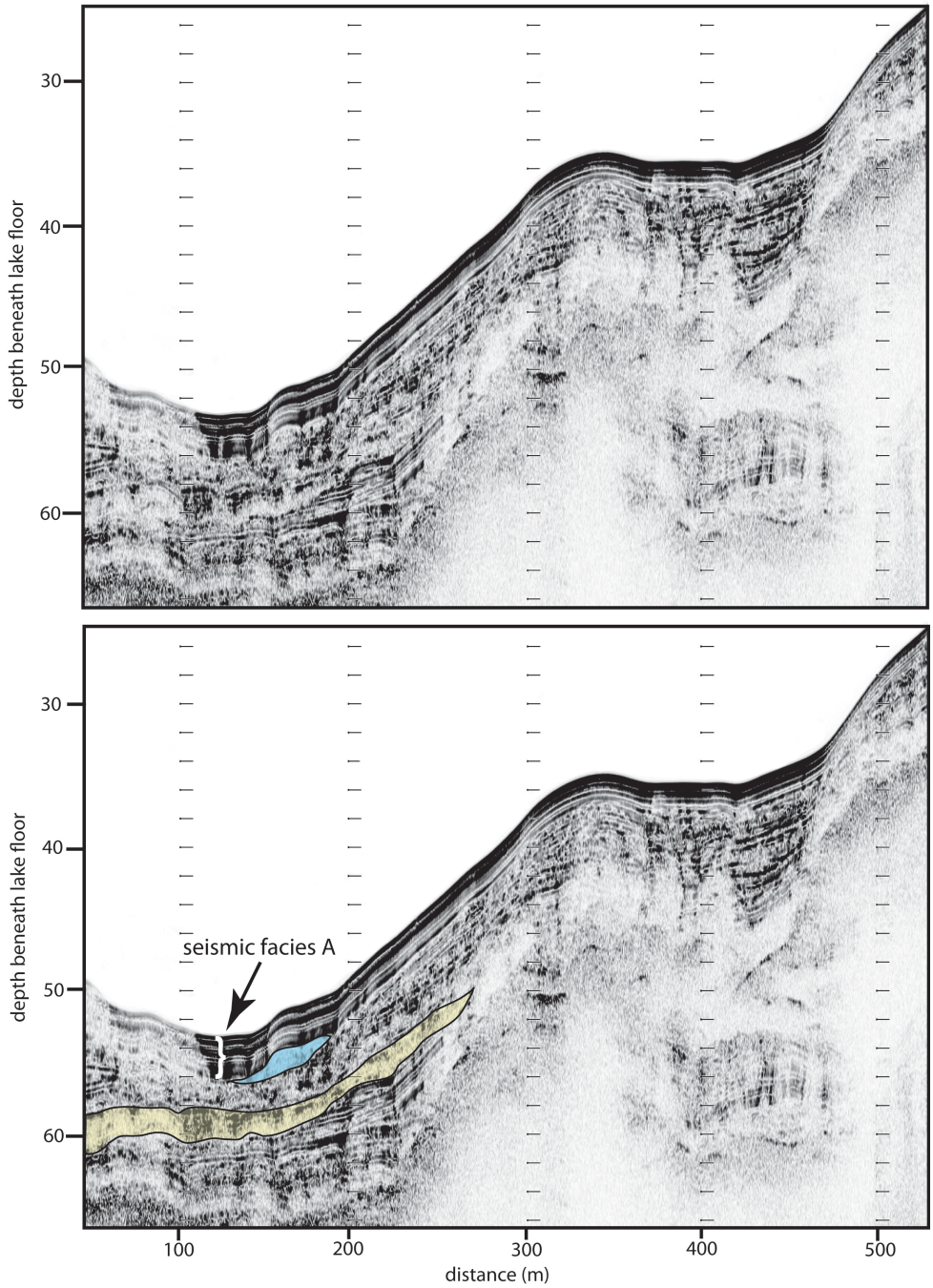

Stop 1 - Figure 9. Mass flow deposits imaged along trackline 59. Note evidence for a mass flow deposit just below seismic facies A (blue shading) as well as an earlier one (yellow shading) preserved at greater depth in the lakebed, which shows evidence for scour into and truncation of strata below. Sediment depth was calculated for an acoustic velocity of 1500 m sec^{-1}.

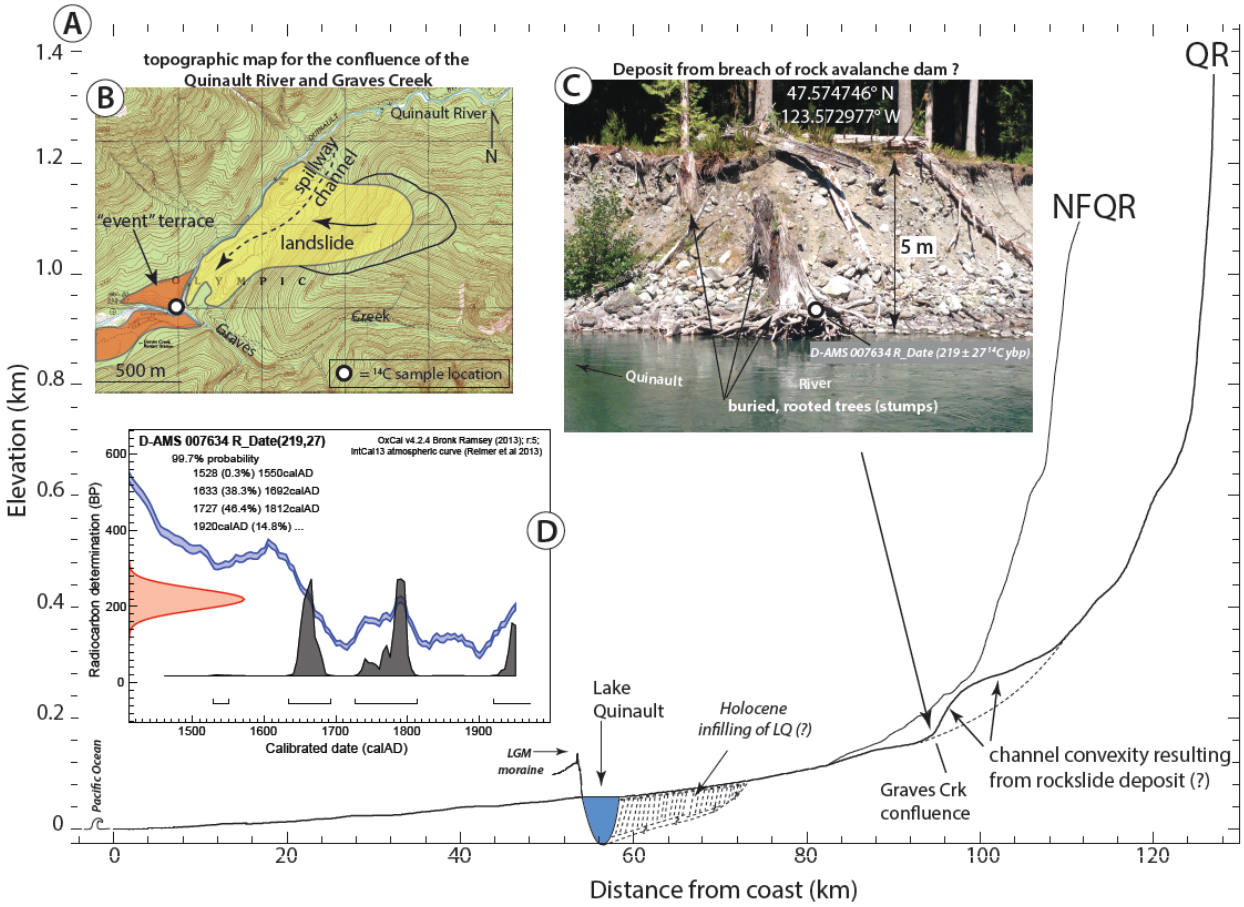

Stop 1 – Figure 10. Possible evidence for seismic triggering fluvial aggradation in the upper Quinault River catchment. **A**. Longitudinal profile of the Quinault and North Fork Quinault Rivers from the Pacific Ocean to their headwaters created from the USGS 10m digital elevation model. A pronounced convexity in the Quinault River profile is observed immediately above the Graves Creek confluence. **B.** Topographic map for the confluence of the Quinault River and Craves Creek reach. The location of an "event" terrace and possible landslide deposit are identified in the orange and yellow polygons, respectively. The photograph depicted in **C** is denoted by the white circle. **C**. Photograph of the 5m tall aggradational terrace along the river right stream bank immediately across from the Graves Creek confluence. Rooted and buried Sitka spruce tree stumps are being exposed by recent channel migration into this terrace deposit. **D**. Radiocarbon calibration for outermost tree ring recovered from beneath bark on the buried tree stump identified in panel **C**.

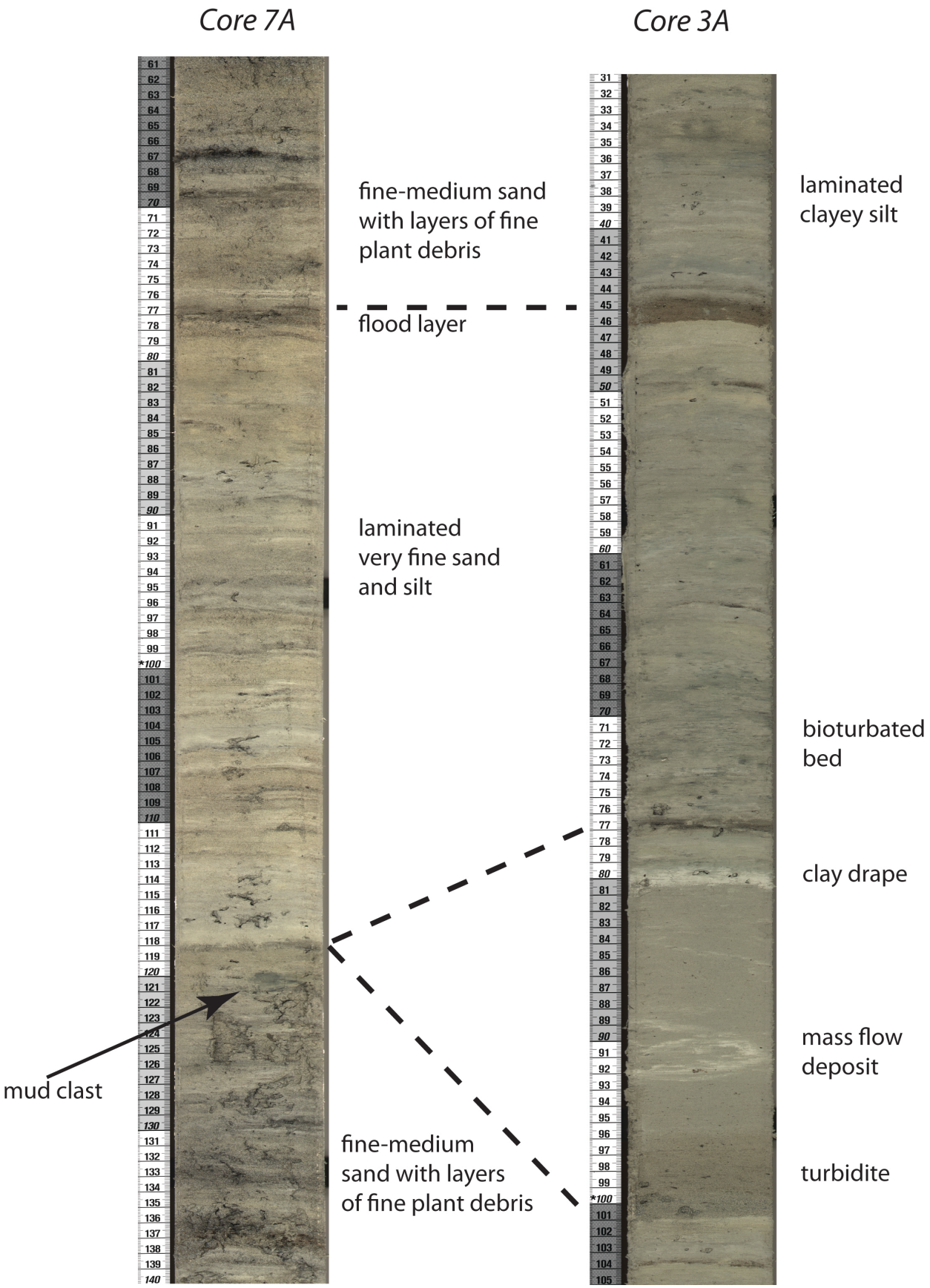
Core 7A
Core 3A
fine-medium sand with layers of fine plant debris
flood layer
laminated very fine sand and silt
mud clast
fine-medium sand with layers of fine plant debris
laminated clayey silt
bioturbated bed
clay drape
mass flow deposit
turbidite

Stop 1 – Figure 11. Figure 13. Correlation between the turbidite/mass flow layer in core 3, interpreted to record a delta-front collapse, with a scour surface in core 7. The overlying, heavily bioturbated bed in core 3 and correlative bed of laminated very fine sand and silt in core 7 are interpreted to mark a temporary reduction of river flow and/or the migration of the Quinault River ingress channel via an avulsion event towards a more distal position with respect to the core sites following the delta-front failure, which likely was triggered by an earthquake.

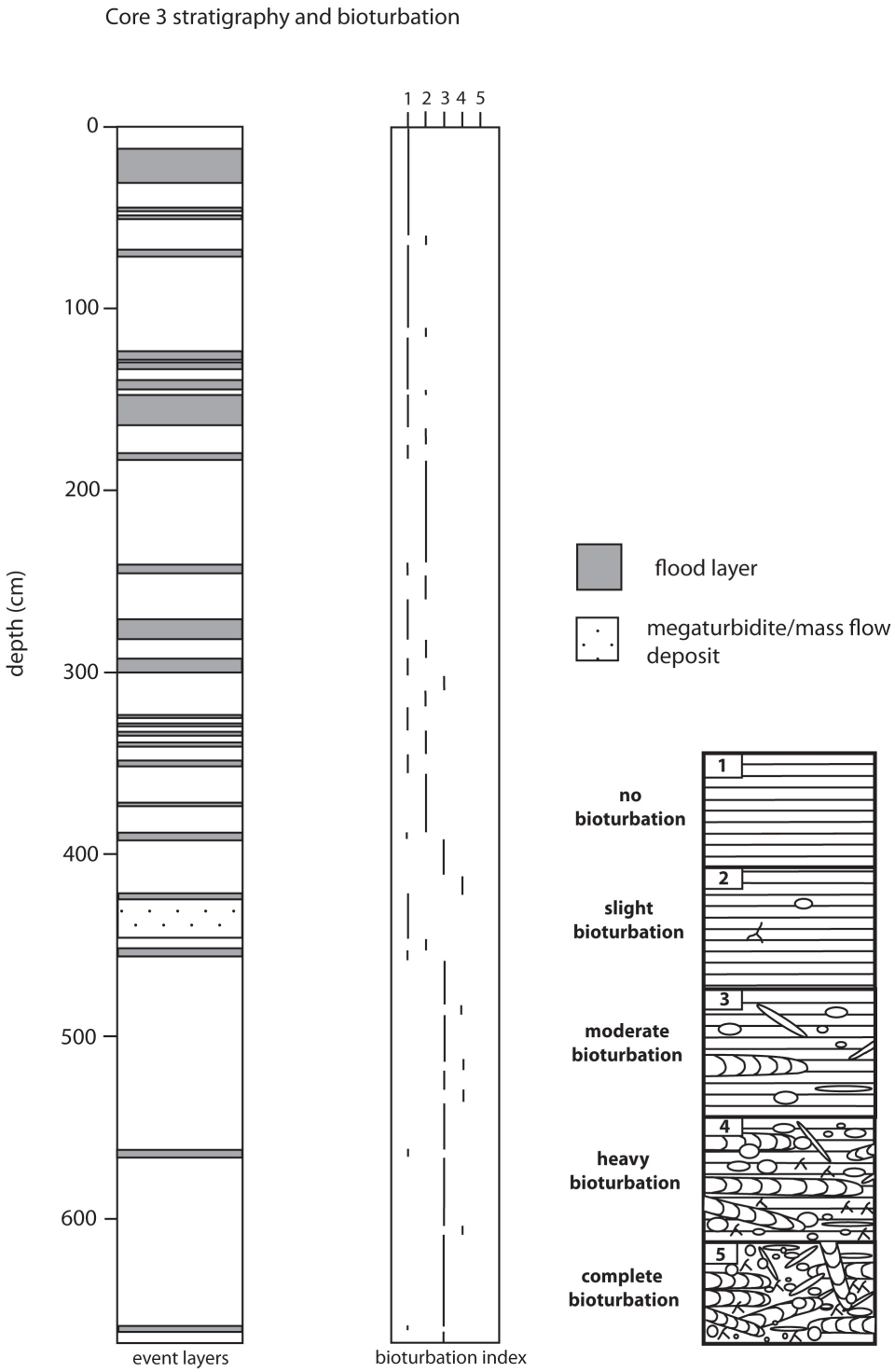

Stop 1 – Figure 12. Figure 11. Stratigraphic column from Core 3, showing position of distinct event layers and the extent of bioturbation, assessed using a visual index similar to that of Droser and Bottjer (1991).

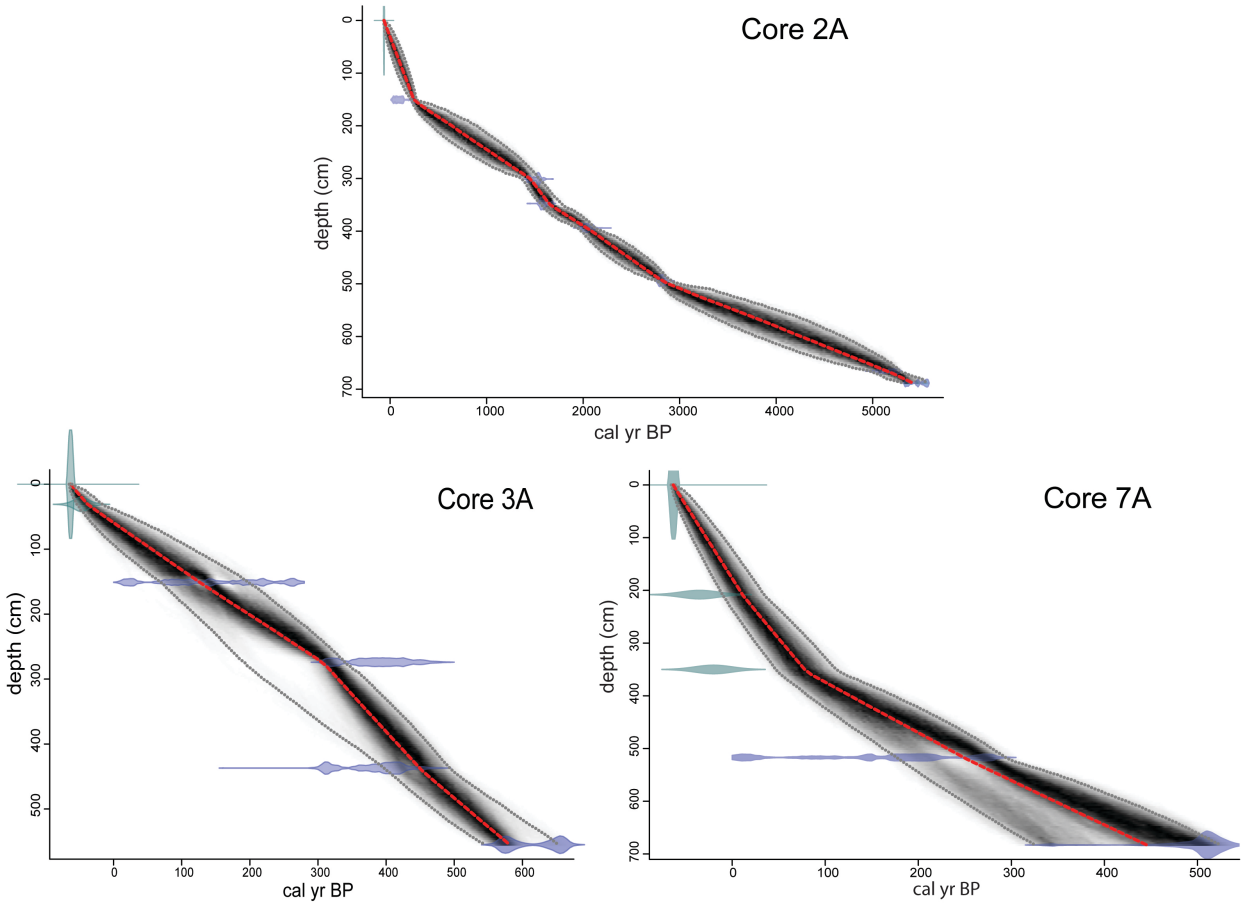

Stop 1 - Figure 13. Age-depth models for cores 2A, 3A, and 7A, constructed using the IntCal13 calibration curve (Reimer et al., 2013) and the Bayesian modelling software Bacon (Blauuw and Christen, 2011). Red line denotes the weighted mean age model and dotted gray lines indicate 95% confidence intervals of the modelled dates. Dark gray shading indicates likely ages, whereas lighter gray shading indicates less likely ages within the confidence limits.

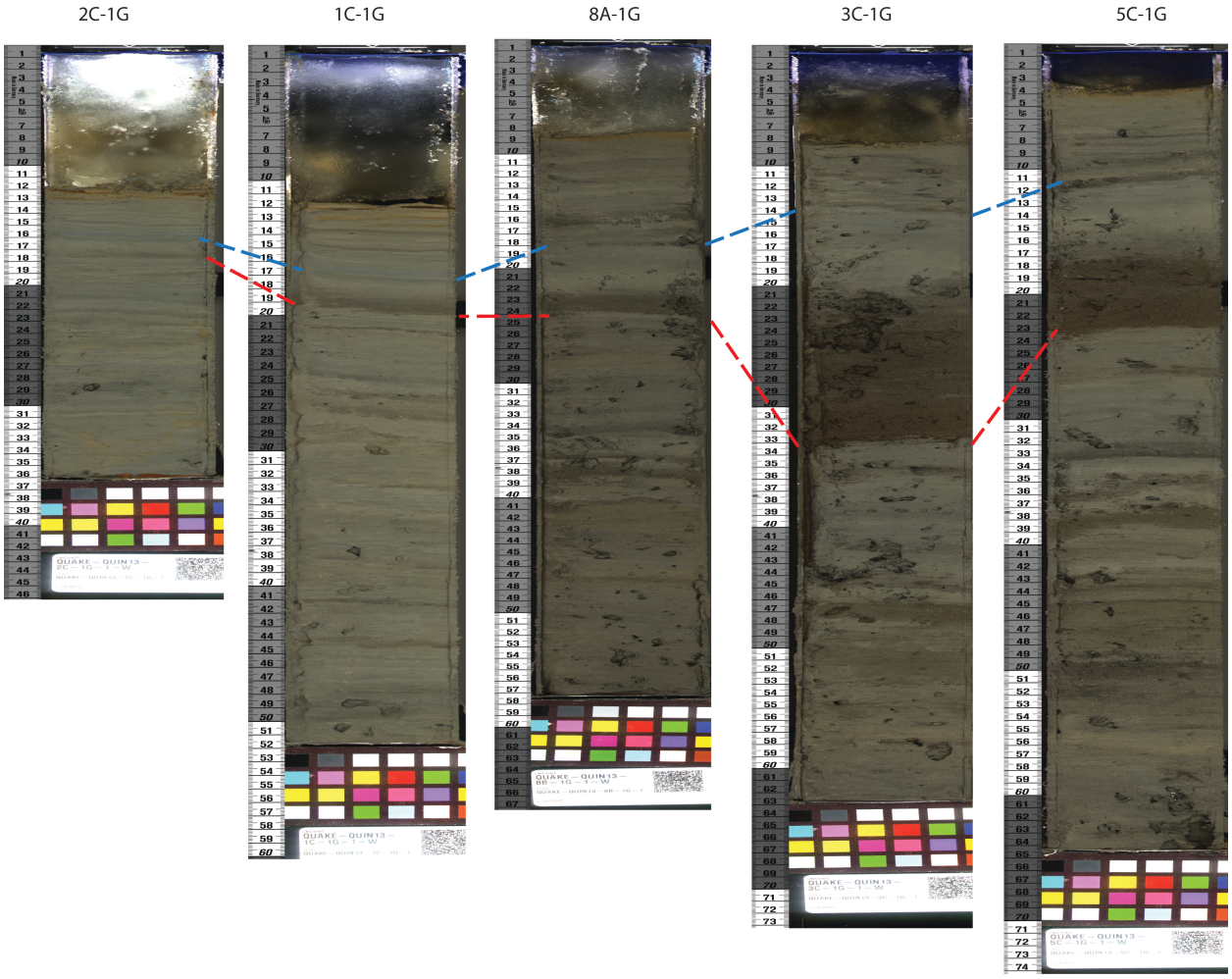

Stop 1 - Figure 14. Core photographs of the uppermost flood layer in Lake Quinault recovered along a transect extending from site 5 near the lake's center to site 2 in High School Bay. At all sites the layer is normally graded, enriched in fine, brown-colored woody plant debris near its base, and capped by fine gray silty clay. Based on average sediment accumulation rates and on calibration of the radiocarbon age of plant debris incorporated into the layer at site 3 to the post-bomb calibration curve (Hua et al. 2013; Table 2), this layer is tentatively attributed to a large March 1997 river flood with an calculated recurrence interval of 33 years based on Quinault River gauging records collected since 1909 (U.S. Geological Survey, 2015).

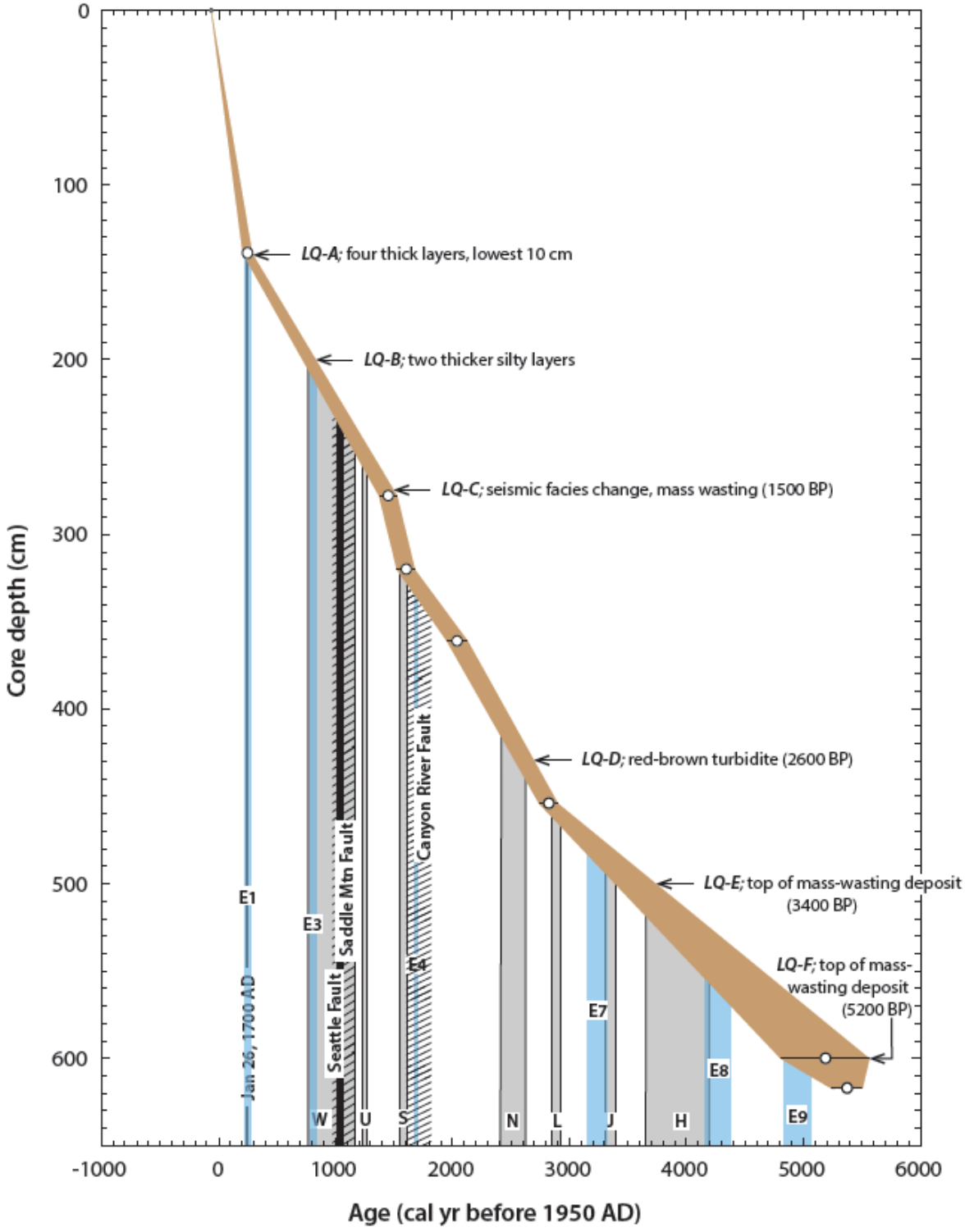

Stop 1 – Figure 15. Figure 17. Comparison of Quinault record to regional paleoseismology.

Figures and references for Yahoo Lake, Stop 4 (Dan Gavin)

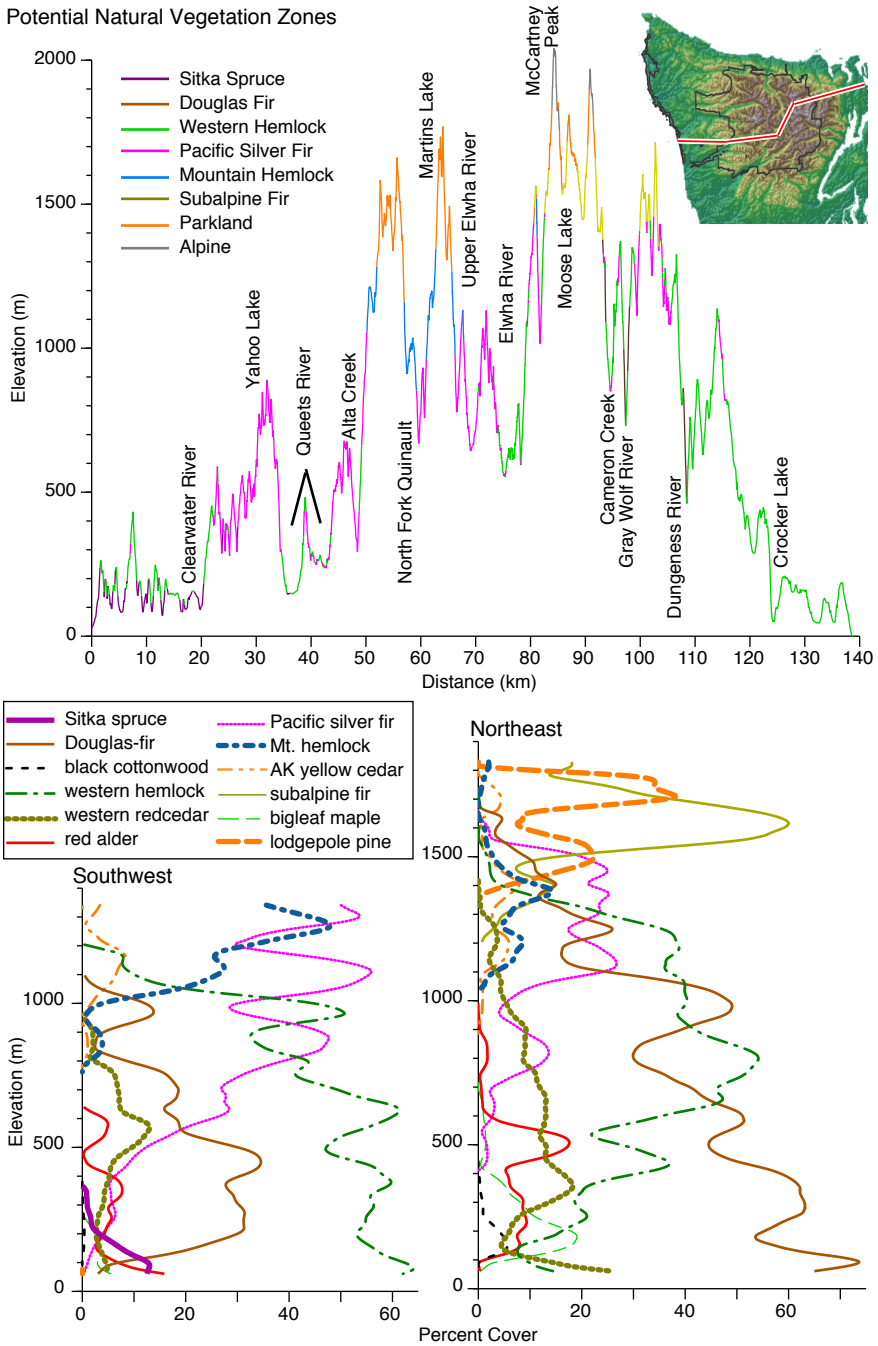

Stop 3 – Figure 1: Elevational transect across the Olympic Peninsula, showing pattern of potential natural vegetation zones. From Gavin and Brubaker (2015) and based on Henderson et al. (2011).

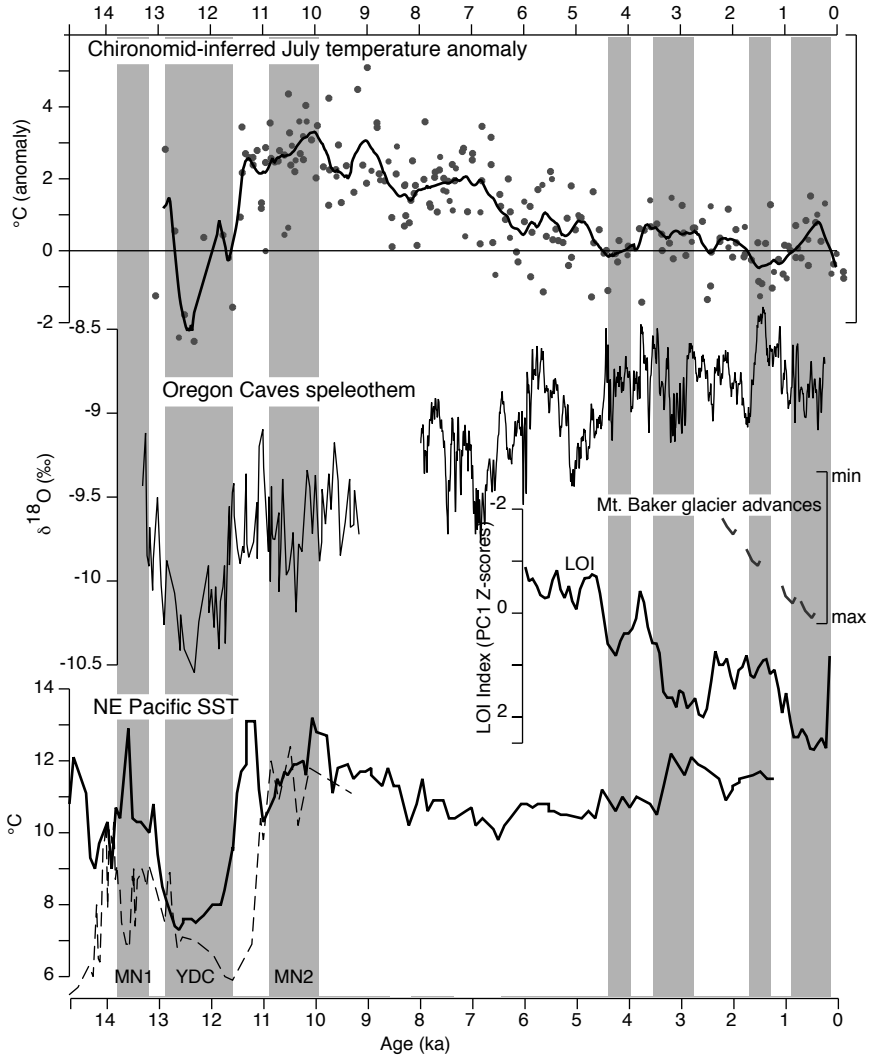

Stop 3 – Figure 2: Paleoclimate indicators from the Pacific Northwest, from Gavin and Brubaker (2015). The chironomid-inferred July temperature anomaly is based on four lakes in southern British Columbia. Points indicate the temperature anomaly from a 0–2-ka base period, and the smooth line shows a locally weighted (loess) smoothing in a 600-year window and its standard error (gray lines). The loss-on-ignition (LOI) index is from glacial-fed lakes in southwest British Columbia that are sensitive to times of glacier advances. Times and relative magnitude of five glacial advances on Mount Baker, Washington, are overlaid on the LOI index. The speleothem oxygen isotope (δ18O) record is from Oregon Caves National Monument. The Northeast Pacific sea-surface temperature (SST) is inferred from alkenone records from a core near northern California, which broadly agrees with a lower-resolution record closer to the Olympic Peninsula (dashed line). Vertical shading indicates times of glacial advances for the McNeeley (MN) 1 and 2 and for the advances from 4.2 ka to present. The Younger Dryas Chronozone (YDC), possibly not a period of glacier advance in the region, is also shown. See Gavin and Brubaker for full set of references.

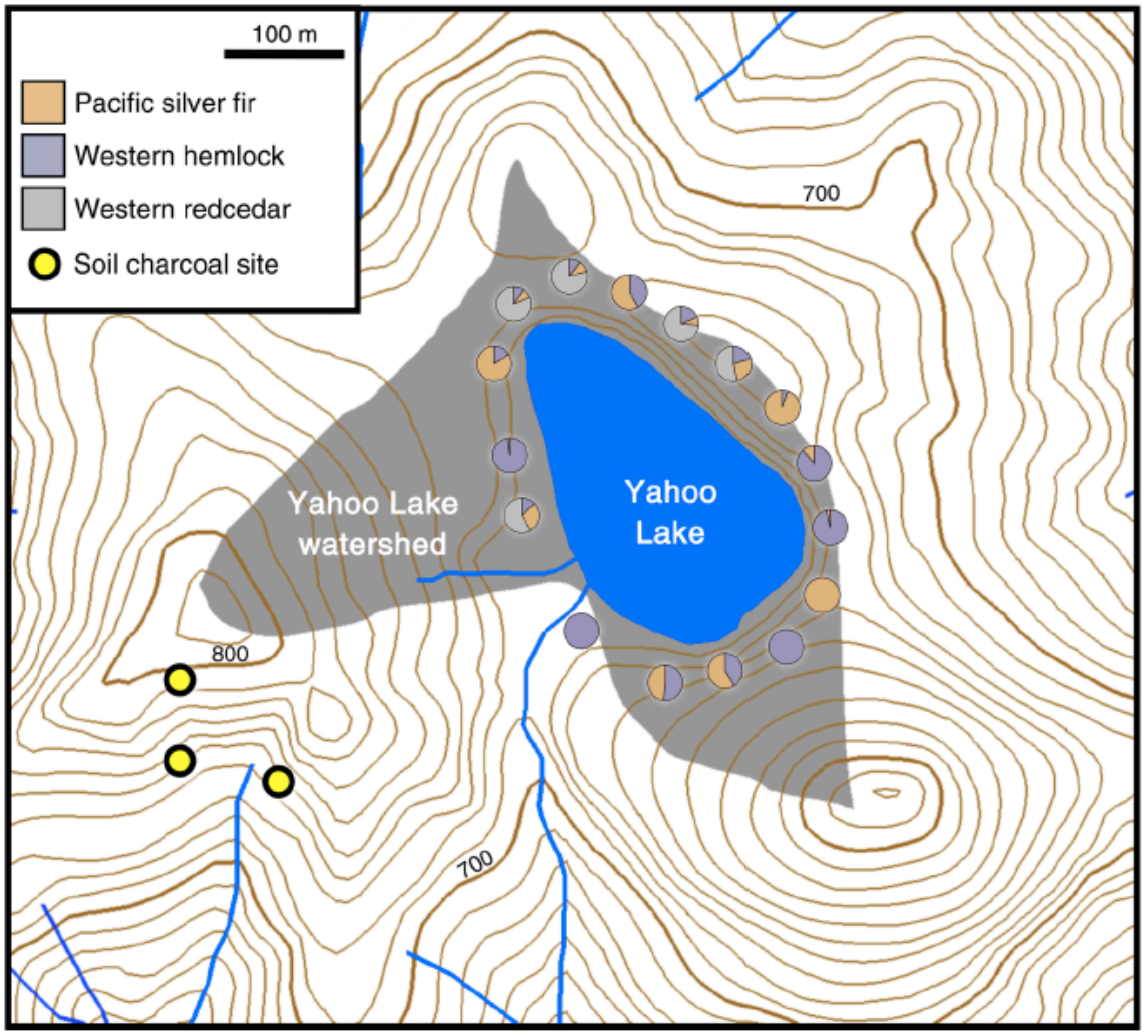

Stop 3 – Figure 3: Yahoo Lake area, showing forest compostion, watershed area, and locations of dated charcoal from Reneau et al. (1989).

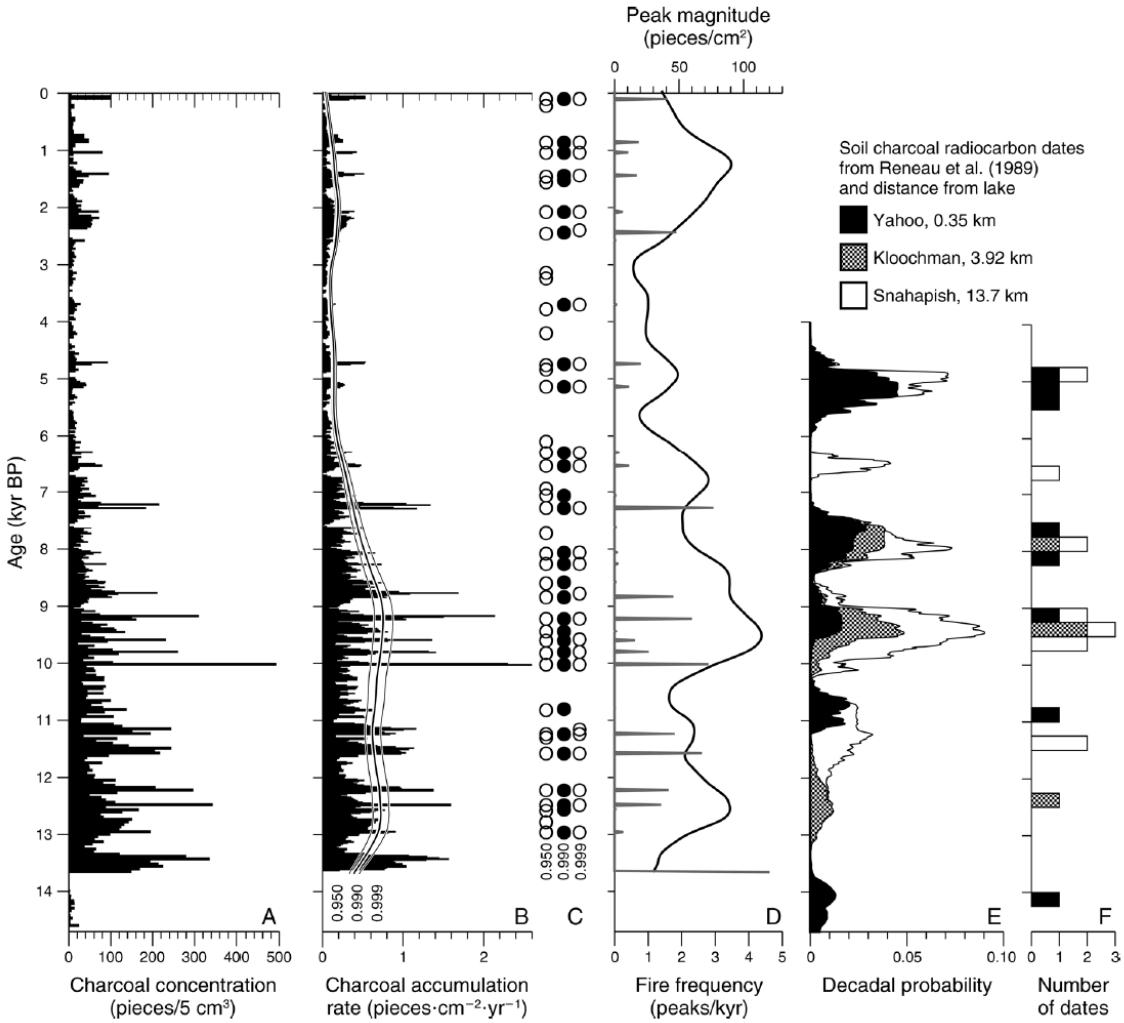

Stop 3 – Figure 4: Charcoal record from Yahoo Lake and soil-charcoal radiocarbon dates from Gavin et al. 2013. (A) Macroscopic charcoal concentration in each 5-cm3 sample. (B) Charcoal accumulation rates interpolated to 20-year intervals. Threshold curves for identifying significant peaks are placed at three levels (95th, 99th, and 99.9th percentiles of the modeled noise distribution). Peak analysis was limited to the samples above a sampling gap from 13.7 kyr to 13.9 kyr. (C) Peaks derived from each of the three thresholds. The 99th percentile (solid circles) was chosen for further analysis. (D) Peak magnitude (horizontal lines) and fire frequency smoothed in a 1000-year moving window. (E) Summed calibrated probability distributions (using INTCAL09) from 21 soil charcoal dates (Reneau et al. 1989). (F) Median calibrated ages of the dates in panel (E).

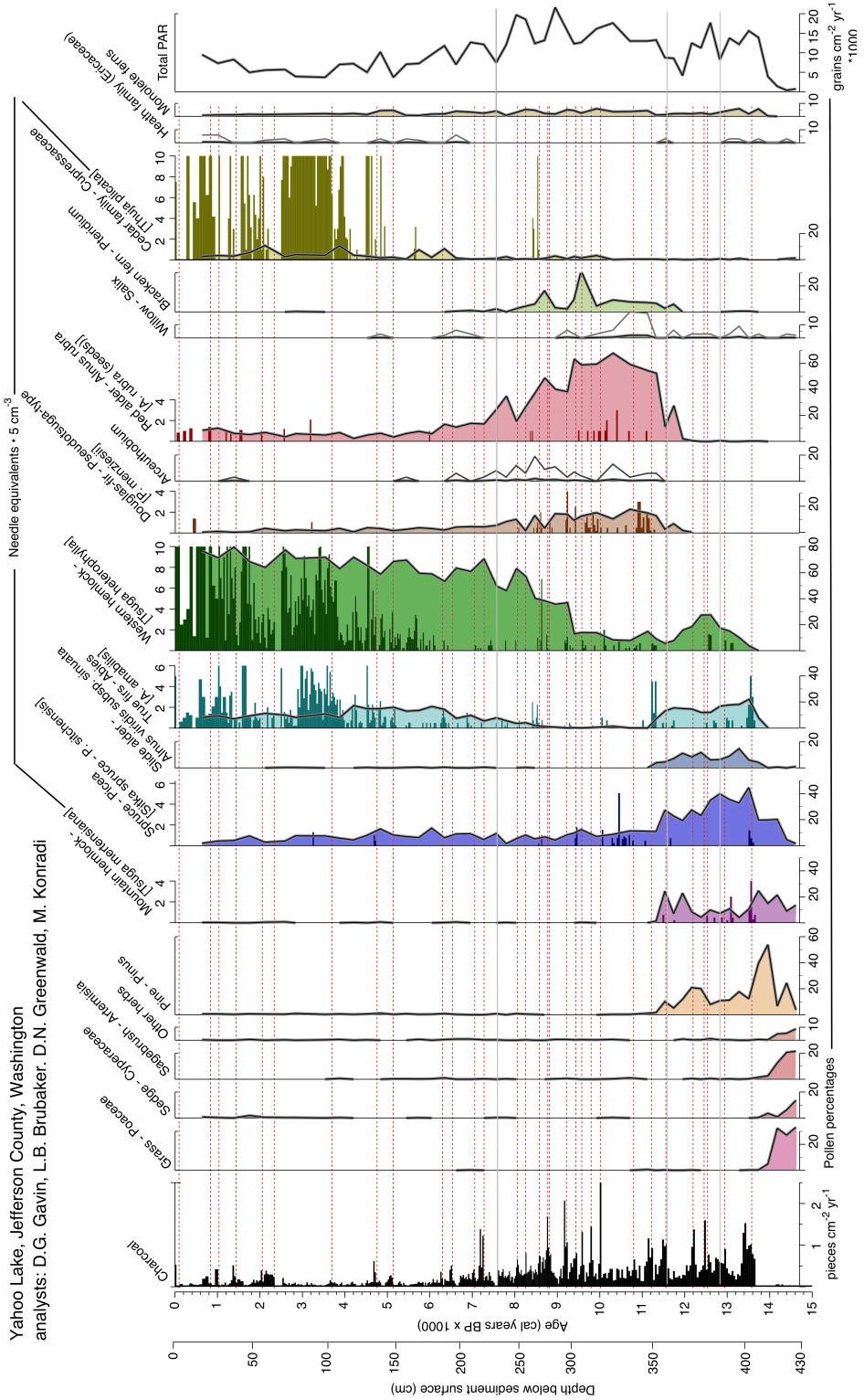

Stop 3 – Figure 5: Pollen and macrofossil diagram for Yahoo Lake (Gavin et al. 2013). Each pollen taxon is labeled above each graph in both common and scientific names. Taxon names in brackets refer to the macrofossil data, graphed as bar charts superimposed over the filled line plot for pollen percentages. Horizontal lines indicate the ages of the Mazama tephra (7.6 ka), and the start and end of the Younger Dryas (12.9–11.6 ka). Gray lines on the pollen graphs indicate 10x exaggeration for rare pollen taxa. Identified fire events from the 1-cm charcoal stratigraphy are shown by dashed red lines.

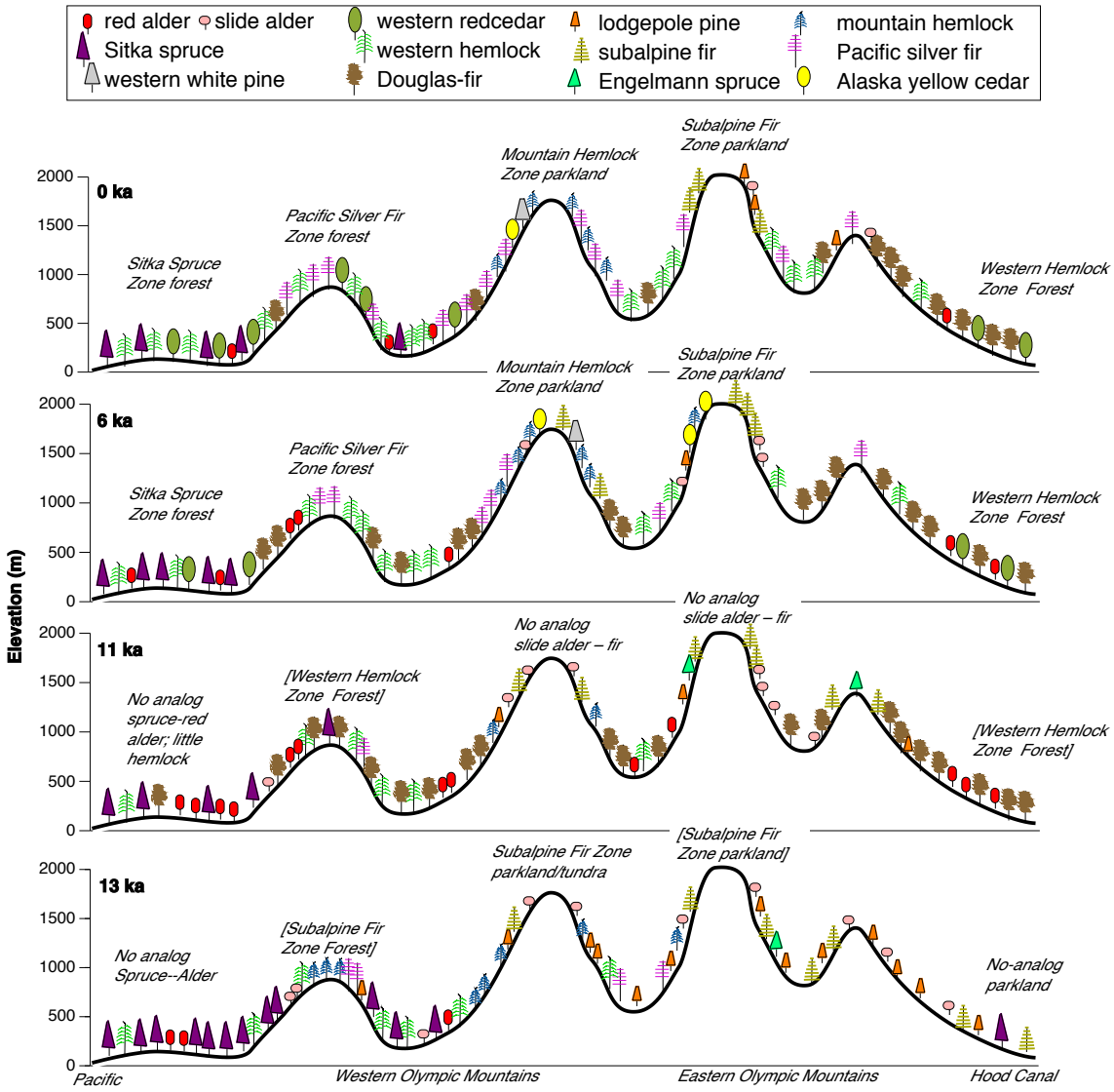

Stop 3 – Figure 6: Schematic diagram showing a profile of dominant tree species on a longitudinal transect across the Olympic Peninsula for four time periods. The analog assignments are given above the location of each pollen record along the transect (west to east: Wentworth, Yahoo, Martins, Moose, and Crocker lakes). Brackets indicate only marginal analogs were found. From Gavin and Brubaker 2015.

Modeling postglacial vegetation dynamics of temperate maritime forests with special regard to snowpack

Christoph Schwörer, Department of Geography, University of Oregon
e-Mail:schworer@uoregon.edu

Past and future forest composition and distribution in temperate mountain ranges is strongly influenced by temperature and snowpack. We used LANDCLIM, a spatially explicit, dynamic vegetation model, to simulate forest dynamics for the last 16,000 years and compared the simulation results to pollen and macrofossil records at five sites on the Olympic Peninsula (Washington, USA). Over the last 16,000 years, simulations driven by a transient Global Circulation Model (GCM) and by a proxy-based temperature reconstruction captured Late-glacial to Late Holocene transitions in forest communities. Overall, the proxy-driven simulations better matched observed vegetation changes than the GCM-driven simulations. This study indicates that despite the moderated climate of the Olympic Peninsula, its forest composition is very sensitive to snowpack-mediated changes in soil moisture.

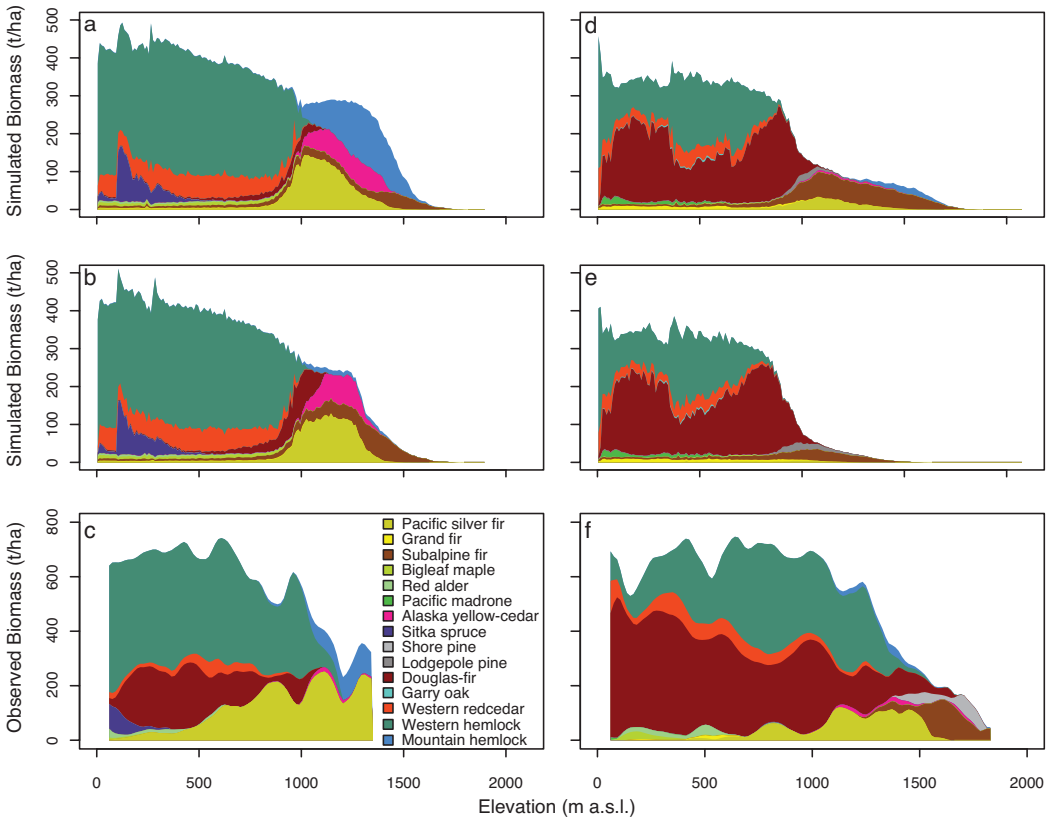

Stop 3 – Figure 7. Elevational distribution and abundance of present-day observed and simulated tree species. A) simulated biomass of individual tree species averaged over the last 150 years. B) same as a) but without the snow accumulation and melt module. C) Percent cover of tree species in 639 ecological plots in the Olympic National Forest (downloaded from Ecoshare.info), multiplied by average species-specific values of aboveground biomass (Smith et al. 1984; Burns et al. 1990a; Burns et al. 1990b). D, e, and f same as a, b and c, but for the east side of the Peninsula

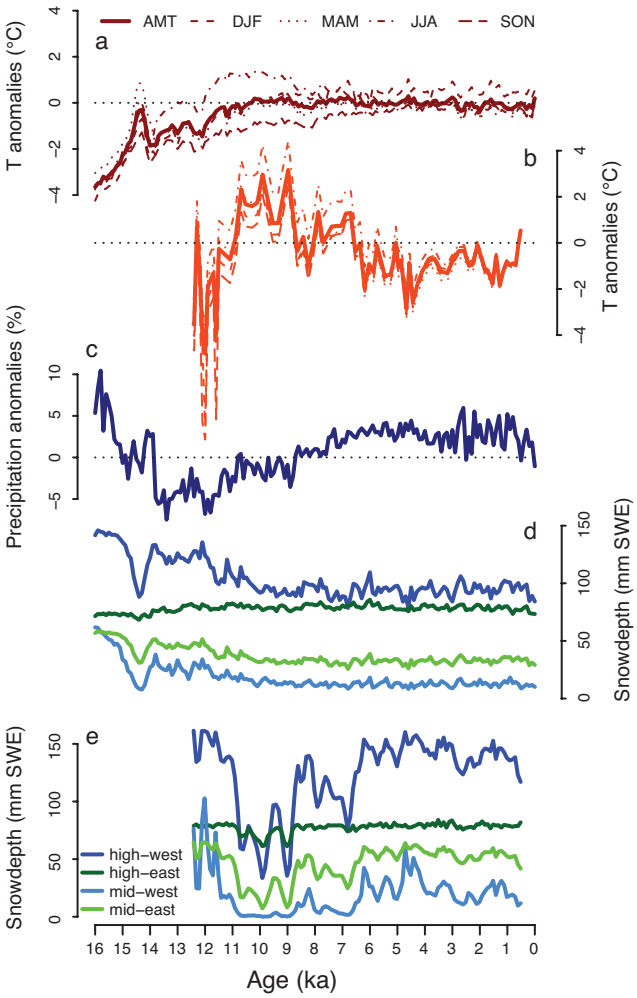

Stop 3 – Figure 8 Time-series of climatic input parameters for the GCM and proxy scenario as well as simulated snowpack for the high- and mid-elevation sites. A) GCM-derived temperature anomalies for annual (AMT) as well as seasonal mean temperatures (DJF = winter, MAM = spring, JJA = summer, SON=fall). B) mean annual and seasonal temperature anomalies used in the proxy scenario, derived from a chironomid-inferred July-temperature reconstruction (Chase et al. 2008) adjusted for changes in insolation. C) GCM-derived precipitation anomalies. D) Simulated snow depths in march for the GCM-scenario at the study sites at middle and high elevations. E) Simulated snow depths in march for the proxy scenario at the study sites at middle and high elevation

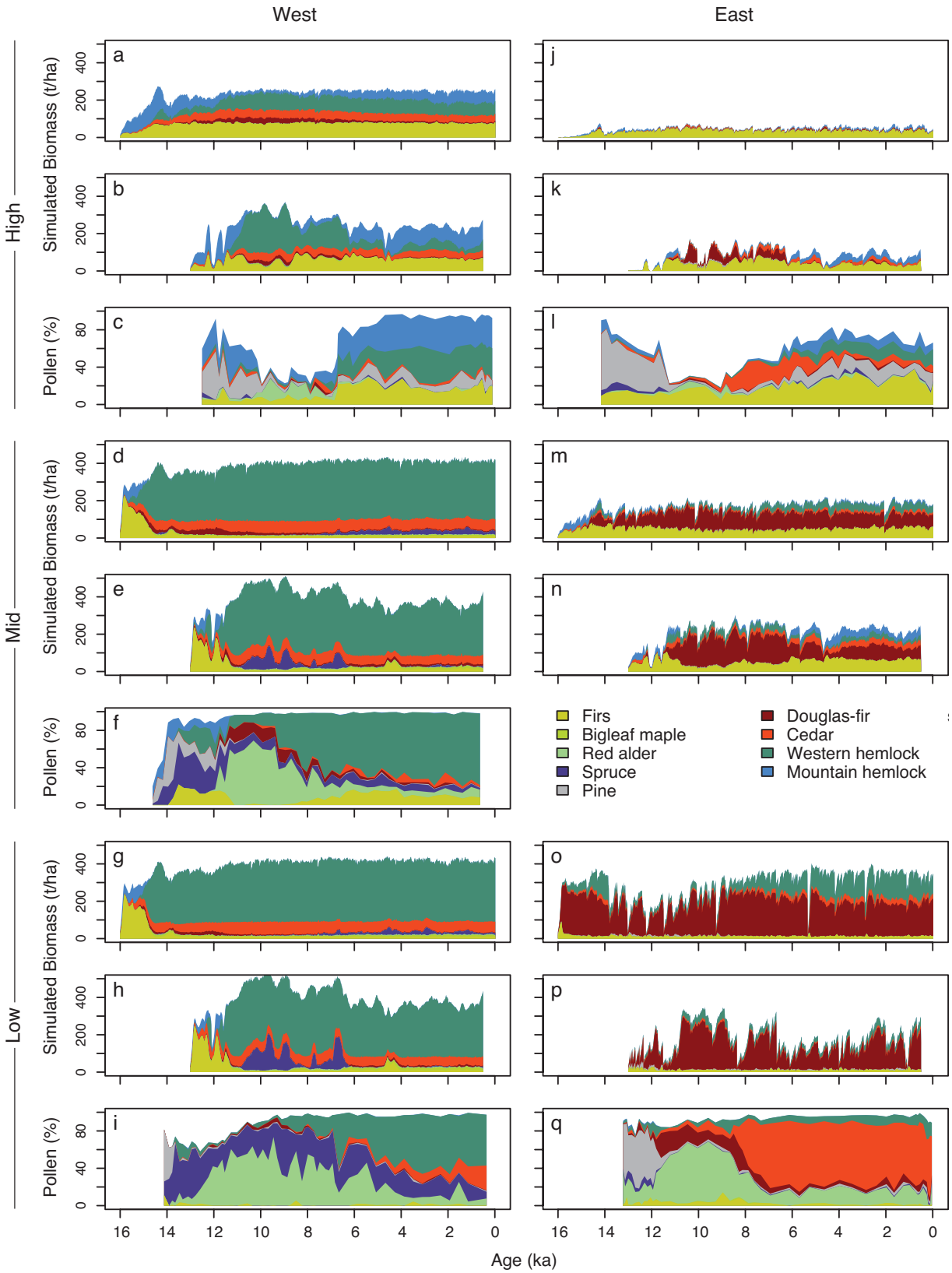

Stop 3 – Figure 9 Simulated biomass in the entire study landscapes for the GCM-(a, d, g, j, m and o) and proxy-scenario (b, e, h, k, n and p) compared to the corresponding pollen records

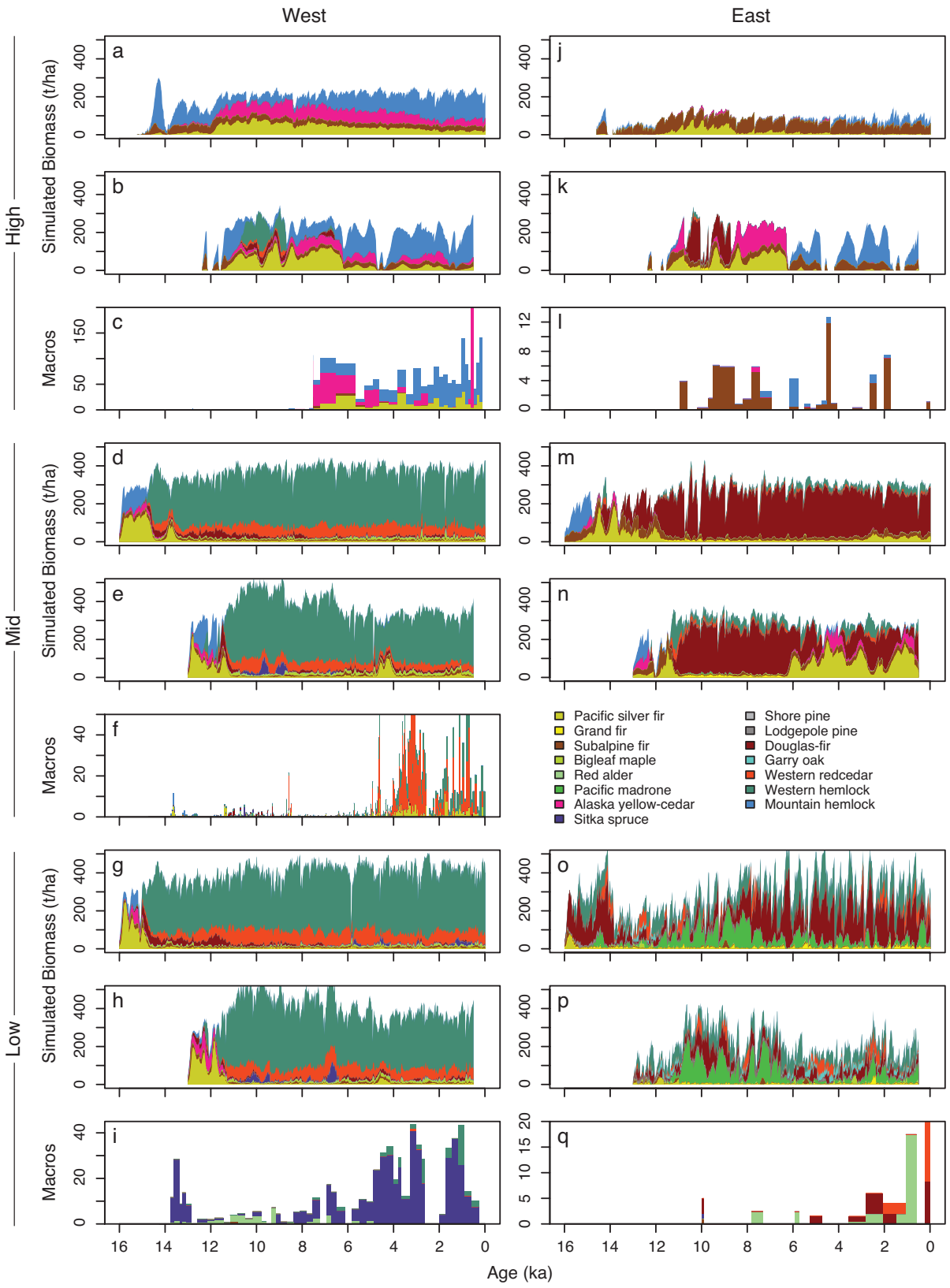

Stop 3 – Figure 10. Simulated biomass within a 250 m radius of the lakes for the GCM- and proxy-scenario compared to the corresponding macrofossil records

References cited in field guide text

Gavin, D. G., J. S. McLachlan, L. B. Brubaker, and K. A. Young. 2001. Postglacial history of subalpine forests, Olympic Peninsula, Washington, USA. Holocene 11:177–188.

Gavin, D. G., L. B. Brubaker, J. S. McLachlan, and W. W. Oswald. 2005. Correspondence of pollen assemblages with forest zones across steep environmental gradients, Olympic Peninsula, Washington, USA. Holocene 15:648–662.

Gavin, D. G., L. B. Brubaker, and D. N. Greenwald. 2013. Postglacial climate and fire-mediated vegetation change on the western Olympic Peninsula, Washington (USA). Ecological Monographs 83:471–489.

Gavin, D. G., and L. B. Brubaker. 2015. Late Pleistocene and Holocene Environmental Change on the Olympic Peninsula, Washington. Springer International Publishing.

Gavin, D. G. 2015. Vegetation stability and the habitat associations of the endemic taxa of the Olympic Peninsula, Washington, USA. Frontiers of Biogeography 7:38–51.

Henderson, J. A., R. D. Lesher, D. H. Peter, and C. D. Ringo. 2011. A Landscape Model for Predicting Potential Natural Vegetation of the Olympic Peninsula USA Using Boundary Equations and Newly Developed Environmental Variables. USDA Forest Service General Technical Report PNW-GTR-941, Portland, OR.

Reneau, S. L., W. E. Dietrich, and M. Rubin. 1989. Analysis of hillslope erosion rates using dated colluvial deposits. The Journal of Geology 97:45.

Stop 4. Clearwater terraces at the Grouse Bridge (Karl Wegmann). This will be an overview stop at the Grouse Bridge over the Clearwater River to discuss Holocene and Pleistocene terrace records in the unglaciated Clearwater drainage. (45 minutes, then return to campground and lodging, or go to optional Stop 5 if time allows)

Karl Wegmann[1] & Frank Pazzaglia[2]

[1]Department of Marine, Earth, and Atmospheric Sciences, North Carolina State University

[2]Earth and Environmental Sciences, Lehigh University

Excerpted from:

Pazzaglia, F.J., Thackray, G.D., Brandon, M.T., Wegmann, K.W., Gosse, J., McDonald, E., Garcia, A.F., Prothero, D., and Swanson, T.W., 2003, Tectonic geomorphology and the record of Quaternary plate boundary deformation in the Olympic Mountains, *in* Swanson, T.W., ed., Western Cordillera and adjacent areas, Volume Geological society of America Field Guide 4: Boulder, CO, Geological Society of America, p. 37-67.

The purpose of this stop is to introduce the concept of a strath, the terrace deposit, and some of the relative and numeric criteria in establishing strath age. Detailed discussions of these topics can be found in Wegmann (1999), Pazzaglia and Brandon (2001), and Wegmann and Pazzaglia (2002, and 2009) (Figures 1 & 2). Terraces are well preserved in the Clearwater drainage (Figue 1). There are two major flights of terraces: a higher, outer, older sequence that is underlain by thick alluvial-fill deposits, and a lower, inner, younger sequence underlain by thin alluvial deposits (Figs. 2 & 5). The terrace exposed here at the Grouse Bridge is a fine example of the lower, inner, younger sequence, and it contains all of the stratigraphic characteristics important to distinguishing and using terraces in tectonic interpretations (Figs. 2 & 3). The lower terraces like the one exposed here are composed of a basal, coarse-grained, 1–3-m-thick axial channel, sandy gravel facies, and overlying fi ne-grained 1–3-m-thick sandy silt overbank facies. The sandy gravel facies locally preserve sedimentary structures consistent with lateral accretion processes, as might be expected for point and transverse bars, which can be seen in the adjacent modern channel. So by analogy, we take the coarse-grained facies of the terrace deposit to represent the bedload being transported when the terrace strath was cut. In contrast, the fine-grained facies represent vertical accretion atop the floodplain, presumably related to deposition during floods.

The 400 km^2 Clearwater River basin, located on the Pacific flank of the actively uplifting Olympic Mountains of western Washington State, contains a well-preserved flight of Pleistocene and Holocene fluvial terraces (Figures 1 & 4; Pazzaglia and Brandon, 2001; Wegmann & Pazzaglia, 2002). We have collected a large data set of numeric ages from the Holocene terraces that is used to elucidate the geomorphic, fluvial, active tectonic and climatic processes that operate at Holocene spatial and temporal scales. Detailed field mapping reveals three prominent Holocene straths and their overlying terrace deposits.

Holocene terrace ages fall into three broad ranges: ca. 9000–11,000 yr B.P. (Qt4), 4000–8000 yr B.P. (Qt5), and 0–3000 yr B.P. (Qt6) (Fig. 6). Terrace deposit stratigraphy, sedimentology, and age distributions allow us to consider two alternative models for their genesis (Fig. 7). The favored model states that the terrace ages are coincident with lateral incision of the Clearwater channel, emplacement of the terrace alluvium, and the carving of the straths. Vertical incision of the Clearwater channel was primarily relegated to the brief (~1000 yr) intervals when we have no record of terraces. Alternatively, the straths were carved as the channel incised vertically during the brief time periods between dated terrace deposits, and the terrace ages record a subsequent long time of alluviation atop the straths and concomitant termination of vertical incision. In both models, we envision a Clearwater River channel at or near sediment carrying capacity with a temporally variable rate of both lateral and vertical incision. Small deviations from this at-capacity condition are driven by variations in the liberation and delivery of hillslope sediment to the channel.

We consider several causes for variable hillslope sediment flux in this tectonically active setting including Holocene climate change and ground accelerations related to earthquakes (Fig. 8). Holocene rates of vertical incision are reconstructed along nearly the entire Clearwater Valley from the wide distribution of dated terraces. Incision rates clearly increase upstream, mimicking a pattern documented for Pleistocene terraces in the same basin (Pazzaglia and Brandon, 2001); however, the rates are 2–3 times those determined for the Pleistocene terraces (Figs. 9 & 10). The faster Holocene incision rates may be interpreted in terms of an increase in the rates of rock uplift. However, we favor an alternative explanation in which the Holocene rates represent a channel rapidly reacquiring its stable, graded concavity following protracted periods of time in the Pleistocene when it could not accomplish any vertical incision into tectonically uplifted bedrock because the channel was raised above the bedrock valley bottom by climatically induced alluviation. These results illustrate how, even in tectonically active settings, representative rates of rock uplift inferred from studies of river incision should be integrated over at least one glacial-interglacial cycle.

Incision rates derived from river terraces are commonly used to infer rock uplift rates; however, an apparent dependence of incision rate on measured time interval may confound directly relating incision to uplift. The time-dependent incision rates are a Sadler effect that have been argued to result from a stochastic distribution of hiatal intervals in river incision , potentially reducing the utility of incision records for interpreting unsteadiness in tectonic processes (e.g., Finnegan et al., 2014). The Clearwater River terrace sequence is a nice example of how time-dependent incision rates can arise from a simple systematic bias in the distance measurement used to calculate incision rate, and thus stochastic causes are not required. Gallen et al. (2015) present a conceptual model that describes the dynamic history of streambed elevation over cycles of terrace formation, illustrating that measured incision rate is time dependent because the stream channel reference frame is not fixed with respect to the geoid. Because it is challenging to reconstruct the full elevation history for a river channel, most researchers use the modern streambed elevation as a reference datum, but we demonstrate that doing so imposes a bias that manifests as an apparent dependence of rate on measured time interval. Fortunately, correction of this bias is straightforward, and allows river incision data to be used in studies of tectonic or climatic unsteadiness.

References

Bronc Ramsey, C., 2000, OxCal version 3.5: Oxford, UK, University of Oxford, downloaded in January 2001, available from http://www.rlaha.ox.ac.uk/orau/index.htm.

Finnegan, N.J., Schumer, R., and Finnegan, S., 2014, A signature of transience in bedrock river incision rates over timescales of 104-107 years: Nature, v. 505, p. 391-394.

Gallen, S.F., Pazzaglia, F.J., Wegmann, K.W., Pederson, J.L., and Gardner, T.W., 2015, The dynamic reference frame of rivers and apparent transience in incision rates: Geology, v. 43, p. 623-626.

Pazzaglia, F.J., and Brandon, M.T., 2001, A fluvial record of rock uplift and shortening across the Cascadia forearc high: American Journal of Science, v. 301, p. 385-431.

Wegmann, K.W., 1999, Late Quaternary fluvial and tectonic evolution of the Clearwater River basin, western Olympic Mountains, Washington State [M.S. thesis]: Albuquerque, University of New Mexico, 217 p.

Wegmann, K.W., and Pazzaglia, F.J., 2002, Holocene strath terraces, climate change, and active tectonics: The Clearwater River basin, Olympic Peninsula, Washington State: Geological Society of America Bulletin, v. 114, p. 731-744.

Wegmann, K.W., and Pazzaglia, F.J., 2009, Late Quaternary fluvial terraces of the Romagna and Marche Apennines, Italy: Climatic, lithologic, and tectonic controls on terrace genesis in an active orogen: Quaternary Science Reviews, v. 28, p. 137-165.

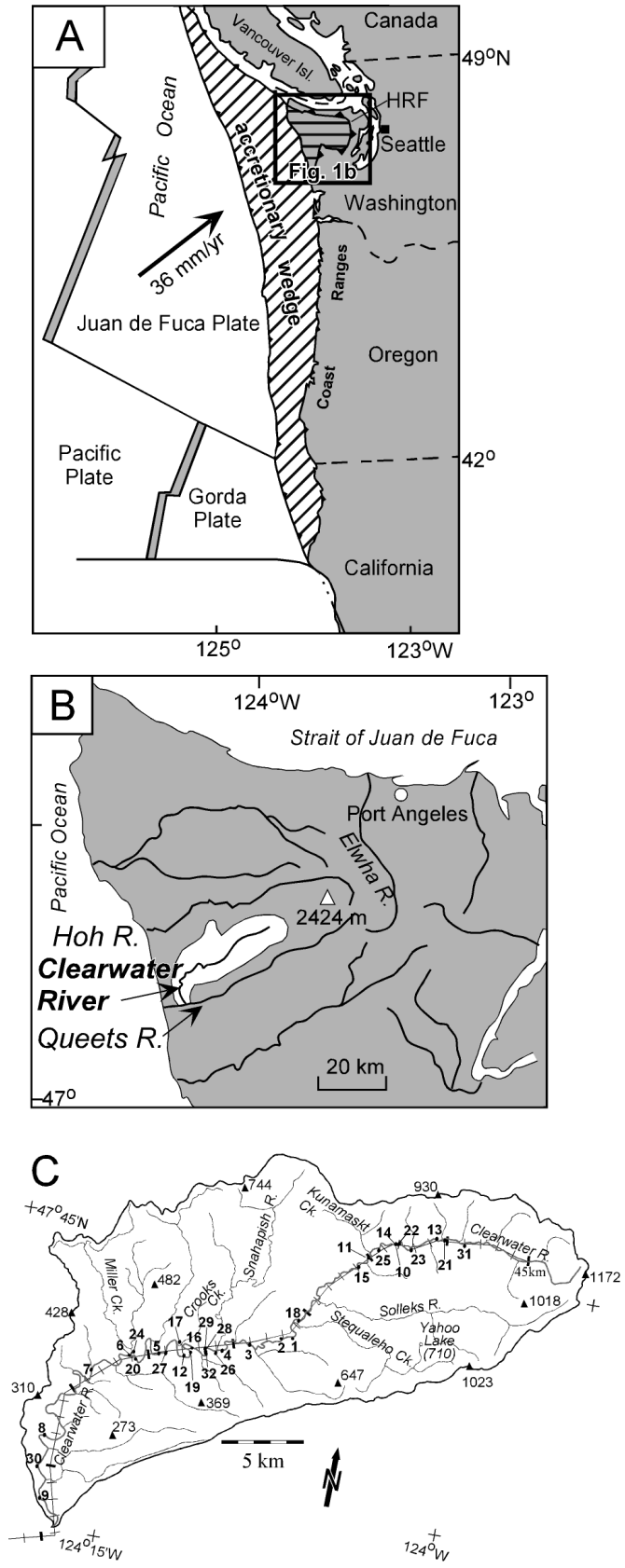

Stop 4 – Figure 1. (A) Location map of the Olympic Mountains showing the major tectonic features of the Cascadia margin. HRF—Hurricane Ridge fault. Note that the Olympic Peninsula is the only part of the Coast Ranges to expose the accretionary wedge. The rectangle around the Olympic Peninsula is enlarged in B. (B) Location of the Clearwater drainage (white) with respect to other major rivers on the Olympic Peninsula. Spot elevation is Mount Olympus. (C) Simplified reference map of the Clearwater basin showing place names indicated in the text, spot elevations (m), and numbered locations of radiocarbon samples referenced in Table 1 of Wegmann & Pazzaglia (2002). Location of radiocarbon dates and features mentioned in the text with respect to their distance from the Pacific Coast are indexed to the cross-hatched line with the 0 km and 45 km labels at its ends paralleling the Clearwater channel. The cross hatches are in one kilometer intervals; 5 km cross hatches are darker.

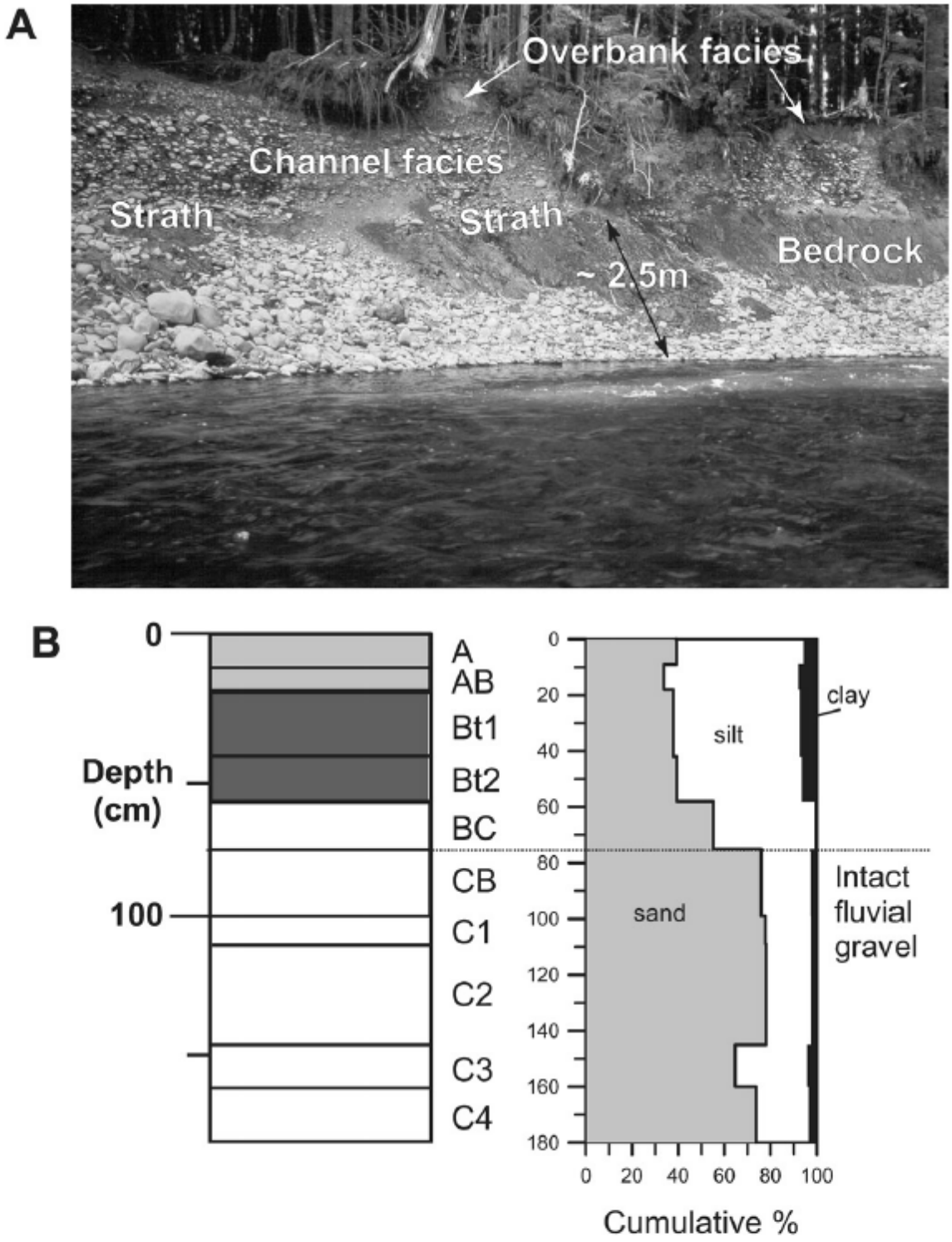

Stop 4 – Figure 2. Annotated photograph of the middle Holocene Qt5 strath and strath terrace exposed at the Grouse Bridge. B: Soil described at the Grouse Bridge site in Qt5.

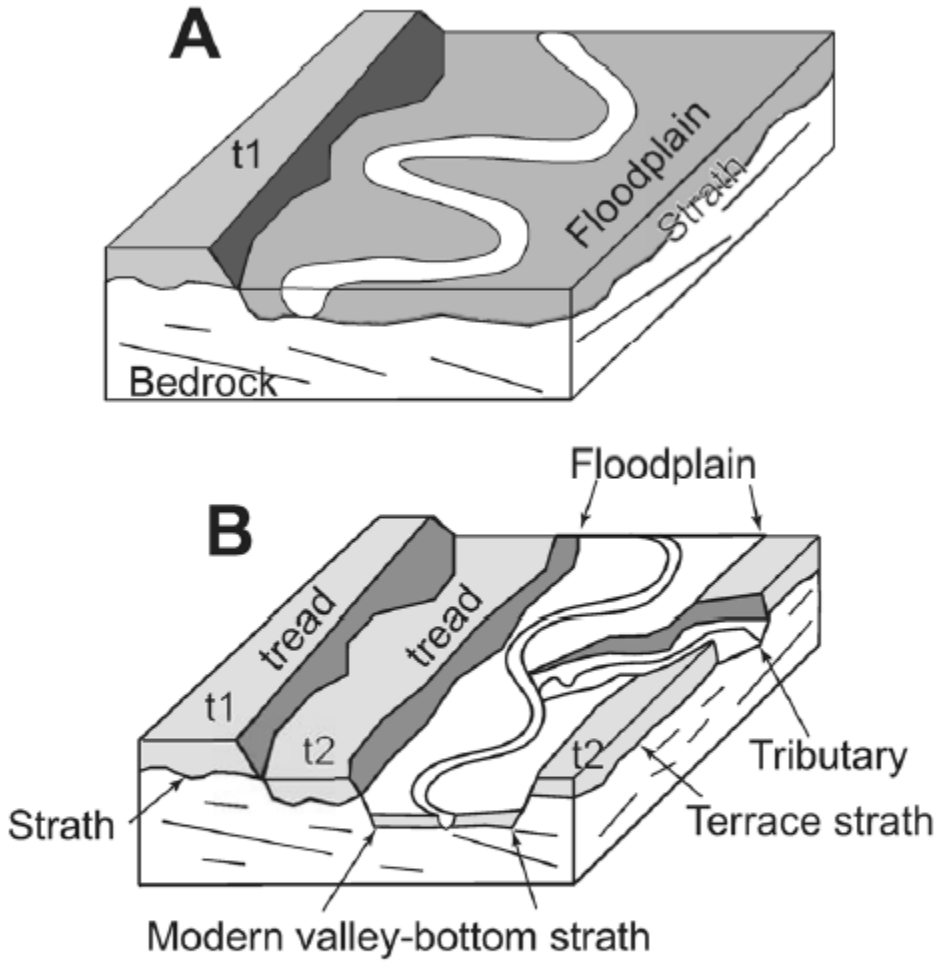

Stop 4 – Figure 3. A: Schematic illustrating the relationship between a terrace (t1, t2), straths, the floodplain, and a valley bottom. B: The correspondence between the width of the floodplain and the width of the valley bottom strath is corroborated by exposure of the valley bottom strath in tributary channels, shown entering from the right part of the diagram.

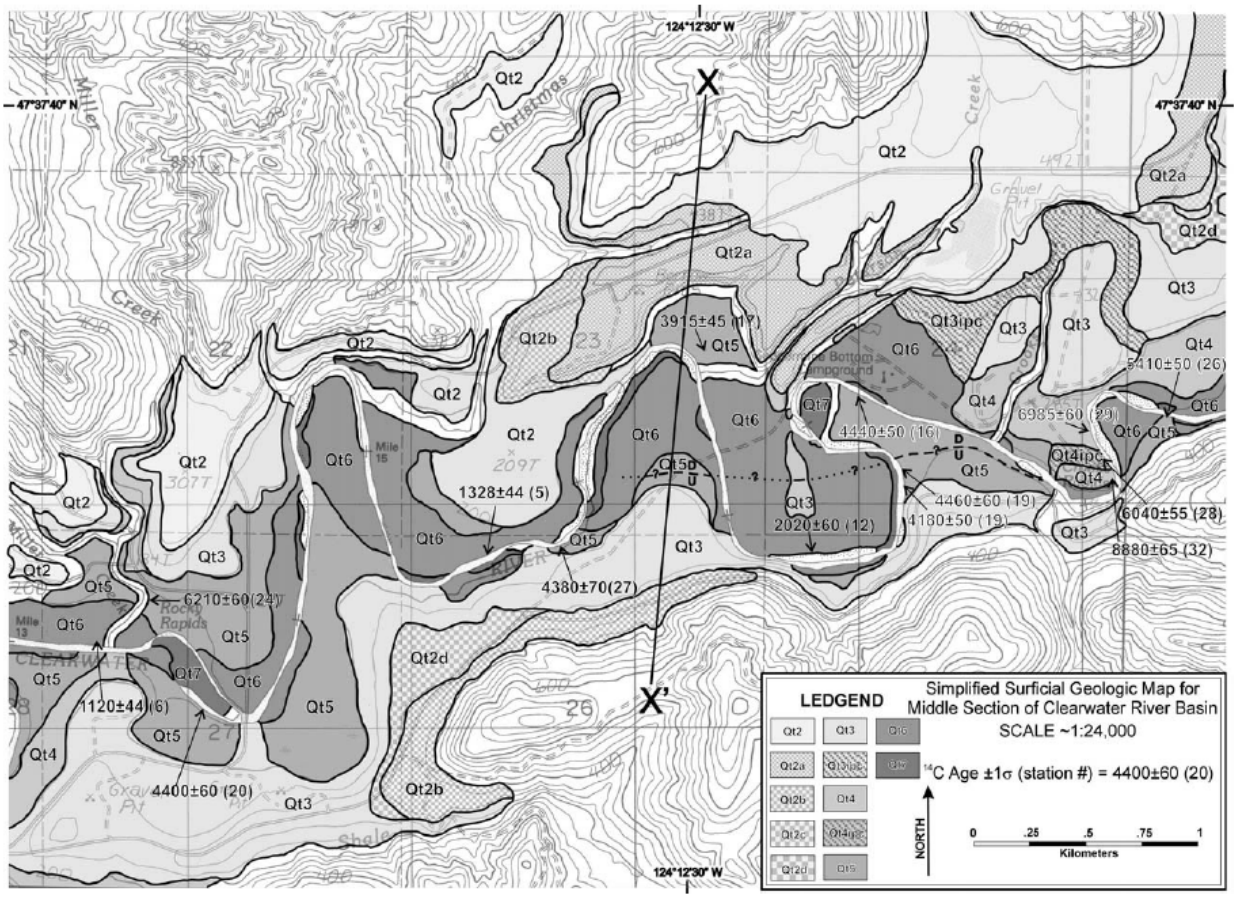

Stop 4 – Figure 4. Map of river terraces in the medial part of the Clearwater Valley (modified from Wegmann, 1999). Letters following terrace names designations: a, b, c, d—treads that share a common strath; ipc—inset paleochannel. X–X is the location of the cross section shown in Figure 4.

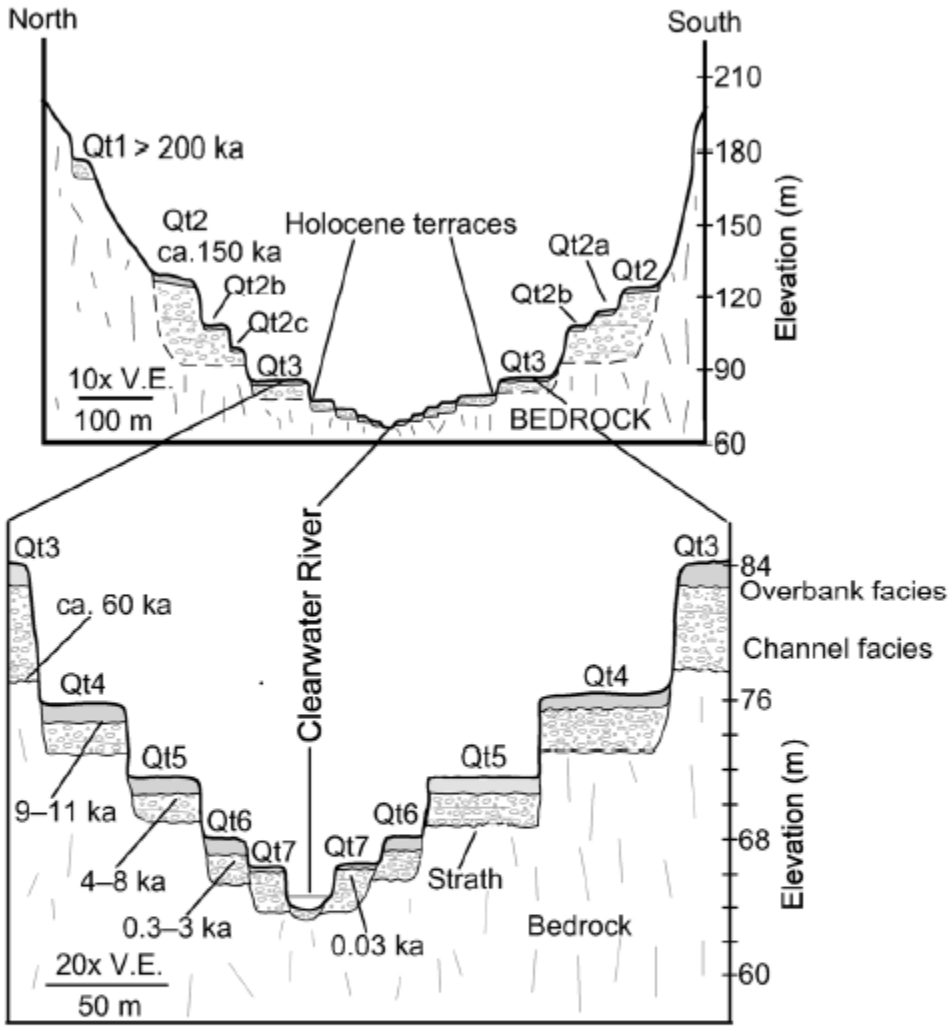

Stop 4 - Figure 5. Composite cross section representing the terrace stratigraphy and general age ranges in the Clearwater drainage. We use the convention of naming terraces in order of increasing age where 1 is the oldest (highest) terrace in the landscape and assigning numbers to straths only. In this manner, terrace Qt2 may have more than one tread, which we designate with lower case alpha numeric subscripts (as Qt2a, Qt2b, etc.) From Wegmann & Pazzaglia (2002).

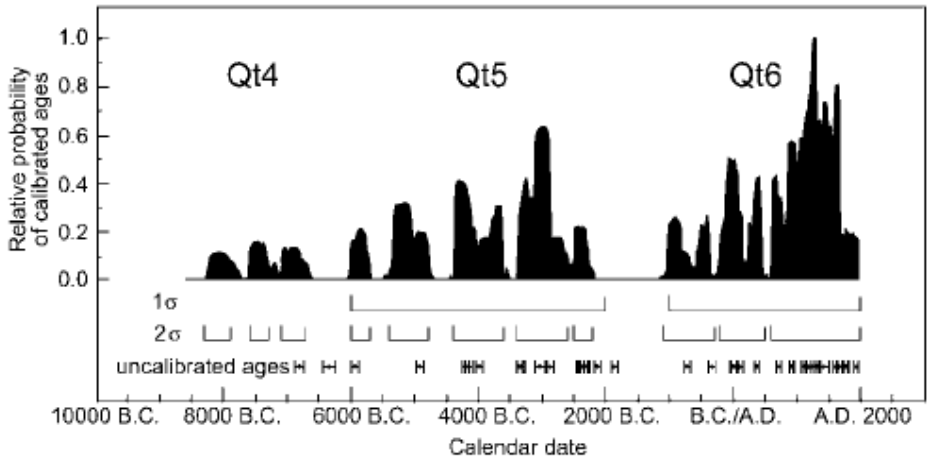

Stop 4 – Figure 6. Probability density and frequency distribution plots for 38 radiocarbon dates (Table 1 of Wegmann & Pazzaglia, 2002) of the Holocene terraces. The plot was produced by calculating calendar ages and their accompanying 1_ errors and then summing the probabilities using the program OxCal (Bronc Ramsay, C., 2000). Note the brackets beneath the frequency histograms. At the 1-sigma confidence level, the groups of ages between ca. 2000–6000 B.C. and A.D. 2000–1000 B.C. statistically coincide with terraces Qt5 and Qt6, respectively. Uncalibrated radiocarbon ages and their respective 1-sigma errors are shown by the small data points at the base of the plot for comparison.

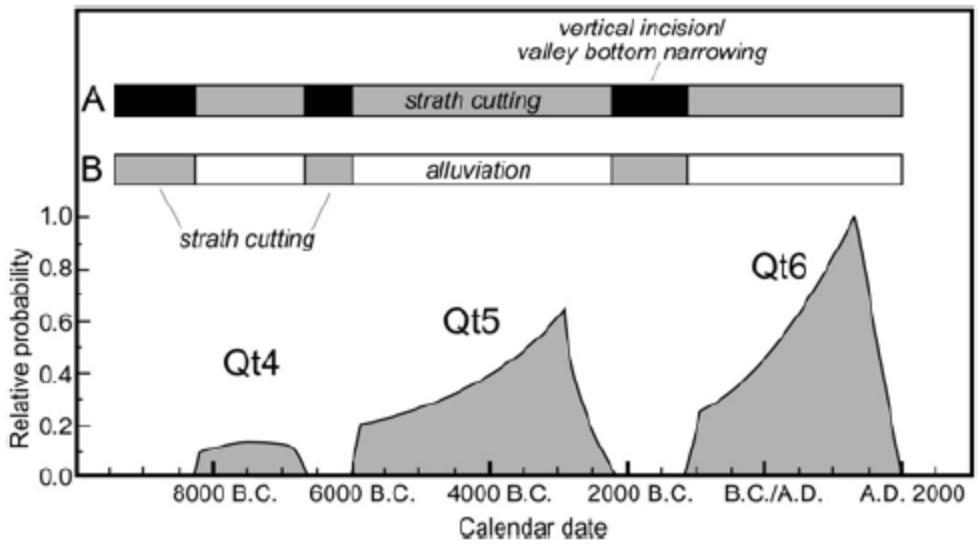

Stop 4 – Figure 7. Conceptual models for strath cutting. White bars indicate alluviation (sediment aggradation atop the strath), black bars indicate valley-bottom narrowing and vertical incision, and gray bars indicate valley-bottom widening, strath cutting, and abandonment of some of the alluvium performing the incision atop the strath. (A) Terrace alluvium and strath cutting are contemporaneous and span the dates collected from the alluvium atop a strath. Temporal gaps represent times of valley-bottom narrowing and vertical incision when the likelihood of strath preservation is very low. (B) The complete termination of vertical incision as the straths are buried by a (relatively) thick alluvial deposit. Deposition of the terrace alluvium is not related to the strath cutting. Straths are cut rapidly by vertical and lateral processes during the temporal gaps, and incision ceases during the time periods represented by dated alluvium.

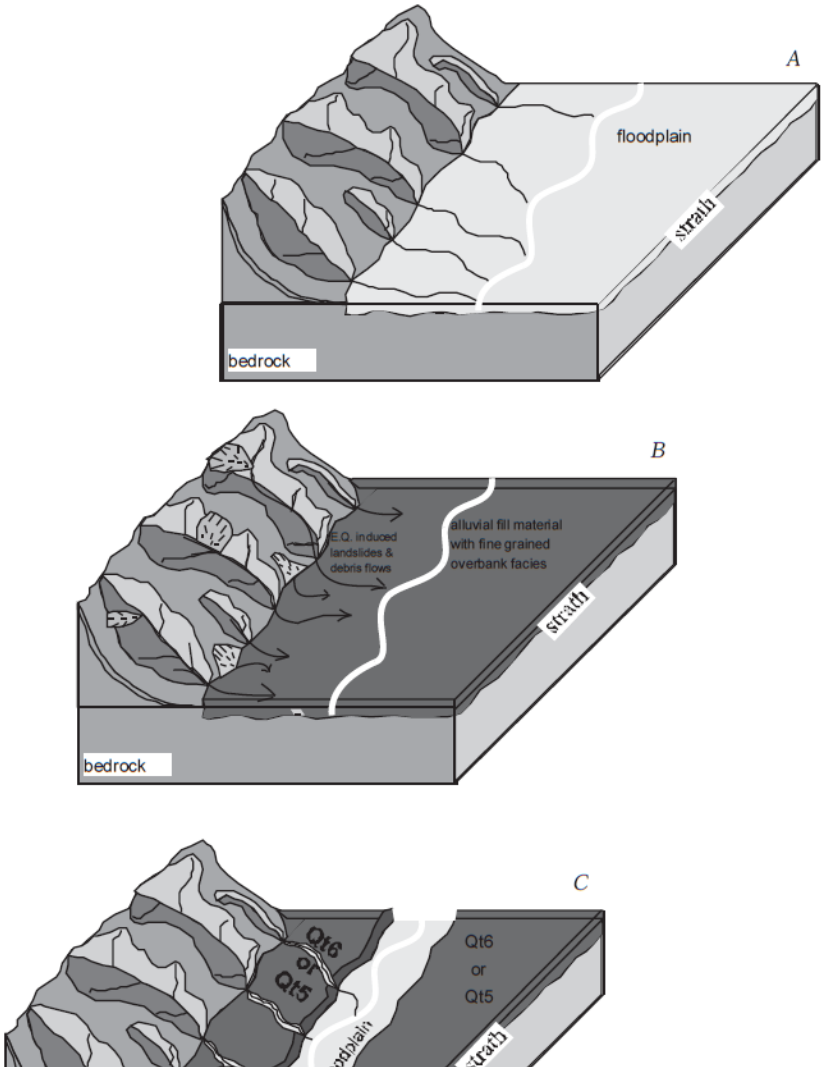

Stop 4 – Figure 8. Exceedingly simplified conceptual cartoon depicting seismic triggering of hillslope sediment evacuation and forced aggradation of the fluvial system that could result in Holocene-scale terraces (Qt5 or Qt6) observed in the Clearwater River basin (from Wegmann, 1999).

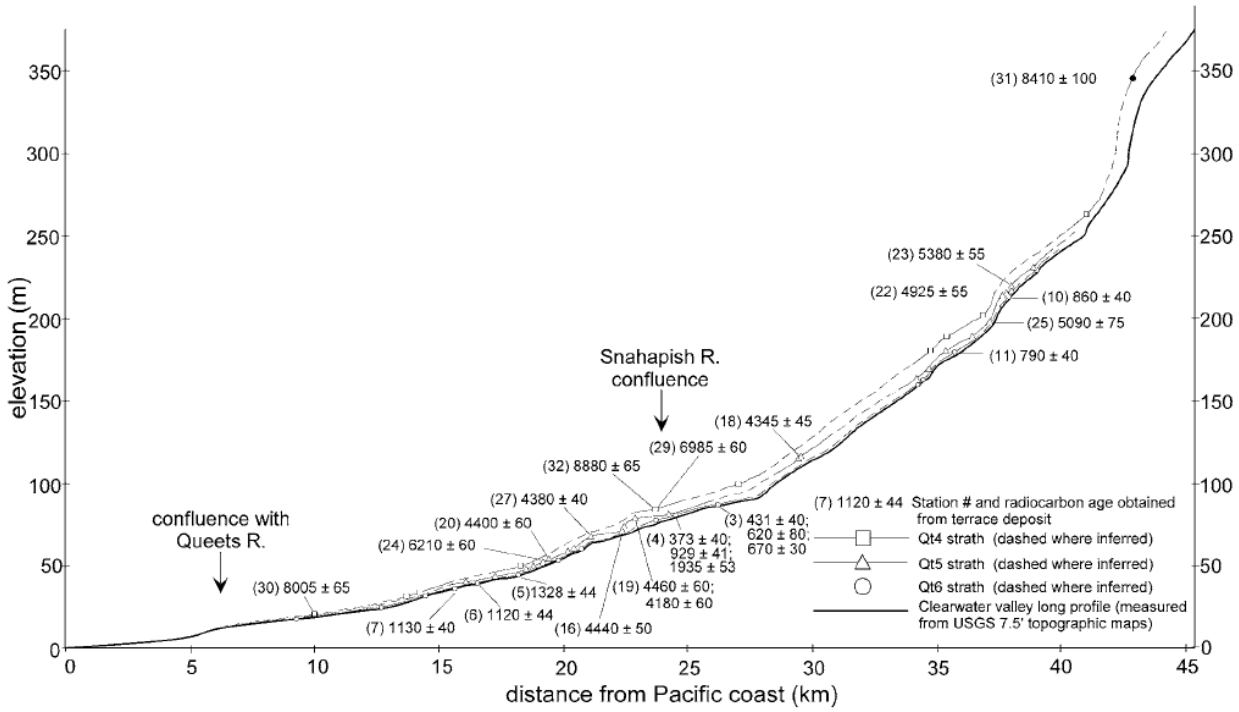

Stop 4 – Figure 9. Longitudinal valley profiles of the Clearwater River and Holocene terraces. The profiles were produced by orthogonally projecting elevation data to a vertical plane oriented down the middle of the Clearwater Valley. Plot does not show terrace Qt7, which essentially lies on the valley's long profile, or terrace Qt5/6, which cannot be clearly represented at this scale.

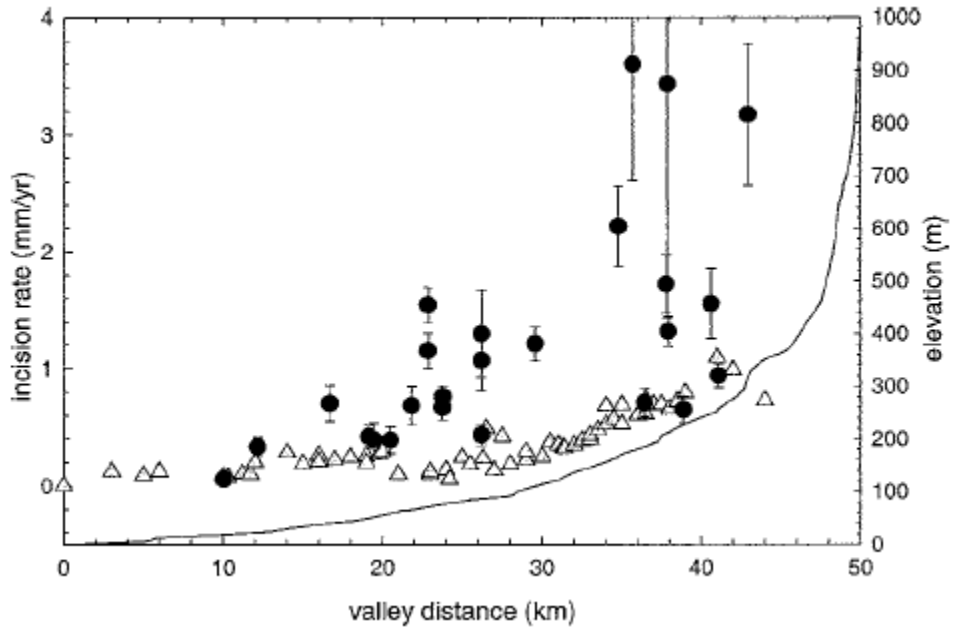

Stop 4 – Figure 10. Incision rates (left vertical axis) determined from Holocene terraces (solid black circles) and Pleistocene terraces (gray triangles – from Pazzaglia & Brandon, 2001) plotted with respect to distance along the valley's long profile (right vertical axis). Rates reflect calendar ages, and error bars on the Holocene data are 1-sigma standard error. Note that the incision rates for both data sets increase upstream.

Glaciation of the Western Olympic Peninsula

Glenn Thackray, Department of Geosciences, Idaho State University, Pocatello, Idaho 83209; thacglen@isu.edu.

Collaborators:
Tammy Rittenour, Utah State University
James Shulmeister, University of Queensland
Cianna Wyshnytzky, M.S. 2013, Utah State University
Katharine Marshall, M.S. 2013, Idaho State University
Amie Staley, M.S. 2015, Idaho State University

The major drainages of the western Olympic Peninsula preserve an extensive record of Middle and especially Late Pleistocene glaciation, and one of the most detailed chronologies of glacial events throughout the last glacial cycle. During the last glaciation, large mountain glaciers descended the Quinault, Queets, Hoh, and Bogachiel valleys several times, leaving an extensive geomorphic and sedimentologic record. Glaciers also descended major valleys on the northern, eastern, and southern flanks of the Olympic Mountains, and the Juan de Fuca and Puget lobes of the Cordilleran Ice Sheet impacted the northern and eastern flanks of the peninsula (Waitt and Thorson, 1983). On the western flank, the lack of ice sheet impacts, the presence of a modestly broad coastal plain, and the proximity to fluctuating Pacific shorelines have rendered the glacial record both well preserved and well exposed.

This field trip will examine evidence of western Olympic glaciation in the Quinault and Hoh valleys and in seacliffs at the mouth of the Queets valley (Fig. 1). We will focus particularly on stratigraphic exposures and new optically stimulated luminescence (OSL) and infrared stimulated luminescence (IRSL) ages that augment the existing radiocarbon chronology.

We will visit a dominant theme of western Olympic glaciation, namely the dominance of marine isotope stage (MIS) 5 through MIS 3 advances in the record. The MIS 2 advances were of far lesser extent than were the earlier advances, and, thus, the region preserves one of the most complete records of Late Pleistocene glacial events in western North America. This pattern appears to result from the dominant effects of Pacific Ocean climate on these maritime glaciers, and bears important implications for understanding the broader record of glaciation in western North America.

Previous Work

Excellent coastal and inland exposures and abundant organic deposits and fossil wood made the western Olympic Peninsula fertile ground for glacial-geologic and paleoecological studies in the 1960s through the 1990s. Recently, detailed glacial-stratigraphic techniques have permitted more detailed understanding of ice-marginal fluctuation. OSL and IRSL have allowed further geochronology, corroborating with and extending the existing radiocarbon chronology, and LiDAR topographic data have led to improved geomorphic mapping and recognition of previously unmapped ice marginal landforms (see Fig. 12 for examples).

Early work in the area focused on the broad-scale delineation of coastal glacial

landforms and inferred glacial events, as well as climatic influences on broad-scale glaciation. Porter (1964), determined average cirque-floor altitudes across the Olympic and Cascade Mountains, and inferred climatic influences on those patterns (Fig. 2). Crandell (1964, 1965) studied the glacial record of the western peninsula in reconnaissance, producing a regional map. Moore (1965) mapped glacial deposits of the Quinault River valley and surrounding areas and identified deposits of three glacial advances (Fig. 3). However, neither of these studies produced firm radiometric ages for deposits of the last glaciation. Heusser (1964, 1972, 1973, 1974, 1978), Florer (1972) and Heusser et al., (1999) analyzed fossil pollen from several peat deposits on the western side of the peninsula and reconstructed vegetation changes in the area for glacial and nonglacial intervals extending beyond 48,000 ^{14}C yr BP. Their work also produced a broad framework of radiocarbon dates for strata in seacliff exposures and for some inland features. Cong and Ashworth (1996) documented beetle assemblages from organic sediments in the seacliffs at Browns Point, north of Kalaloch, and interpreted paleoclimatic conditions from those assemblages (Stop 5, and Ashworth portion of this field guide).

The chronology of western Olympic glaciation has been derived largely from three projects in the 1990s and another since 2011, and the findings of those studies will be the subject of field trip discussion. Thackray (1996, 2001, 2008) described the geomorphology and stratigraphy of the Hoh and Queets valleys and the coastal stratigraphy and tectonic deformation between the Hoh and Raft rivers (1998). Gerstel and Lingley (2000) described similar geomorphologic and stratigraphic features in the Bogachiel valley and associated drainages. The fluvial and tectonic geomorphology of the unglaciated Clearwater Valley, which lies between Hoh and Queets valleys, was studied in detail by Pazzaglia and Brandon (2001), Pazzaglia et al. (2003), Wegmann (1999), Wegmann and Pazzaglia (2002), and Belmont et al., (2007) and will also be examined and discussed on this field trip.

The glacial geomorphology, stratigraphy, and geochronology of the Hoh, Queets, and Quinault valleys have been extended and updated through a project active since 2011, involving Idaho State University (Thackray, Marshall, Staley), Utah State University (Rittenour, Wyshnytzky), and the University of Queensland (Shulmeister). As noted, OSL and IRSL dating, improved radiocarbon dating methods, and newly available LiDAR topographic data have proven to be a boon to renewed study of the glacial sequences. Marshall (2015), identified two previously unidentified ice marginal sequences in the lowermost Hoh valley (Lyman Rapids A and B) and demonstrated MIS 5b(?) through MIS 4 ages for the Lyman Rapids A-C sequences (Fig. 4). She also refined the geomorphology of the MIS 3 Hoh Oxbow glacial sequence, and determined that two main ice limits date between 30-40 ka. Those results confirmed and extended the radiocarbon chronology of Thackray (2001). Staley (1915) revisited Quinault valley glaciation, a half-century after Moore's (1965) study. She delineated new details in the glacial geomorphology and produced a detailed OSL chronology, confirming the general nature of Moore's geomorphic sequence and documenting multiple MIS 5(?) through early MIS 3 advances (Fig. 5 and 12). She also determined an MIS 2 age for the youngest moraine in the sequence, which provides the sill for Lake Quinault. The Quinault glacial record and the post-glacial lacustrine record will be prominent subjects of this field trip. The Hoh and Quinault chronologies include similarly dominant MIS

5(?)-3 glacial events, though the two records also reveal important contrasts. In particular, the Hoh valley sequence includes late MIS 3 advances (ca. 40-30 ka) that are apparently missing in the Quinault valley record, while the Quinault sequence includes unique early MIS 3 advances (ca. 40-70 ka). Figure 11 summarizes the chronology.

Wyshnytzky (2013) and Wyshnytzky et al. (2015) documented the detailed glacial record of the South Fork Hoh valley, and produced an expanded and more detailed record of MIS 2 ice limits and associated stratigraphy (Fig. 6 and 7). Finally,

The western Olympic region has been the subject of several professional field trips since the 1990s, and portions of this guide are adapted from the associated field guides. Thackray and Pazzaglia (1994) and Pazzaglia et al. (2003) produced field guides associated with Geological Society of America meetings in Seattle, focused on glaciation, Clearwater fluvial evolution, and tectonic geomorphology. Thackray and Pazzaglia (1996) led a Friends of the Pleistocene field trip to the region with a similar focus. More recently, an Association of Women Geologists-Association of Engineering Geologists field trip examined aspects of engineering geology and hydrology of the region, as well as the glacial-interglacial stratigraphy (Gerstel et al., 2011).

Finally, the western Olympic Peninsula and the Olympic Peninsula in general have been the subject of numerous studies incorporating geomorphology, thermochronology, geophysics, and Quaternary geology, and there is an extensive literature. These include a) influences of large woody debris, natural and introduced, on major rivers, as well as associated engineering projects (Tim Abbe and others), b) landslide hazard and mitigation (Tom Badger and Washington DOT, Wendy Gerstel), c) soil hydrology (Casey Hanell and others, Washington Department of Natural Resources), d) linkages between geomorphology and anadromous fish (David Montgomery and others) and e) exhumation history of the Olympic uplift (Mark Brandon and others). There are many others—this is in no way an exhaustive list!

References Cited (or not cited but relevant)

Baldwin, E.M., 1939, Late-Cenozoic diastrophism along the Olympic Coast: Unpublished M.S. Thesis, State College of Washington, 46 pp.

Belmont, Patrick, F. J. Pazzaglia, and John C. Gosse. "Cosmogenic 10 Be as a tracer for hillslope and channel sediment dynamics in the Clearwater River, western Washington State." *Earth and Planetary Science Letters* 264.1 (2007): 123-135.

Crandell, D. R., 1964, Pleistocene glaciations of the southwestern Olympic Peninsula, Washington: U. S. Geological Survey Professional Paper 501-B, p. B135-B139.

Crandell, D. R., 1965, The glacial history of western Washington and Oregon *in* H. E. Wright and D. G. Frey (eds.). The Quaternary of the United States. Princeton University Press, p. 341-353.

Florer, L. E., 1972, Quaternary paleoecology and stratigraphy of the sea cliffs, western Olympic Peninsula, Washington: Quaternary Research, v. 2, p. 202-216.

Gerstel, W., Badger, T., Hanell, C., Thackray, G., Abbe, T., Shelmerdine, W., and Walsh, T. 2011. Glaciations, tectonics, slope and river processes within large western Peninsula drainages and beach bluffs near Kalaloch. Association of Environmental

and Engineering Geologists/Association For Women Geoscientists Guidebook. http://www.aegwashington.org/media/fieldtrips/2011/2011_FT_Guidebook.pdf
Gerstel, W.J., Lingley, W.S.J., 2000, Geologic Map of the Forks 1:100,000 Quadrangle, Washington, *Washington Division of Geology and Earth Resources, Open File Report 2000-4*, scale 1:100,000.
Heusser, C. J., 1964, Palynology of four bog sections from the western Olympic Peninsula, Washington: Ecology, v. 45, p. 23-40.
Heusser, C. J., 1972, Palynology and phytogeographical significance of a late Pleistocene refugium near Kalaloch, Washington: Quaternary Research, v. 2, p. 189-201.
Heusser, C. J., 1973, Environmental sequence following the Fraser advance of the Juan de Fuca lobe, Washington Quaternary Research, v. 3, p. 284-306.
Heusser, C. J., 1974, Quaternary vegetation, climate, and glaciation of the Hoh River Valley, Washington, Geological Society of American Bulletin, v.85, p.1547-1560.
Heusser, C.J., 1978, Palynology of Quaternary deposits of the lower Bogachiel River area, Olympic Peninsula, Washington: Canadian Journal of Earth Sciences, v. 15, p. 1568-1578.
Heusser, C.J., Heusser, L.E., Peteet, D.M., 1999, Humptulips revisited: a revised interpretation of Quaternary vegetation and climate of western Washington, USA, *Paleogeography, Paleoclimatology, and Paleoecology,* 150, 191-221.
Marshall, K.J., 2013, Expanded Late Pleistocene glacial chronology for Western Washington, U.S.A and the Wanaka-Hawea Basin, New Zealand, using luminescence dating of glaciofluvial outwash, *M.S. Thesis Idaho State University*.
Pazzaglia, F. J. and Brandon, M. T., **2001**, A fluvial record of long-term steady-state uplift and erosion across the Cascadia forearc high, western Washington State: American Journal of Science, v. 301, no. 4-5, p. 385-43.
Pazzaglia, F.J., Thackray, G.D., Brandon, M.T., Wegmann, K.W., Gosse, J., McDonald, E., Garcia, A.F., and Prothero, D., 2003,Tectonic geomorphology and the record of Quaternary plate boundary deformation in the Olympic Mountains, *in* Swanson, T.W., ed., Western Cordillera and adjacent areas: Boulder, Colorado, Geological Society of America Field Guide 4, p. 37–67.
Porter, S.C., 1964, Composite Pleistocene snow line of Olympic Mountains and Cascade Range, Washington, *Geological Society of America Bulletin,* 75, 477-482.
Rau, W. W., 1973, Geology of the Washington coast between Point Grenville and the Hoh River: Washington Department of Natural Resources, Geology and Earth Resources Division Bulletin 66, 58 pp.
Rau, W. W., 1975, Geologic map of the Destruction Island and Taholah quadrangles, Washington: Washington Department of Natural Resources, Geology and Earth Resources Division Map GM-13, scale 1:62,500.
Staley, A.E., 2015, Glacial Geomorphology and Chronology of the Quinault Valley, Washington, and Broader Evidence of Marine Isotope Stages 4 and 3 Glaciation Across Northwestern United States, *M.S. Thesis, Idaho State University.*
Tabor, R.W., and Cady, W.M., 1978, Geologic map of the Olympic Peninsula: U.S. Geological Survey Map I-994, 2 sheets, scale 1:125,000.
Thackray, G.D., 1996, Glaciation and neotectonic deformation on the western Olympic Peninsula, Washington [Ph.D. dissertation]: Seattle, Washing- ton, University of Washington, 139 p.

Thackray, G.D., 1998, Convergent-margin deformation of Pleistocene strata on the Olympic coast of Washington, USA, *in* Stewart, I.S., and Vita-Finzi, C., eds., Coastal tectonics: Geological Society [London] Special Publication 146, p. 199–211.

Thackray, G.D., 2001, Extensive Early and Middle Wisconsin glaciation on the western Olympic Peninsula, Washington, and the variability of Pacific moisture delivery to the northwestern United States: Quaternary Research, v. 55, p. 257–270.

Thackray, G. D. (2008). Varied Climatic and Topographic Influences on Late Pleistocene mountain glaciation in the western United States. *Journal of Quaternary Science*, 23(6): 671-681.

Thackray, G.D. and F.J. Pazzaglia. 1994. Quaternary stratigraphy, tectonic geomorphology, and fluvial evolution of the western Olympic Peninsula, Washington, *in* D.A. Swanson and R.A. Haugerud, eds., Geologic Field Trips in the Pacific Northwest, Geological Society of America Annual Meeting, Seattle, Washington, v. 2, p. A1-29.

Thackray, G.D and F.J. Pazzaglia. 1996. Quaternary Glaciation and Tectonism on the Western Olympic Peninsula, Washington. Guidebook for the Friends of the Pleistocene, Third Annual Pacific Northwest Cell Field Conference.

Waitt, R.B. and R.M. Thorson. 1983. The Cordilleran ice sheet in Washington, Idaho, and Montana, in S.C. Porter, ed., Late Quaternary Environments of the United States; Volume 1: The Late Pleistocene. University of Minnesota Press, p. 53-70.

Wegmann, K.W., 1999, Late Quaternary fluvial and tectonic evolution of the Clearwater River basin, western Olympic Mountains, Washington State [M.S. thesis]: Albuquerque, University of New Mexico, 217 p.

Wegmann, K.W., and Pazzaglia, F.J., 2002, Holocene strath terraces, climate change, and active tectonics: The Clearwater River basin, Olympic Peninsula, Washington State: Geological Society of America Bulletin, v. 114, p. 731-744.

Wyshnytzky, C.E., 2013, Constraining ice advance and linkages to paleoclimate of two glacial systems in the Olympic Mountains, Washington and the Southern Alps, New Zealand, *M.S. Thesis Utah State University*.

Wyshnytzky, C.E., Rittenour, T.M., Nelson, M.S., Thackray, G.D., 2015, Luminescence dating of Late Pleistocene proximal glacial sediments in the Olympic Mountains, Washington, *Quaternary International,* 362, 116-123.

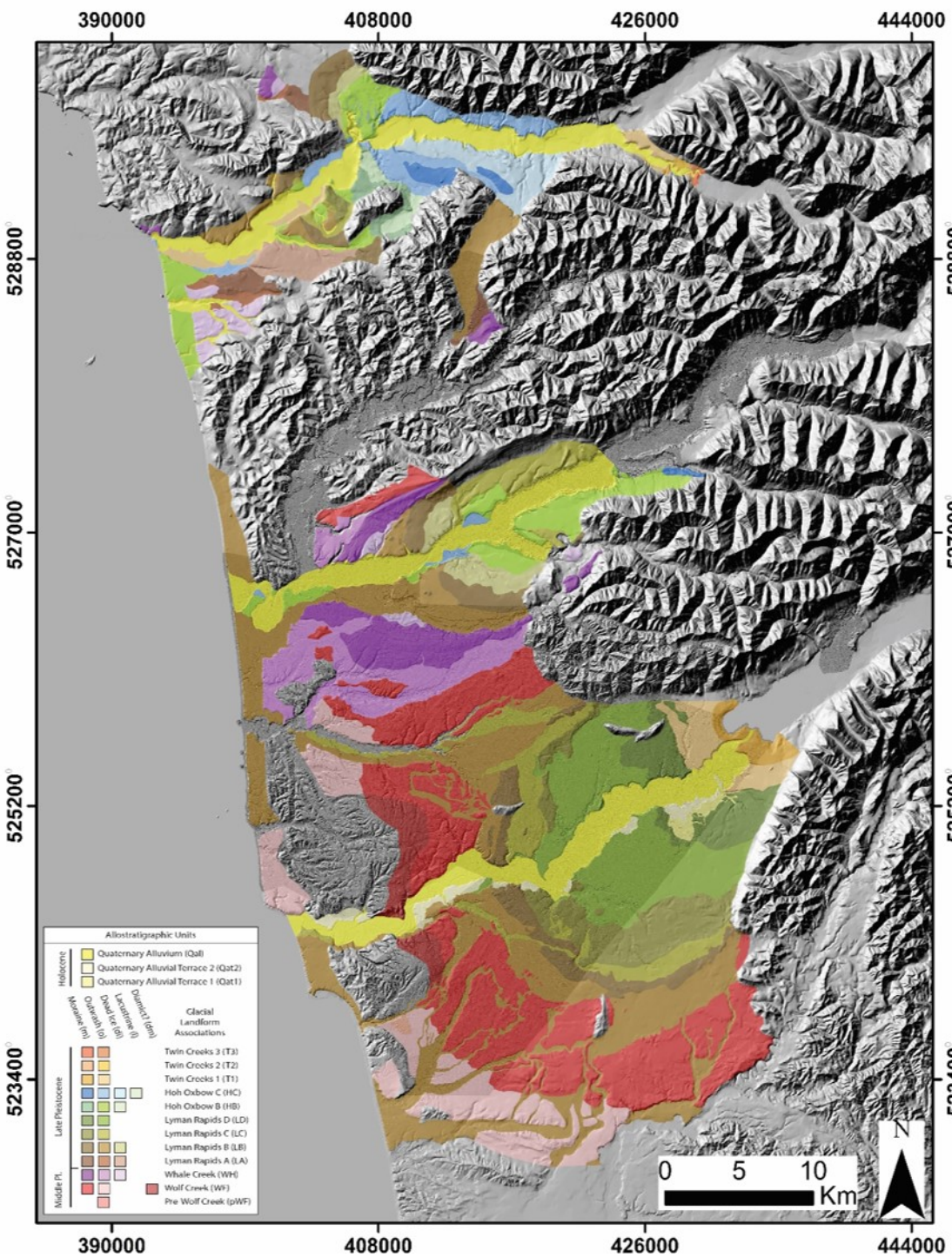

Figure 1. Map of glacial landforms in the Hoh, Queets, and Quinault valleys. Incorporates mapping by Thackray, 1996, 2001; Marshall, 2013; Wyshnytzky, 2013; and Staley, 2015, and builds upon early work by Moore (1965) in the Quinault valley.

Figure 2 (following page(s)). Map and profiles of cirque floor altitudes across the Olympic and Cascade Mountains. From Porter (1964)

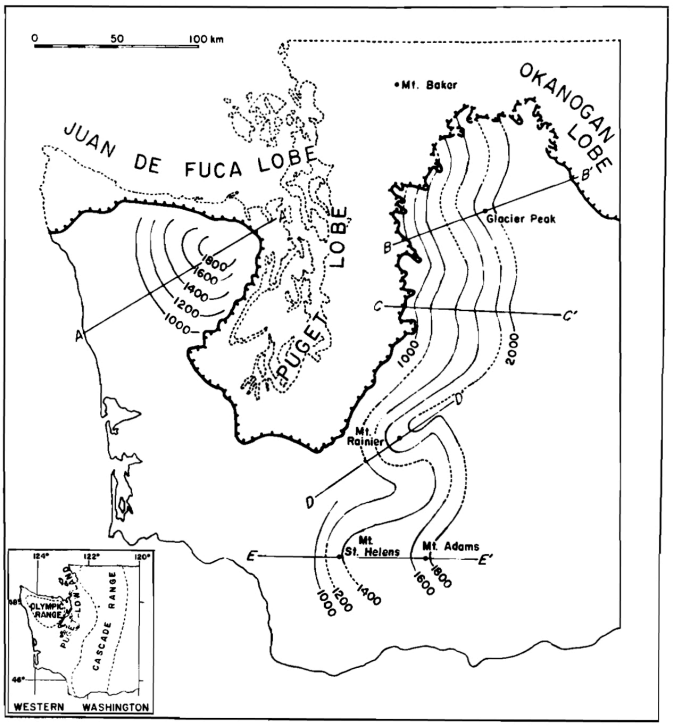

Figure 1. Form lines connecting the floors of lowest north-facing Pleistocene cirques in the Olympic and Cascade ranges (altitudes in meters). Form lines are dashed where control is poor or source is unreliable. Southern limit of Canadian ice during latest (Vashon) glaciation shown by heavy ticked line (dashed where poorly known).

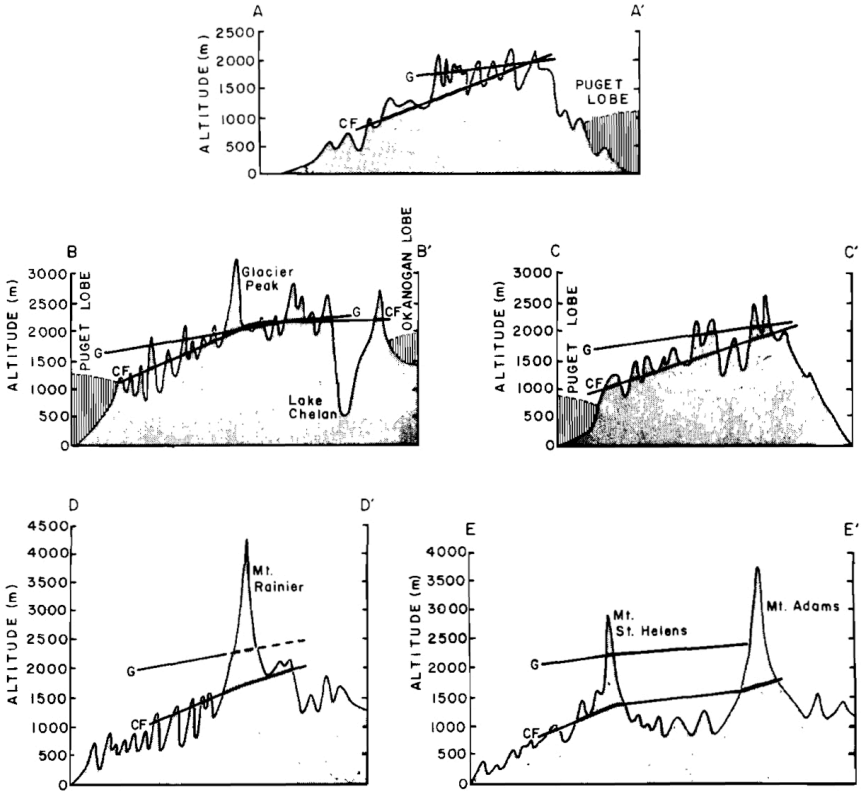

Figure 3. Sections across the Olympic and Cascade ranges comparing altitudes of small modern glaciers (G) with altitudes of lowest north-facing Pleistocene cirque floors (CF)

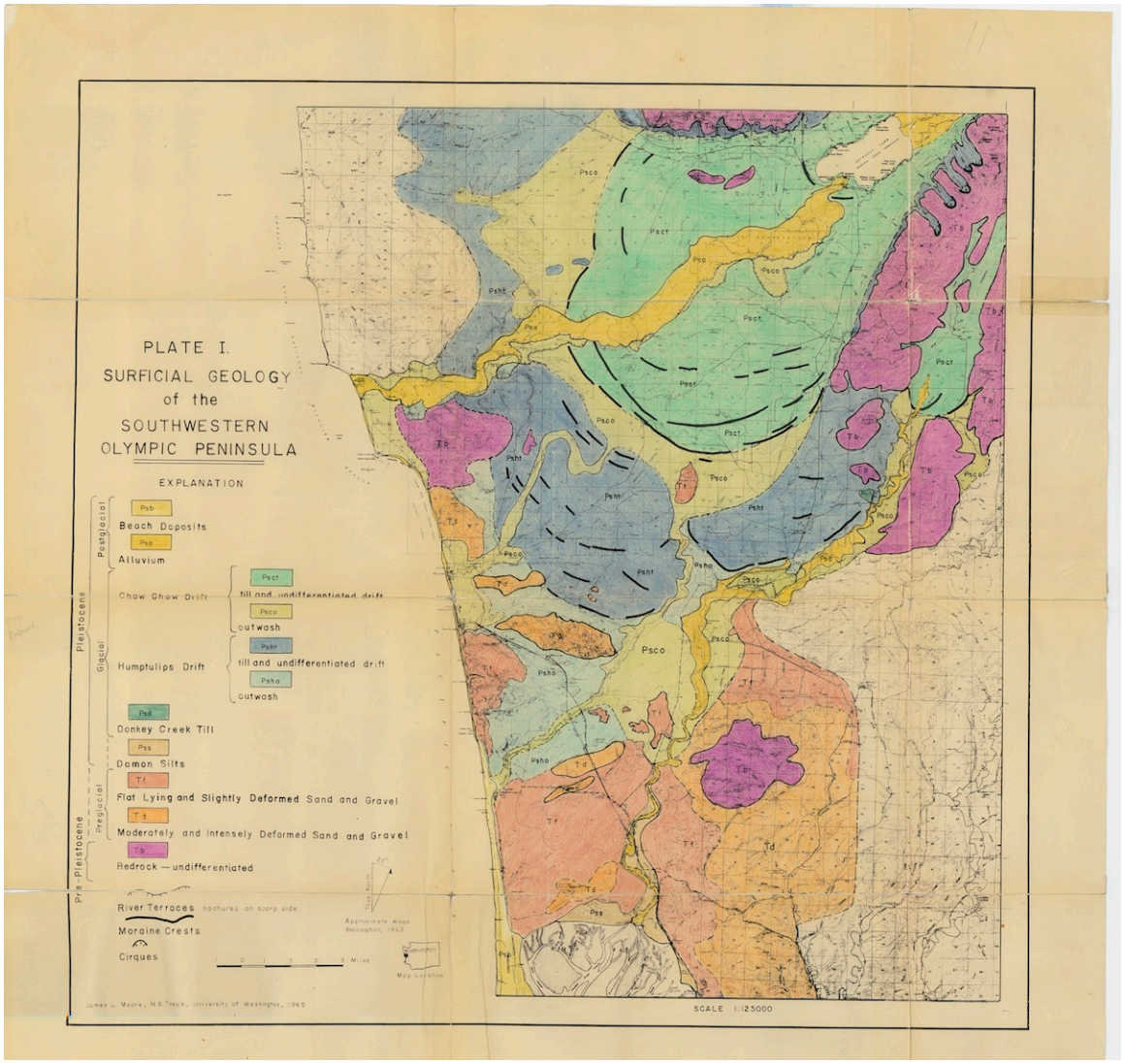

Figure 3. Surficial geologic map of the Quinault valley and surrounding areas. From Moore (1965), University of Washington MS thesis.

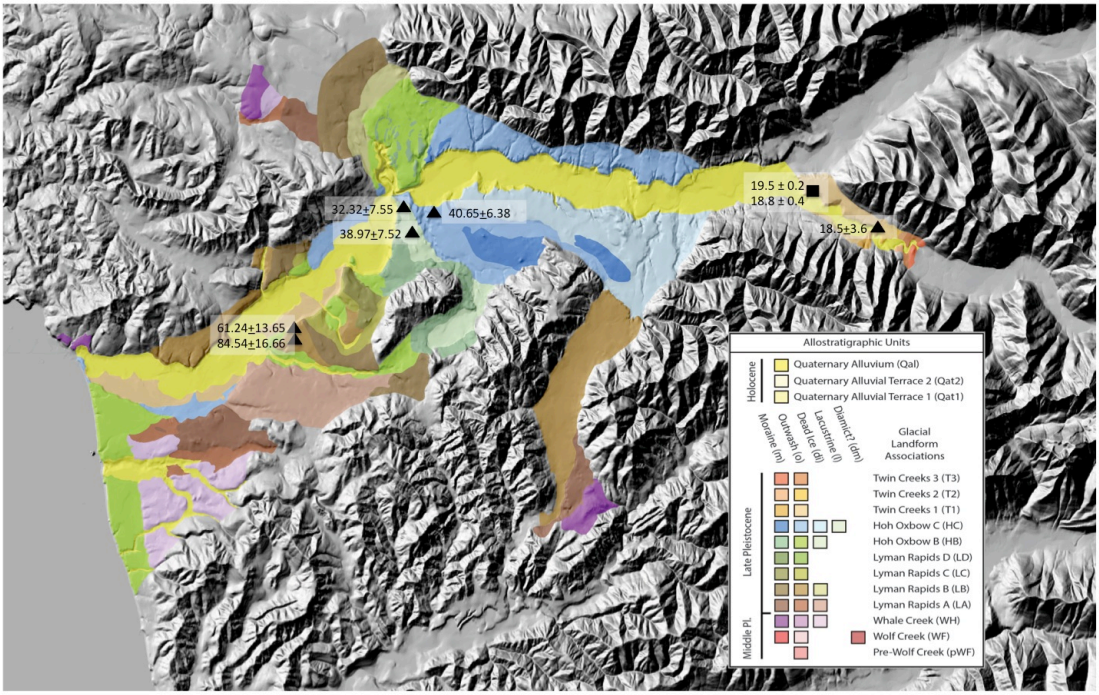

Figure 4. Map of glacial landforms in the Hoh valley, with OSL and radiocarbon ages pertinent to surficial map units. Note that numerous additional radiocarbon and OSL dates constrain the ages of units buried in the valley and coastal stratigraphy and provide a detailed chronology of ice fluctuations. This figure incorporates mapping and geochronology from Thackray, 1996 and 2001, Marshall, 2013, Wyshnytzky, 2013, and Wyshnytzky et al., 2014.

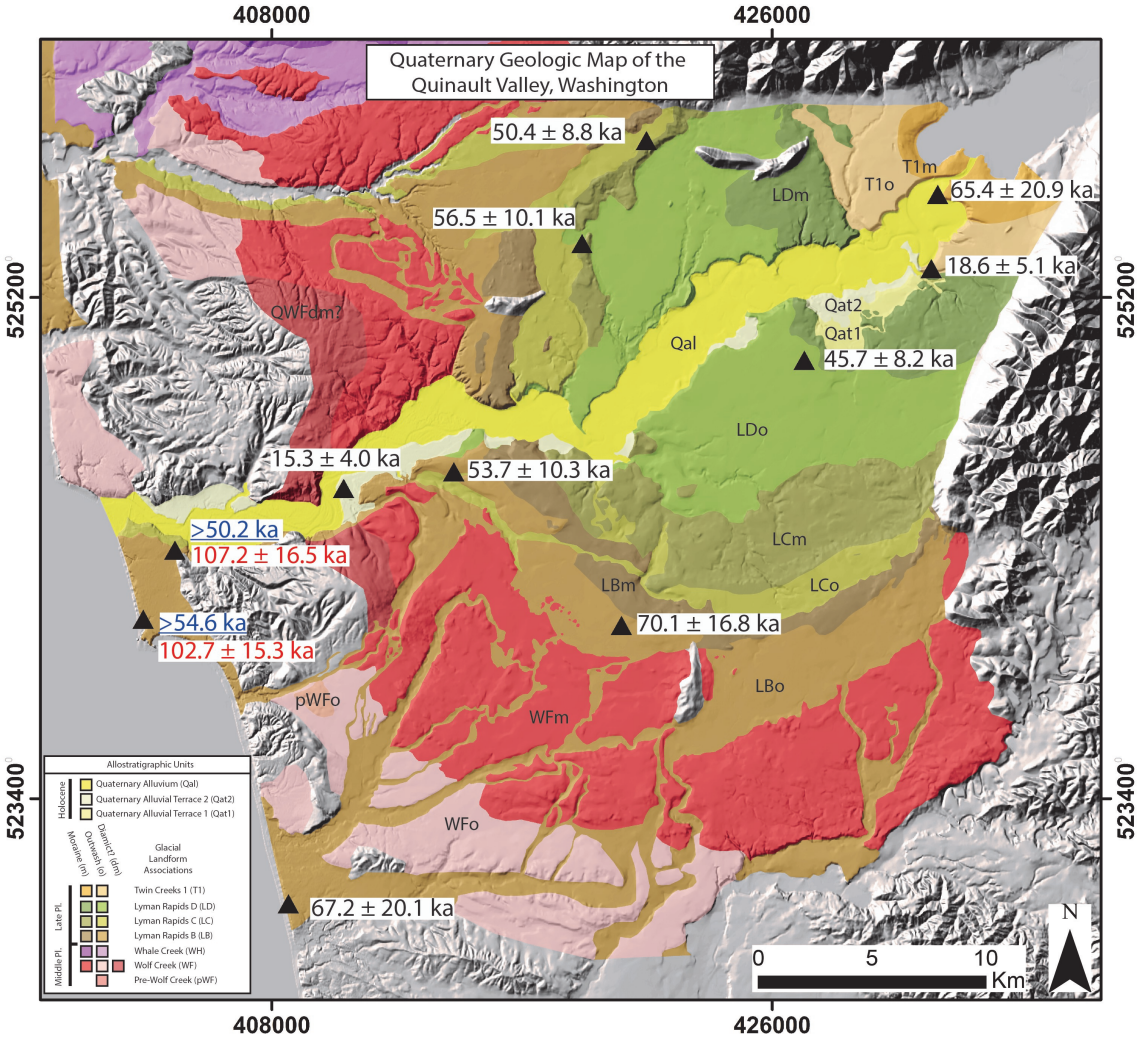

Figure 5. Map of glacial landforms in the Hoh valley, with OSL and radiocarbon ages pertinent to surficial map units. Note that numerous additional radiocarbon and OSL dates constrain the ages of units buried in the valley and coastal stratigraphy and provide a detailed chronology of ice fluctuations. This figure incorporates mapping and geochronology from Staley (2015) in the Quinault valley and Thackray, 1996, 2001, and Marshall, 2013, for the Queets valley.

Figures 6 and 7. Stratigraphy and geochronology of the South Fork Hoh valley, are included as Figures 1a and 1b in the roadlog description for Stop 7.

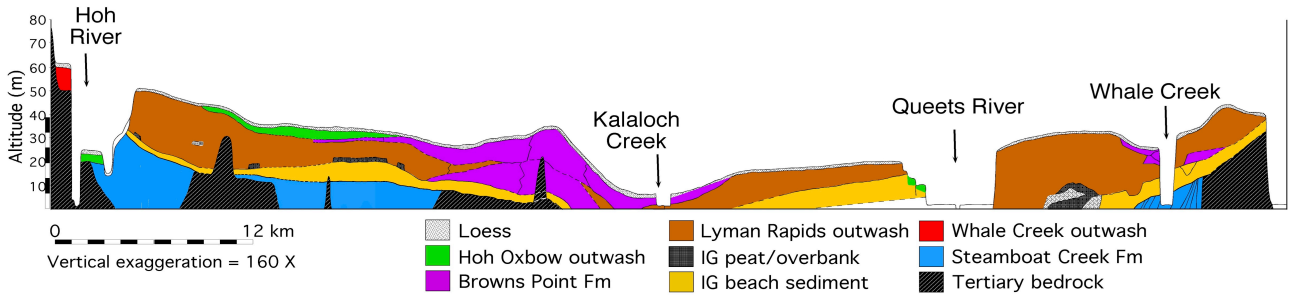

Figure 8. Generalized seacliff stratigraphy between the Hoh and Raft rivers. North is to the left. Note extreme vertical exaggeration.

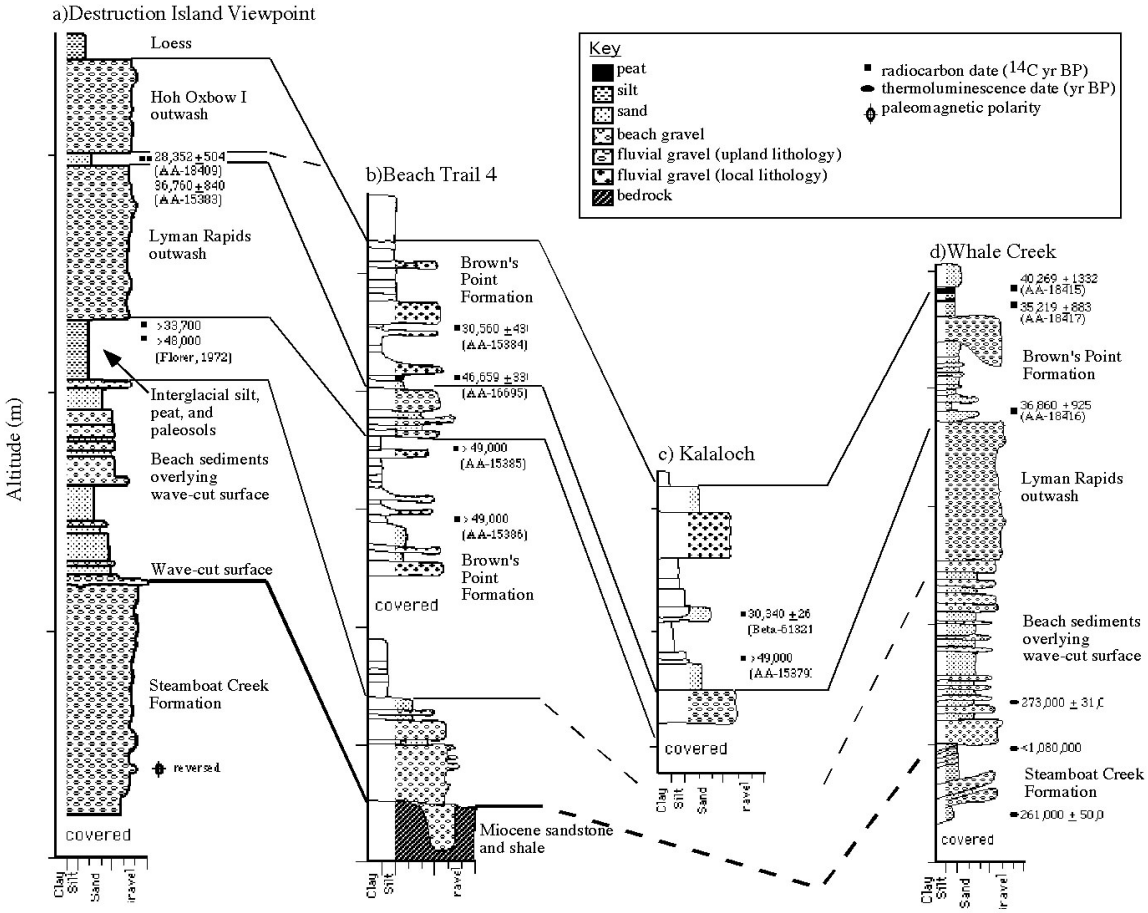

Figures 9 and 10 (combined). Correlated stratigraphy and radiocarbon geochronology of four prominent coastal exposures between the Hoh and Raft Rivers. See Figure 8 for reference. Stop 2 (Whale Creek) and Stop 6 (Kalaloch) will reference these figures. From Thackray (1996 and 1998).

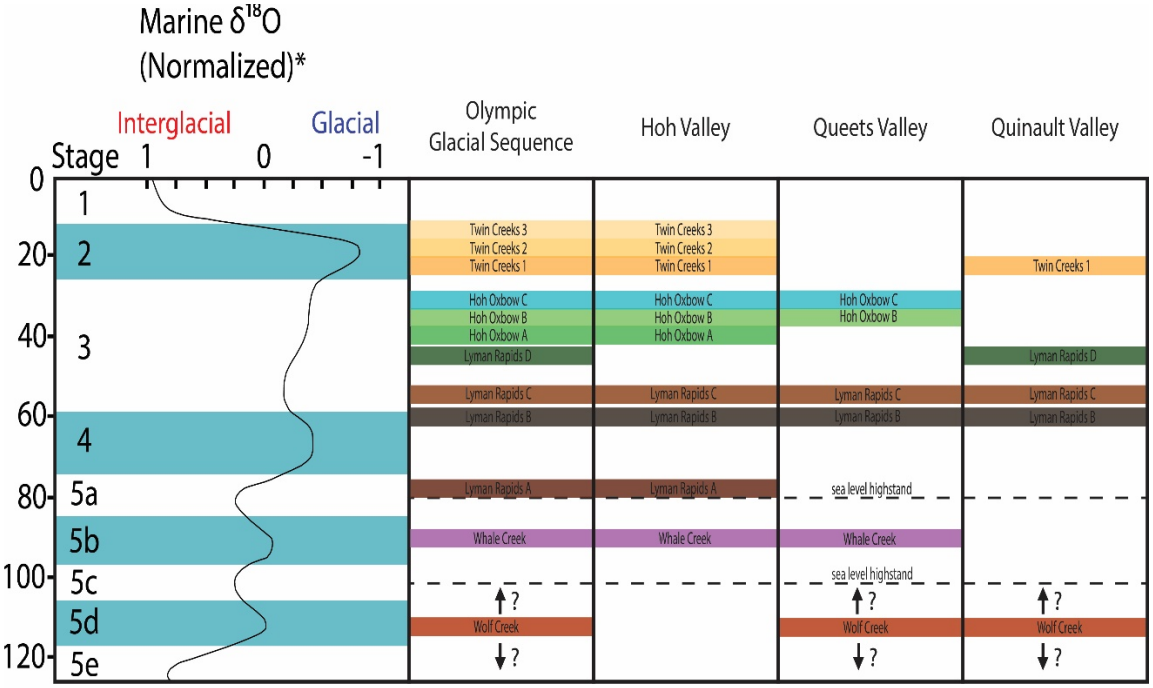

Figure 11. Standard Marine Isotope Stage Curve (Kaufman *et al.,* 2003, data from Martinson, 1987) modified to include western Olympic valley glacial sequence from Thackray (1996, 2001), Marshall (2013), Wyshnytzky (2013), Wyshnytzky et al. (2015), and Staley (2015). Vertical scale is in tens of thousands of years.

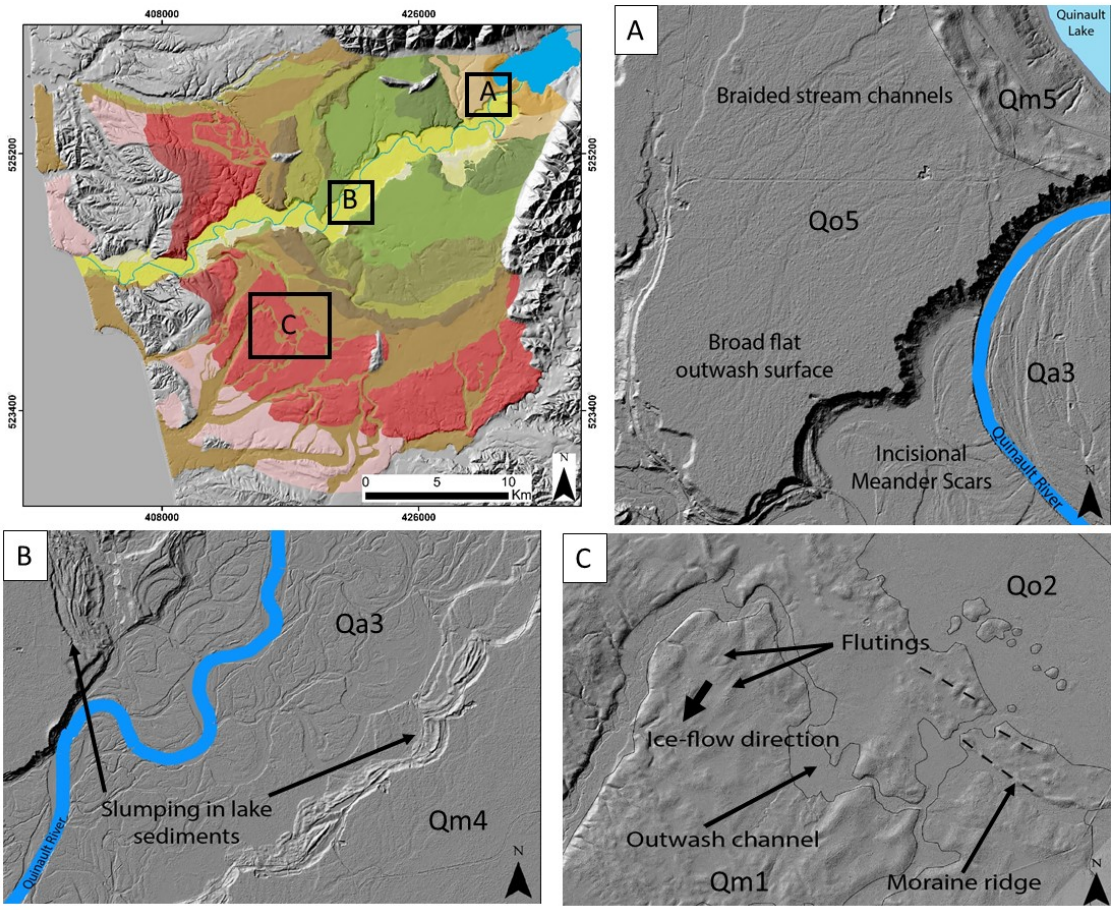

Figure 22. Key landforms identified from the 1-m bare-Earth LiDAR in the Quinault valley, Washington. A) Moraine-outwash pair at head of the lower Quinault River. Paleo braided streams are apparent. B) Slumping along the southern bank of Quinault River, indicating distribution of buried lake sediments. C) Flutings, paleo outwash channel, and individual moraine ridges. Paleo ice-flow direction is inferred based on fluting orientation. (Figure 2.3 of Staley, 2015).

Stop 8. Evidence for Post-glacial Surface Rupture on the Lake Creek—Boundary Creek Fault from Chirp Seismic Investigations at Lake Crescent

Karl Wegmann[1], DelWayne Bohnenstiehl[1], and Elana Leithold[1] & Patrick Pringle[2]

[1] Dept. of Marine, Earth, and Atmospheric Sciences, North Carolina State University
[2] Dept. of Science, Centralia College

Excerpted from:
Wegmann, K.W., Bohnenstiehl, D.R., Leithold, E.L., and Pringle, P., in prep, Holocene earthquakes on the Lake Creek-Boundary Creek Fault revealed by Chirp seismic investigations of Lake Crescent, Washington: Bulletin of the Seismological Society of America.

Improving the estimates of sizes, recurrence intervals, and effects of late Quaternary earthquakes in the Puget Sound region is one of the priority research topics for the Pacific Northwest hazards community. Herein we present preliminary evidence supporting the hypothesis that the Lake Creek – Boundary Creek Fault (LCBCF) has experienced multiple post-glacial rupture events at Lake Crescent, Washington (Figure 1). One or more of these events is likely to have triggered rock avalanches, drainage reorganization, and isolation of aquatic species. The LCBCF is an east-west trending oblique slip fault on the northern flank of the Olympic Peninsula near the town of Port Angeles. The LCBCF is one of a number of steeply-dipping crustal faults in the Puget Sound region recognized primarily in the past decade or so as exhibiting evidence for latest Pleistocene - Holocene surface rupture based on the evaluation of high-resolution lidar-derived digital elevation models (Haugerud, 2002; Polenz et al., 2004; Schasse et al., 2004) and subsequent fault trenching investigations (Nelson et al., 2007). The LCBCF is one of several fault zones in the Puget Sound region accommodating north-south contraction and clockwise rotation of the western Washington portion of the Cascadia forearc (e.g., Wells et al., 1998).

In the summer of 2013 we acquired 75 km of chirp seismic reflection imagery for Lake Crescent for the purpose of identifying whether or not the sediments in this lake preserve a paleo-earthquake record (Wegmann et al., 2014). From this data we observe stratigraphic evidence for as many as five deformation events in proximity to the trace of the LCBCF, where lacustrine sediments are folded and faulted, and the amplitude of folding increases with depth across seismic event horizons. In addition, sediment thickness between event horizons remains relatively uniform, suggesting that this fault might exhibit a characteristic earthquake recurrence interval, assuming that the average sediment accumulation rate has remained constant between earthquake events. We also observe several large subaqueous mass-wasting deposits along the lake margins that are traceable upslope to previously mapped subaerial rock avalanches. Importantly, the thickness of lacustrine sediment that has accumulated on top of the subaqueous mass-wasting deposits is the same as that which has accumulated since the last earthquake event along the trace of the fault, suggesting that these rock avalanches were seismically triggered by the LCBCF, perhaps in the past few thousand years. This most recent earthquake and rock avalanche may be recorded in the oral history of local Native American tribes.

Lake Crescent is a deep glacially-carved lake occupying portions of two steep-sided fault-controlled valleys (Figure. 2; Tabor, 1975). Mountain peaks rise up to 1,370 m (4,500 ft) from the bottom of the Lake, the bottom of which, at 190 m deep, is several tens of meters below sea level. The lake dates to c.14 ka, following retreat of the Juan de Fuca lobe of the Cordilleran ice sheet to the east (Heusser, 1973; Polenz et al., 2004; Wegmann et al., 2012). Lakes Crescent and Sutherland share a common heritage, as they were one lake into the middle-to-late Holocene (Tabor, 1975; Logan and Schuster, 1991). Several large rockslide-avalanche deposits are mapped along the trace of the LCBCF between the Elwha River and Lake Crescent (Brown et al., 1960; Logan and Schuster, 1991; Schasse, 2003), and field evidence indicates that the deep ancestral lake was divided into two parts by coalescing rock avalanches from the north and south side of the valley, which altered the regional drainage pattern. We believe it is likely that these rock avalanches generated a lake tsunami, as has been recorded in other settings where rapidly-moving rock masses enter deep bodies of water (e.g., the 1963 Vajont dam disaster in Italy (Hendron & Patton, 1987), Lake Geneva in AD 563 (Kremer et al., 2012), and in glacial fiords in Alaska (Miller, 1960) and Chile (Lastras et al., 2013).

Ancestral Lake Crescent drained east along the trace of the LCBCF to the Strait of Juan de Fuca via Indian Creek and the Elwha River (Fig. 2). Following the blockage of this drainage by the Lake Southerland and possibly also by the Mount Storm King rockslide complexes, the water level in Lake Crescent rose 25 m (80 ft) until it overtopped a low divide in the Boundary Creek valley (Fig. 2). Lake Crescent now drains to salt water via the Lyre River. In 2010, we radiocarbon dated growth rings from a drowned tree that is rooted in 18 m (60 ft) of water from the west end of Lake Crescent to 4,340 ± 50 calendar years before present (Pringle et al., 2010). This initial date is our present estimate for the most recent earthquake along the Lake Crescent section of the LCBCF. A more recent landslide found along the north shore of Lake Crescent contains submerged upright tree trunks, one of which was dated to 280 ± 60 ^{14}C ybp (Logan and Schuster, 1991), providing a potential temporal overlap with the last megathrust event in AD 1700 on the Cascadia Subduction zone.

Seismic Evidence for Multiple LCBCF Earthquakes: In 2013 we collected ~75 km of Chirp seismic imagery from Lake Crescent using an Edgetech SB-512i system towed near the surface using a small catamaran system. Examples of undeformed lacustrine sediments from the west and east basins of Lake Crescent are shown on Figure 3. We recognize and are able to correlate a thick (1-2 m), seismically transparent mass wasting deposit (MWD – Unit B on Fig. 3) across the entire lake. Undeformed, finely layered sediments drape the MWD (Unit A on fig. 3). Seismic stratigraphy is observed to depths of 20 m beneath the lake bottom (e.g., Line D, Fig. 3), and our initial interpretation is that the gross stratigraphic architecture is controlled by periodic MWDs correlated to landslides and underwater slumps within the lake basin. Importantly, we are able to correlate the interpreted MWD layers across the two basins of the lake, suggesting that they are not localized features. This observation informs ***our hypothesis*** that a complete (?) late Pleistocene through Holocene record of surface rupture on the LCBCF is recorded in the MWD event layers of Lake Crescent. In order to test this hypothesis we have recently (last week) cored and will radiocarbon date sediments from Lake Crescent

in collaboration with colleagues at the National Lacustrine Core Facility at the University of Minnesota (LacCore).

In Figure 4 we present seismic reflection evidence suggesting that at least **five** earthquake rupture events (E1 – E5) are recorded in the upper 10 to 15 m of Lake Crescent sediments. We observe distinct disruption, folding, and offset of seismic layers across the trace of the main strand and splay of the LCBCF zone beneath the east basin of the lake (Fig. 2 & 4). Our interpreted Event Layer 1 (EV1) is the same thick, seismically-transparent MWD unit (B) shown on Lines A & B (Fig. 3) and observed all across the lake. The EV1-MWD layer is capped by undeformed sediments of seismic Unit A. Thus, we believe that the basal age of Unit A will provide a limiting constraint on the timing of the most recent earthquake on the LCBCF. We predict that the base of seismic Unit A will date to ~ 4,200 cal year before present.

Several of our seismic transects crossed subaqueous portions of the rock avalanche deposits. Seismic Line C (Fig. 4) is one such line. Here we observe several 10s of meters of topography across the rock avalanche deposit. Inter-deposit depressions have collected lacustrine sediments since emplacement. Importantly, from these small depositional basins we observe only ~ 2 m of undeformed stratified sediments, very similar in appearance to seismic Unit A. We do not observe the seismically transparent MWD unit B on top of the rock avalanche deposits, suggesting that they occurred in response to the last earthquake event on the LCBC Fault. Alternatively, the rock avalanches could have been triggered by a different source such as upper crustal faults in the Puget Sound region (e.g., Sherrod & Gomberg, 2014 and references therein), or by the 1700 AD or prior megathrust events on the subduction interface (e.g., Atwater & Hemphill-Haley, 1997; Goldfinger et al., 2012; Enkin et al., 2013). Seismically-triggered rock avalanches are well known from the eastern Olympic Mountains, where a number of them appear to have been triggered by one or more earthquakes about 1000 years before present (e.g., Schuster et al., 1992; Logan et al., 1998).

Earthquakes that triggered rockslides are important mechanisms for the isolation and genetic diversity of aquatic organisms. Waterfalls along the Lyre River prevent anadromous fish from migrating into Lake Crescent to spawn. Anadromous ancestral populations of rainbow, now known as the Beardslee Trout (*Oncorhynchus mykiss irideus f. beardsleei*) and coastal cutthroat trout (*Oncorhynchus clarki clarki f.crescentii*) were isolated in Lake Crescent during the lake-separating mass wasting event, and have since become genetically distinct from non-isolated regional populations (Meyer & Fradkin, 2002; Brenkman et al., 2014).

Brown, Grower, and Snavely (1960) and Tabor (1975) both recognized that Lakes Crescent and Sutherland were separated by a major landslide and that this landslide may have been triggered by a seismic. There is also Native American oral history that might record this earthquake-triggered landslide event. A Quileute legend purports that during a great battle between the Clallam and Quileute nations, *"…after watching the bloodshed for two long days, Mount Storm King became angry. On the third day he broke off a great piece of rock from his head and hurled it down into the valley killing all who were fighting… (T)hrough the valley flowed a small river. The rock hurled by Mount Storm King dammed this stream*" (Clark 1953).

References:

Atwater, B.F., and Hemphill-Haley, E., 1997, Recurrence intervals for great earthquakes of the past 3,500 years at northeastern Willapa Bay, Washington, U.S. Geological Survey Professional Paper 1576: Reston, VA, U.S. Geological Survey, p. 108.

Blakely, R.L., Sherrod, B.L., Wells, R.E., Weaver, C.S., McCormack, D.H., Troost, K.G., and Haugerud, R.A., 2004, The Cottage Lake aeromagnetic lineament: possible onshore extension of the southern Whidbey Island fault, Washington: U.S. Geological Survey Open-File Report 04-1204, v. 1.1, 60 p.

Brenkman, S.J., Duda, J.J., Kennedy, P.R., and Baker, B.M., 2014, A legacy of divergent fishery management regimes and the resilience of rainbow and cutthroat trout populations in Lake Crescent, Olympic National Park, Washington: Northwest Science, v. 88, p. 280-304.

Brown, R.D., Jr., Gower, H.D., and Snavely, P.D., Jr., 1960, Geology of the Port Angeles–Lake Crescent area, Clallam County, Washington, Oil and Gas Investigations Map OM-203: Washington, D.C., U.S. Geological Survey.

Clark, E.E., 1953, Indian legends of the Pacific Northwest: Berkeley, University of California Press.

Enkin, R.J., Dallimore, A., Baker, J., Southon, J.R., and Ivanochko, T., 2013, A new high-resolution radiocarbon Bayesian age model of the Holocene and Late Pleistocene from core MD02-2494 and others, Effingham Inlet, British Columbia, Canada; with an application to the paleoseismic event chronology of the Cascadia Subduction Zone1: Canadian Journal of Earth Sciences, v. 50, p. 746-760.

Goldfinger, C., Nelson, C.H., Morey, A., Johnson, J.E., Gutierrez-Pastor, J., Eriksson, A., Karabanov, E., Patton, J., Gracia, E., and Enkin, R., 2012, Turbidite event history: Methods and implications for Holocene paleoseismicity of the Cascadia subduction zone, US Department of the Interior, US Geological Survey.

Haugerud, R., 2002, Lidar evidence for Holocene surface rupture on the Little River fault near Port Angeles, Washington [abstract]: Seismological Research Letters, Volume 73, p. 249.

Hendron, A.J., and Patton, F.D., 1987, The Vaiont slide—a geotechnical analysis based on new geologic observations of the failure surface: Engineering Geology, v. 24, p. 475-491.

Heusser, C.J., 1973, Environmental sequence following the Fraser advance of the Juan de Fuca lobe, Washington: Quaternary Research, v. 3, p. 284-306.

Kremer, K., Simpson, G., and Girardclos, S., 2012, Giant Lake Geneva tsunami in ad 563: Nature Geoscience, v. 5, p. 756-757.

Lastras, G., Amblas, D., Calafat, A.M., Canals, M., Frigola, J., Hermanns, R.L., Lafuerza, S., Longva, O., Micallef, A., and Sepúlveda, S.A., 2013, Landslides Cause Tsunami Waves: Insights From Aysén Fjord, Chile: Eos, Transactions American Geophysical Union, v. 94, p. 297-298.

Lidke, D.J., Johnson, S.Y., McCrory, P.A., Personius, S.F., Nelson, A.R., Dart, R.L., Bradley, L.-A., Haller, K.M., and Machette, M.N., 2003, Map and data for Quaternary faults and folds in Washington State: US Geological Survey Open-File Report 03-0428, 15p., 1 pl.

Logan, R.L., and Schuster, R.L., 1991, Lakes divided: The origin of Lake Crescent and Lake Sutherland, Clallam County, Washington: Washington Geology, v. 19, p. 38-42.

Logan, R.L., Schuster, R.L., Pringle, P.T., Walsh, T.J., and Palmer, S.P., 1998, Radiocarbon ages of probable coseismic features from the Olympic Peninsula and Lake Sammamish, Washington: Washington Geology, v. 26, p. 59-67.

Meyer, J., and Fradkin, S., 2002, Summary of fisheries and limnological data for Lake Crescent, Washington: Olympic National Park Report, National Park Service, Port Angeles, WA.

Miller, D.J., 1960, The Alaska earthquake of July 10, 1958: giant wave in Lituya Bay: Bulletin of the Seismological Society of America, v. 50, p. 253-266.

Moran, P., Cox, S., Embrey, S., Huffman, R., Olsen, T., and Fradkin, S., 2012, Sources and sinks of nitrogen and phosphorus to a deep, oligotrophic lake, Lake Crescent, Olympic National Park, Washington, Scientific Investigations Report 2012-5107: Washington, D.C., US Geological Survey, p. 68.

Nelson, A.R., Personius, S.F., Buck, J., Bradley, L.-A., Wells, R.E., and Schermer, E.R., 2007, Field and Laboratory Data from an Earthquake History Study of Scarps of the Lake Creek-Boundary Creek Fault, Between the Elwha River and Siebert Creek, Clallam County, Washington, US Geological Survey.

Polenz, M., Wegmann, K.W., and Schasse, H.W., 2004, Geologic map of the Elwha and Angeles Point 7.5-minute quadrangles, Clallam County, Washington: Washington Division of Geology and Earth Resource Open File Report 2004-14, 1 sheet, scale 1:24,000.

Pringle, P., Wegmann, K., Pontbriand, D., and Walker, W.W., 2010, Some recent discoveries pertaining to subfossil forests in the Pacific Northwest—Examples from Lake Crescent and Lower Dry Beds Lakes, Olympic Mountains, Washington: Northwest Scientific Association, Annual Meeting, v. 82, p. 77-78.

Schasse, H.W., 2003, Geologic map of the Washington protion of the Port Angeles 1:100,000 quadrangle: Washington Division of Geology and Earth Resources Open File Report 2003-6.

Schasse, H.W., Wegmann, K.W., and Polenz, M., 2004, Geologic map of the Port Angeles and Ediz Hook 7.5-minute quadrangles, Clallam County, Washington: Washington Division of Geology and Earth Resource Open File Report 2004-13, 1 sheet, scale 1:24,000.

Schuster, R.L., Logan, R.L., and Pringle, P.T., 1992, Prehistoric Rock Avalanches in the Olympic Mountains, Washington: Science, v. 258, p. 1620-1621.

Sherrod, B., and Gomberg, J., 2014, Crustal earthquake triggering by pre-historic great earthquakes on subduction zone thrusts: Journal of Geophysical Research: Solid Earth, p. 2013JB010635.

Tabor, R.W., and Tabor, R., 1975, Guide to the geology of Olympic National Park, University of Washington Press Seattle.

Wegmann, K.W., Bohnenstiehl, D.R., Bowman, J.D., Homburg, J.A., Windingstad, J.D., and Beery, D., 2012, Assessing Coastal Landscape Change for Archaeological Purposes: Integrating Shallow Geophysics, Historical Archives and Geomorphology at Port Angeles, Washington, USA: Archaeological Prospection, v. 19, p. 229-252.

Wegmann, K.W., Leithold, E.L., and Bohnenstiehl, D.R., 2014, How important is seismically-induced erosion above the Cascadia subduction zone? Insights from the stratigraphy of large lakes on the Olympic Peninsula, Washington State, *in* Gillespie, A., and Montgomery, D., eds., Proceedings of the 23rd Biennial Meeting of the American Quaternary Association, Volume 23: University of Washington, Seattle, WA, American Quaternary Union, p. 35-37.

Wells, R.E., Weaver, C.S., and Blakely, R.J., 1998, Fore-arc migration in Cascadia and its neotectonic significance: Geology, v. 26, p. 759-762.

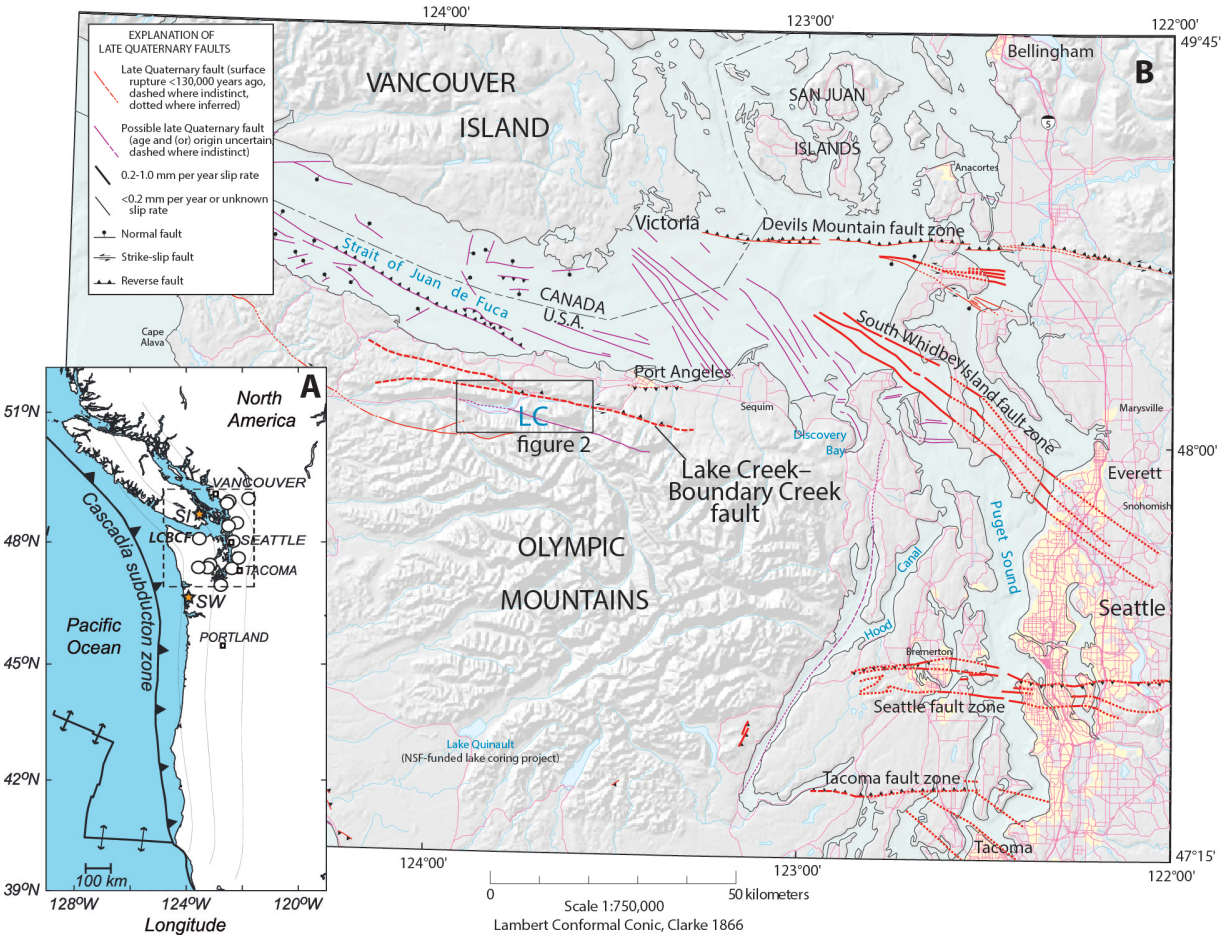

Stop 8 - Figure 1. Active tectonics of the Cascadia margin. **A**. Map of the Cascadia subduction zone showing locations of known late Holocene upper plate earthquakes (open circles), modified from Sherrod & Gomberg (2014). Dashed rectangle shows location of enlarged map. **B**. Map of the Olympic Peninsula and Puget Sound region in northwest Washington State showing known and possible late Quaternary faults from Lidke et al. (2003) and Blakely et al. (2004). Study area along the Lake Creek-Boundary Creek fault in the vicinity of Lake Crescent outlined by rectangle. Figure modified from Nelson et al. (2007).

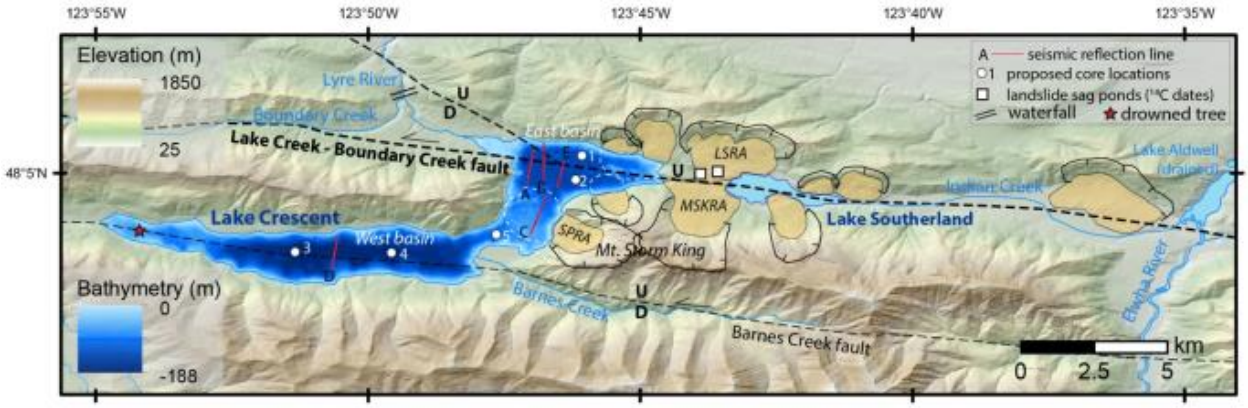

Stop 8 - Figure 2. Topographic map of the Lake Crescent study area with potential earthquake-triggered landslides along the LCBCF (orange polygons). We identify the Barnes Creek Fault; although we saw no evidence for deformation of lake sediments in numerous chirp seismic lines that crossed the fault. Proposed lake sediment core and landslide ^{14}C collection sites are identified, as are the selected seismic lines highlighted in Figs. 3 & 4. SPRA, MSKRA, and LSRA are the Sledgehammer Point, Mount Storm King, and Lake Southerland rock avalanche deposits, respectively.

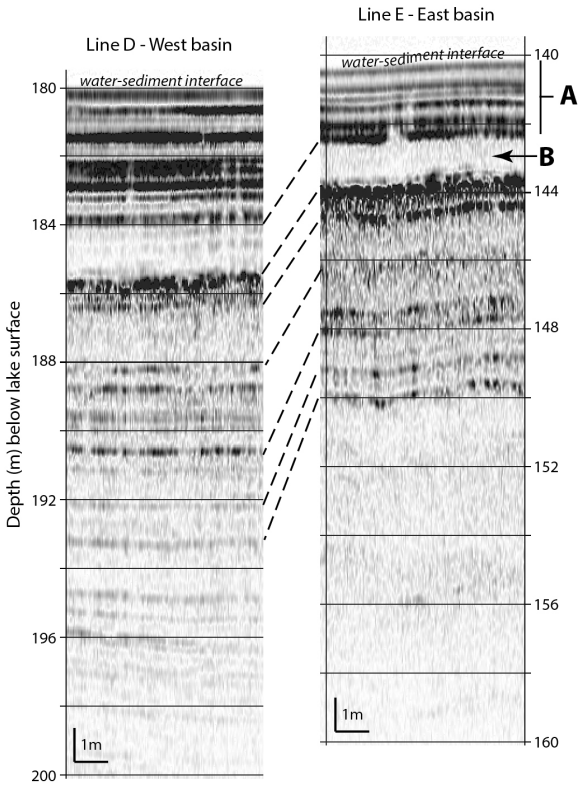

Stop 8 - Figure 3. Representative Chirp seismic stratigraphy for the West and East basins of Lake Crescent (see Fig. 2 for locations). A thick transparent layer (**seismic unit B**) is observed lake wide between 2 and 4 m deep. We interpret this layer as a mass wasting deposit (MWD) correlated to landslides and underwater slumps. The MWD layer is not observed on the rock avalanche deposits (Fig. 4), indicating that it is contemporaneous with it. Sediment package **A** has accumulated since the last LCBCF. Note that after deposition of Unit **B** the Sledge hammer point rock avalanche separated the lake into two deep basins resulting in higher sedimentation rates in the western basin. Note the difference in depth between the water-sediment interface of Lines D and E. Moran et al. (2012) report sedimentation rates of 0.9 mm/yr and 0.6 mm/yr from ~2.5 m deep cores from the West and East deep-water basins of Lake Crescent, respectively.

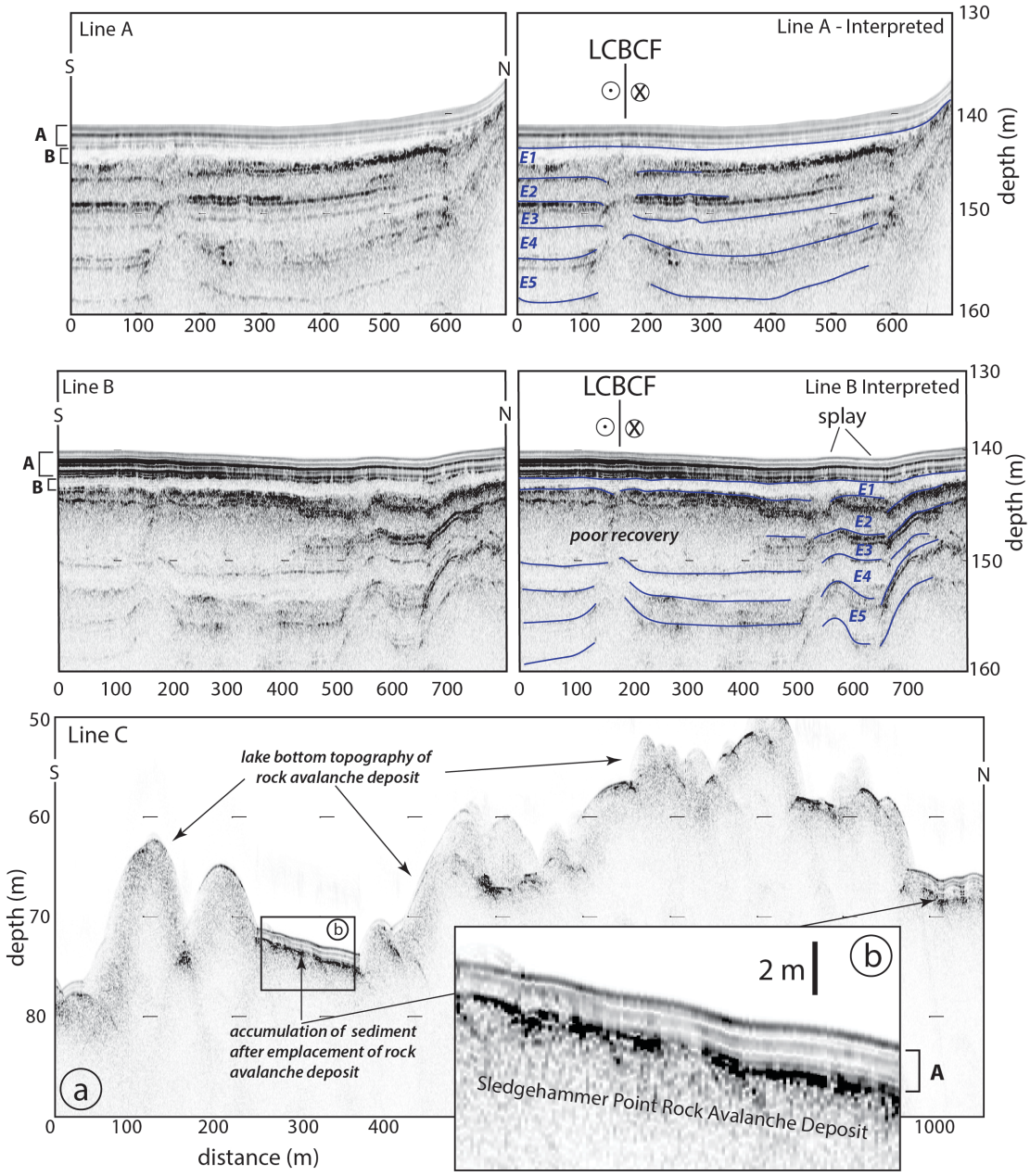

Stop 8 - Figure 4. Chirp seismic images and interpretation of sediment deformation (top & middle) caused by repeated earthquakes (E1 – E5) on the LCBC and splay faults beneath Lake Crescent. Unit **A** is younger than the most recent earthquake as it caps the unit **B** MWD layer (E1). Sediment depth to the top of the Unit **B** MWD is 2 m. Bottom: seismic image Line C across the Sledgehammer Point rock avalanche deposit at about 60 m water depth. Inset shows detail of 2 m of sediments that have accumulated in depressions on the slide mass since emplacement. Note vertical exaggeration.

Elwha River Dam Removal and River Channel Restoration
FOP Field Trip Stops 10 and 11

Compiled by: Lisa Ely and **Bryon Free**, Dept. of Geological Sciences, Central Washington University; and **Andy Ritchie**, U.S. National Park Service

STOP 10. Glines Canyon Dam Site. Glines Canyon Dam removal, sediment transport from the former Lake Mills Reservoir, and overview of the Elwha River Restoration Project.

The removal of the two dams on the Elwha River (Fig. 1) was the largest dam removal project in history. The dam removal process began in 2011. The downstream Elwha Dam (constructed in 1913) was fully removed by September 2012, and the Glines Canyon Dam at this field trip stop (constructed in 1927) was removed by August 2014. The two dam removals were undertaken to restore natural fish passage and habitat to the river. The dams collectively impounded 21 million m^3 of sediment, 16 million m^3 of which was stored in the reservoir behind the Glines Canyon Dam at this site (Warrick et al., 2015). The dams were lowered incrementally to allow the river to rework the sediment within the reservoir and maximize the sediment transport downstream (Fig. 2; Randle et al., 2015). Lowering the dams in stages minimized the hazards associated with dam removal, reduced the cost of removing the sediment, and allowed the sediment releases to be scheduled to avoid spawning seasons and other downstream impacts (Duda et al., 2011; Magirl et al., 2011).

The Glines Canyon Dam sat at the head of a 2-km-long, narrow bedrock canyon, and remnants of the former dam are visible from this overlook (Fig. 3). The water in the reservoir was incrementally lowered from 2011-2012, allowing the river delta to prograde across the reservoir basin toward the dam. At this site, sand and gravel deltaic sediments overlie fine-grained lakebed sediments deposited in the former reservoir (Fig. 4). Cut stumps of the pre-dam old-growth forest reemerged as the lake was lowered; some are still capped with lacustrine sediments. Large logs and stumps strewn across the terraces cut into the delta sediments accumulated in the reservoir over the life of the dam and have recently been reworked by the river. Ongoing research on the Elwha River by University of Washington Ph.D. student Vivian Leung demonstrates that the large woody debris creates channel complexity that enhances the erosion and removal of the reservoir sediment (Leung and Montgomery, 2010).

In October, 2012, the reservoir was completely drained and the coarser sand and gravel fluvial sediments began to be released downstream. Within the first 2 years of dam removal, 37% of the sediment had flushed out of the reservoir (Randle et al., 2015). Terraces of the prograded delta remain along the margins of the reservoir basin, marking some of the baselevel stages as the dam was lowered. These are rapidly revegetating through natural processes and revegetation projects, which increases the stability of the new river banks. The two largest discharges since the inception of the dam removal in December, 2014 and February, 2015 mobilized a significant amount of sediment within the reservoir, creating the most recent evidence of fluvial erosion and deposition visible from the dam overlook. The

amount of future erosion will depend on the growth rate of bank-stabilizing vegetation and the timing of additional large discharge events.

STOP 11. Altair Bridge over the Elwha River.

The Altair Bridge site is the farthest upstream of four study sites between the two dams on the Elwha River that were monitored for the effects of the dam removal on the channel before, during and after the dam removal process from 2012-2015 (Figs. 1 and 5). Changes in the river channel were quantified through annual repeat Terrestrial LiDAR (TLS), bimonthly sediment distribution surveys, and periodic large woody debris (LWD) mapping (Fig. 2). The results form the basis of a Central Washington University Masters thesis by Bryon Free (2015). The data presented for this field trip stop are from his MS thesis. This study, along with numerous others that are part of the Elwha River Restoration Project, provides empirical data to support models of sediment transport and channel response for future dam removal projects.

Although ~90% of the sediment released from the two dams from September 2011-September 2013) reached the coast (Warrick et al., 2015), the retention of the additional sediment and large woody debris resulted in substantial channel changes that continue to date. The complexity and particular geomorphic characteristics of each site were major factors in the deposition and accumulation of the new influx of woody debris and sediment from the dam removal. The Altair Bridge site lies at the first expansion of the Elwha River channel below the dam site as it exits the 2-km Glines Canyon. Prior to the initial release of coarse sediment from the dam in October 2012, this site consisted of four armored and incised channels separated by heavily vegetated, established islands (Fig. 6), which have now partially coalesced (Fig. 7). Except for a single log jam and a few scattered logs, the copious woody debris visible from the bridge has accumulated since the inception of the dam removal.

The initial sediment pulse filled the riffles and pools throughout the entire middle reach of the river within the first few months (East et al, 2015). Within the 300-meter Altair reach, sediment deposition greatly outpaced erosion in the first year, with a minimum net accumulation of 5000 m^3 above the low-flow water surface (Fig. 7). In contrast, net erosion and deposition were approximately equal in the second year (Fig. 7), partly due to a 9-month hiatus in the dam removal that limited the influx of new sediment (Fig. 2). As the initial sediment wave dissipated and the river continued to transport sediment from the reservoir, the timing of the sediment deposition and erosion was increasingly dictated by the discharge of the river (Figs. 8 and 9). As the individual pieces of woody debris coalesced into log jams, it influenced the sediment deposition by armoring the banks of channels, creating low-velocity pools, and directing the flow of water and sediment (Fig. 10). Over the past 3 years, the combined deposition of sediment and woody debris blocked the right-hand channel and caused a dominant channel to form on the left. This channel has migrated 20-30 m to the west, and eroded entire campsites from the former Altair campground. Overall, at the four study sites, the preexisting geomorphology influenced the capture and retention of sediment and large woody debris to a large

degree, which affected subsequent channel changes in a continuing feedback process.

References

Duda, J.J., Warrick, J.A., Magirl, C.S., 2011. Coastal and lower Elwha River, Washington, prior to dam removal—history, status, and defining characteristics. In: Duda, J.J., Warrick, J.A., Magirl, C.S. (Eds.), Coastal Habitats of the Elwha River, Washington—Biological and Physical Patterns and Processes Prior to Dam Removal. U.S. Geological Survey Scientific Investigations Report 2011-5120, p. 1–26.

East, A. E., Pess, G. R., Bountry, J. A., Magirl, C. S., Ritchie, A. C., Logan, J. B., Randle, T. J., Mastin, M. C., Minear, J. T., Duda, J. J., Liermann, M. C., McHenry, M. L., Beechie, T. J., and Shafroth, P. B., 2015, Large-scale dam removal on the Elwha River, Washington, USA: River channel and floodplain geomorphic change: Geomorphology, v. 228, p. 765-786.

Free, B.J., 2015, Quantifying channel responses to the removal of the Glines Canyon Dam in the middle reach of the Elwha River, Washington. M.S. Thesis, Central Washington University, 90 p. Thesis is imminently available to download from www.geology.cwu.edu/grad/

Leung, V. and Montgomery, D.R., 2010. Spatial patterns of streambed morphology around woody debris: flume experiments and field observations on the effects of woody debris on streambed morphology. American Geophysical Union Fall Meeting, abstract #EP43D-0781.

Magirl, C. S. Curran, C. A.; Rich, S. W.; Warrick, J. A.; Czuba, J. A.; Czuba, C. R.; Gendaszek, A. S.; Shafroth, P. B.; Duda, J. J.; Foreman, J. R., 2011, Baseline hydrologic studies in the lower Elwha River prior to dam removal, Chap 4 *in* Duda, J.J., Warrick, J.A., and Magirl, C.S., eds., Coastal habitats of the Elwha River, Washington—Biological and physical patterns and processes prior to dam removal: U.S. Geological Survey Scientific Investigations Report 2011–5120 p. 75-111.

Magirl, C.S., Hilldale, R.C., Curran, C.A., Duda, J.J., Straub, T.D., Domanski, M., Foreman, J.R., 2015. Large-scale dam removal on the Elwha River, Washington, USA: fluxes of river sediment. Geomorphology 246, p. 669–686.

Randle, T.J., Bountry, J.A., Ritchie, A.C., Wille, K.B., 2015. Large-scale dam removal on the Elwha River, Washington, USA: erosion of reservoir sediment. Geomorphology 246, p. 709–728.

Warrick, J.A., Bountry, J.A., East, A.E., Magirl, C.S., Randle, T.J., Gelfenbaum, G., Ritchie, A.C., Pess, G.R., Leung, V., Duda, J.J., 2015. Large-scale dam removal on the Elwha River, Washington, USA: fluxes of river sediment. Geomorphology 246, p. 729–750.

Wheaton, J. M., Brasington, J., Darby, S. E. and Sear, D. A., 2010, Accounting for uncertainty in DEMs from repeat topographic surveys: improved sediment budgets. Earth Surface Process and Landforms, v. 35, no. 2, p. 136–156.

Figures for FOP Field Trip Stops 10 and 11 on the Elwha River.

All figures are from Free, Bryon J., 2015, Quantifying channel responses to the removal of the Glines Canyon Dam in the middle reach of the Elwha River, Washington. M.S. Thesis, Central Washington University, 90 p.

Elwha Figure 1. Elwha Restoration Project Map, northwestern Washington State on the Olympic Peninsula. Base map is the 2012 aerial LiDAR provided by the USGS. From B. Free (2015).

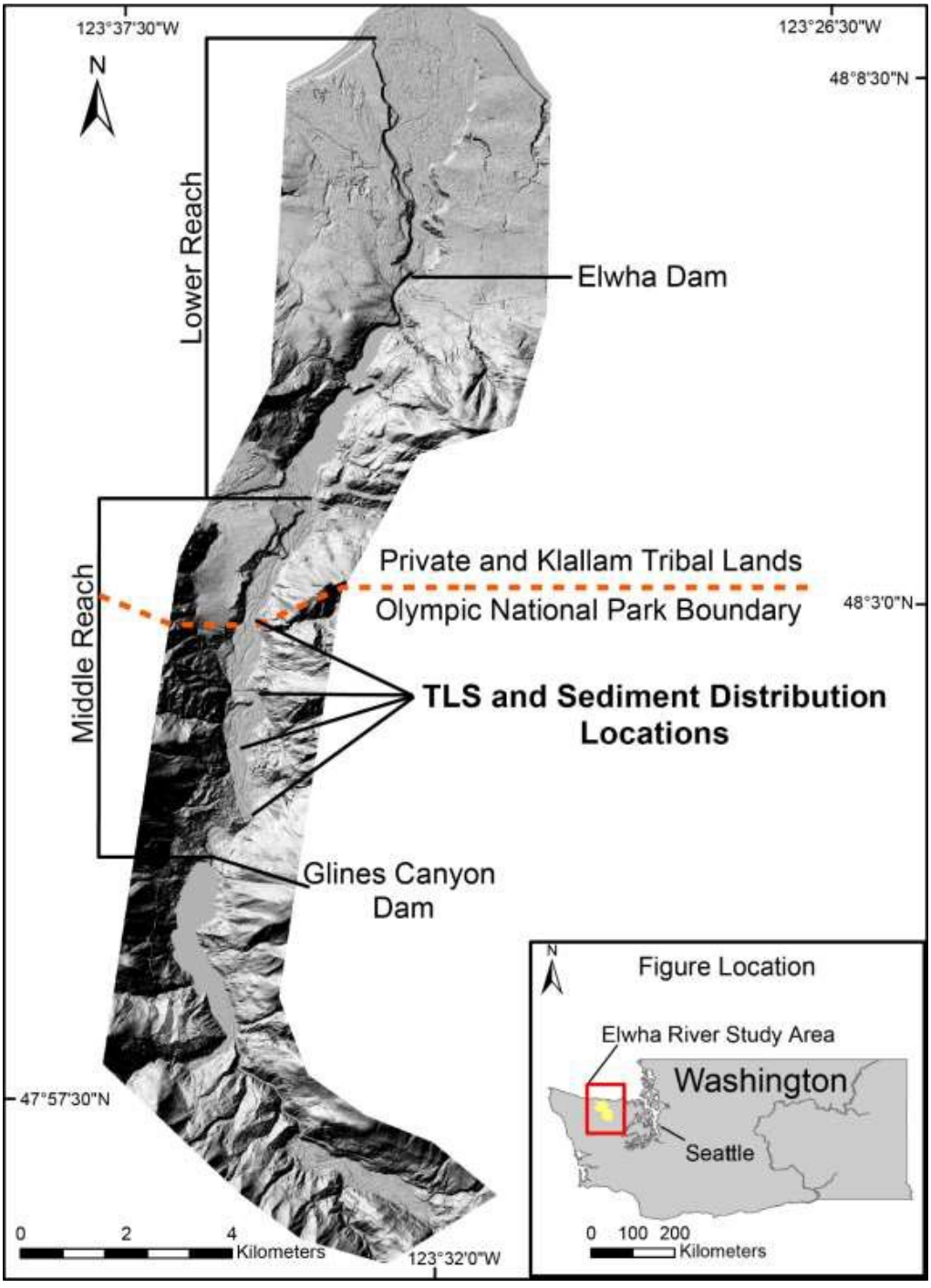

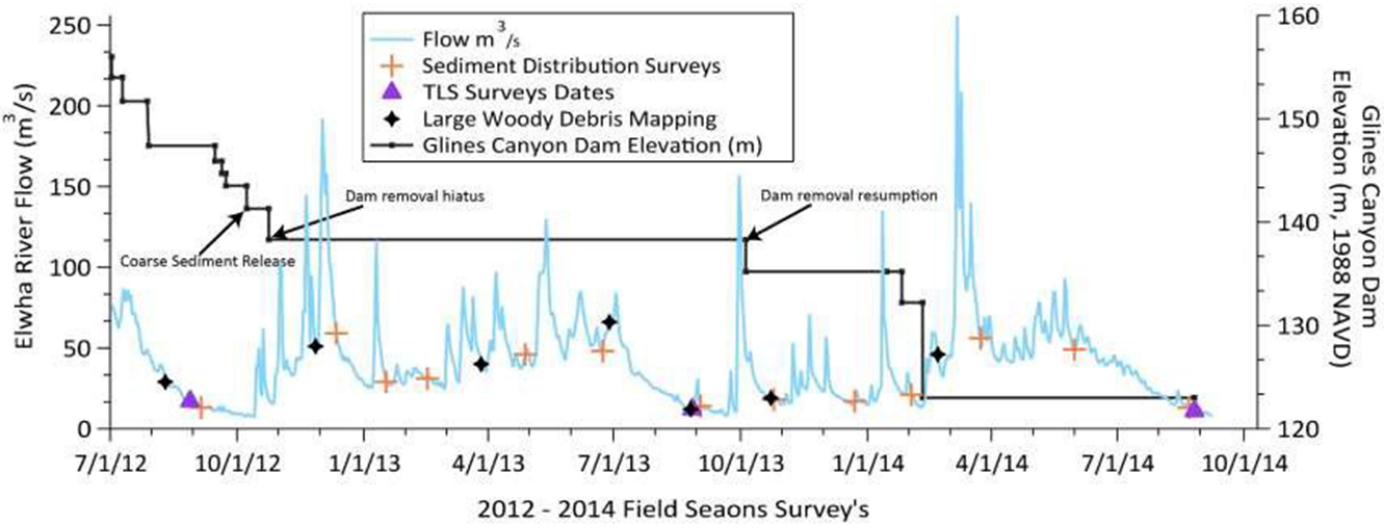

Elwha Figure 2. Elwha River hydrograph at the USGS gauging station # 12045500 located 12 km downstream of Glines Canyon Dam at Hwy 101 McDonald Bridge. The black line delineates the dam drawdown sequence. Dates of TLS surveys, sediment measurements, and wood mapping by Free (2015) in the downstream river channel are also included. B. Free (2015).

Elwha Figure 3a. Glines Canyon Dam in July, 2012 with diminishing reservoir in foreground.

Elwha Figure 3b. Reservoir basin from Glines Canyon Dam site in May, 2015. Note vegetation establishing on delta terraces; in-situ stumps in lake sediments.

Elwha Figure 4a. Delta prograding into diminishing reservoir behind Glines Canyon Dam, July 2012.

Elwha Figure 4b. In-situ pre-dam cut stump capped by lake sediments from former reservoir. In stratigraphy, fine-grained lake sediments are overlain by recently deposited sand and gravel from prograding delta. Photo taken in July, 2012.

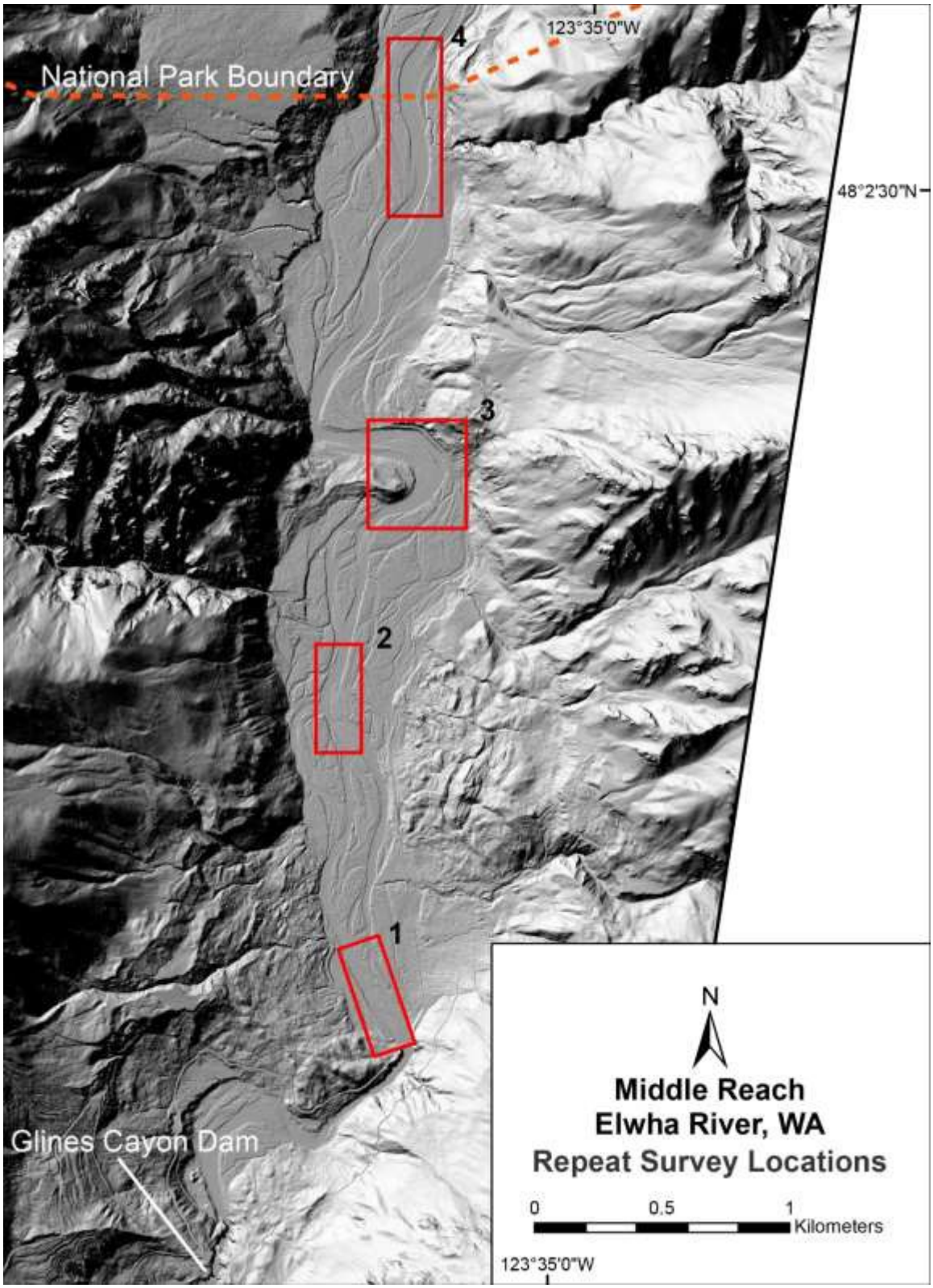

Elwha Figure 5. Elwha River Study Sites 1-4. Site 1 is the Altair Bridge at STOP 11 of the FOP field trip (B. Free, 2015).

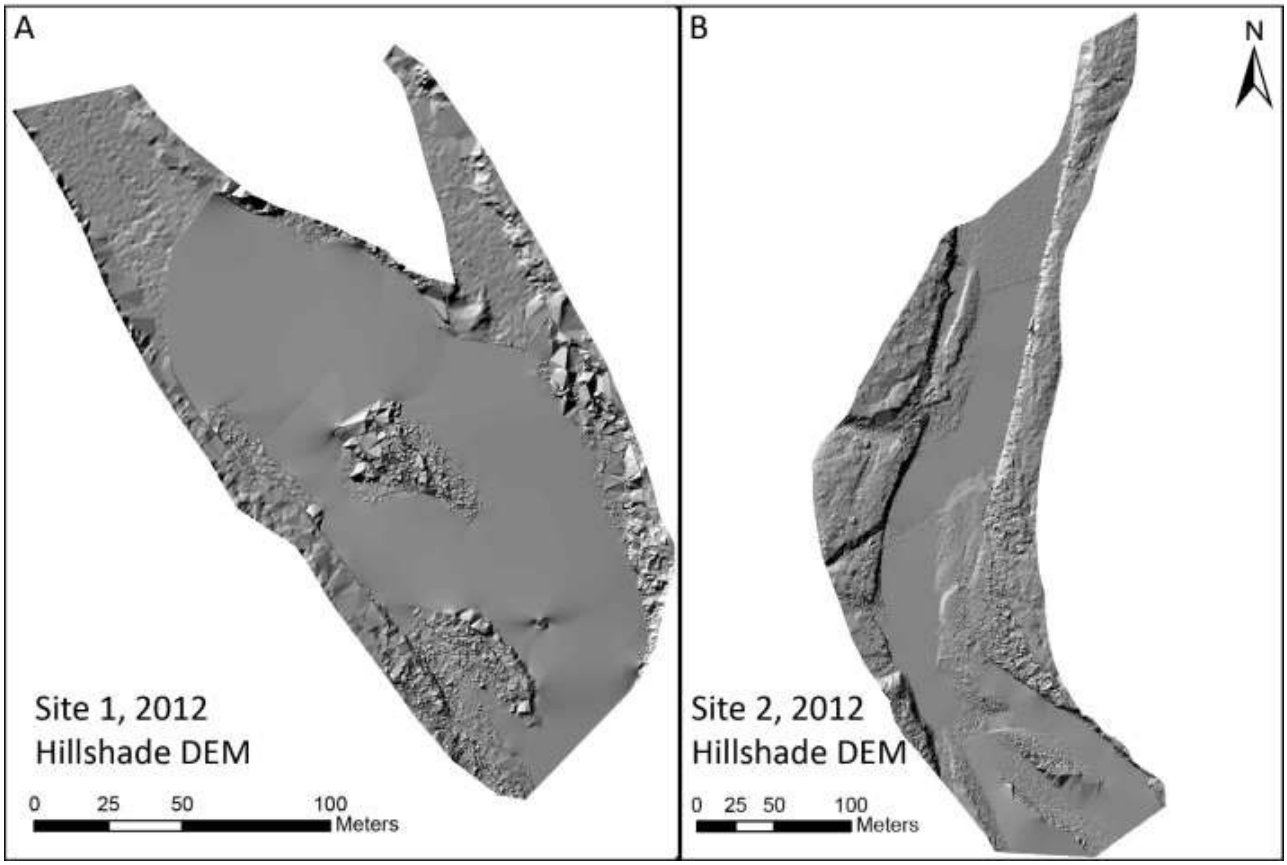

Elwha Figure 6: A**:** Site 1 (Altair Bridge, FOP STOP 11), in August 2012. Hillshade surface prior to coarse sediment release with several flowing channels. B**:** Site 2, August 2012. Hillshade surface prior to coarse sediment release with a single channel and prominent point bar. B. Free (2015).

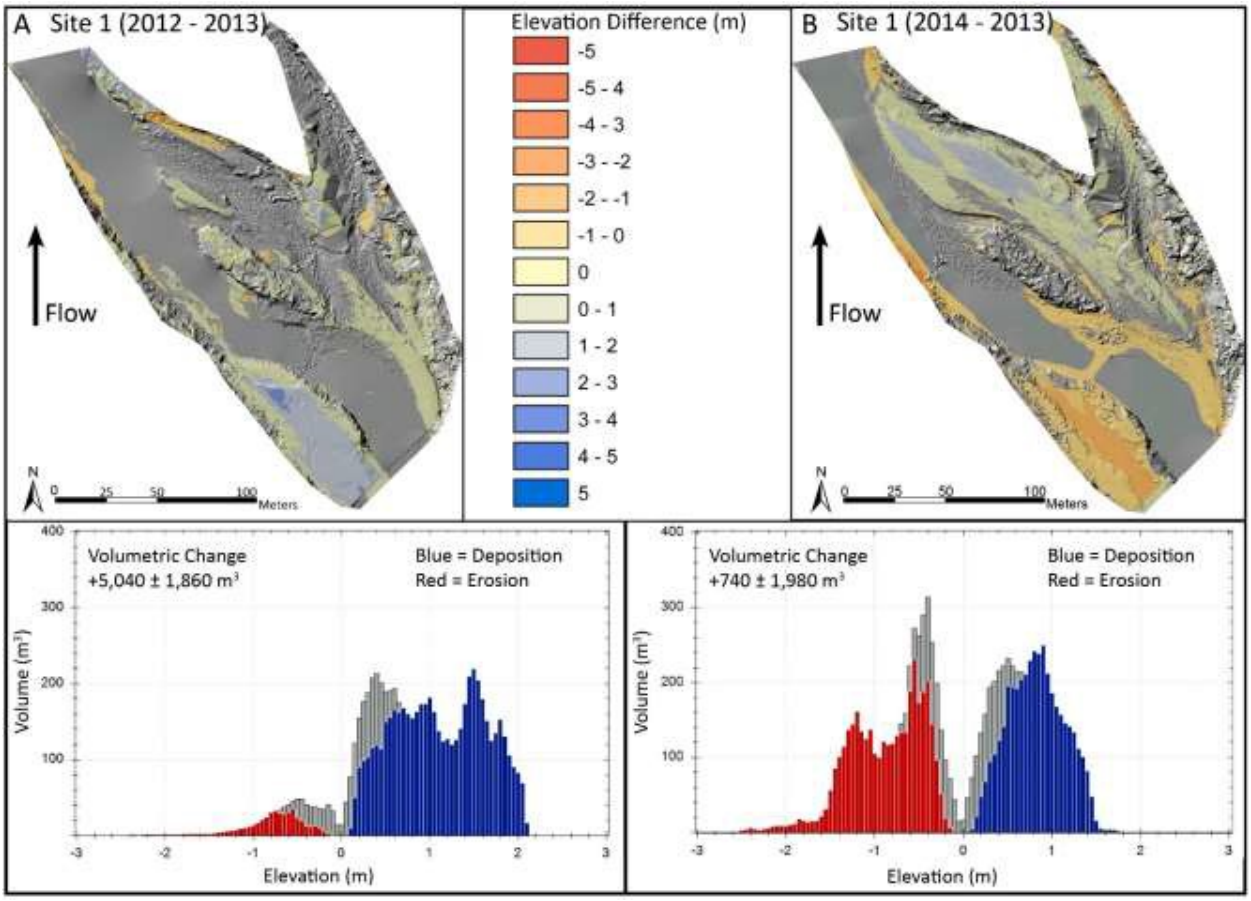

Elwha Figure 7a. DEM of Difference (DoD) at Site 1 (Altair) showing changes in the vertical elevation of the ground surface between TLS surveys. Large amounts of deposition can be seen in Year 1 of dam removal, while in Year 2 net deposition and erosion are equivalent. Grey areas in the map are surfaces that were not used in the differencing calculations due to water surface errors. The histograms depict the changes in volume and elevation from erosion (red) and deposition (blue); grey indicates the potential error in the calculations. DoD calculated using methods from Wheaton, 2010. From B. Free (2015).

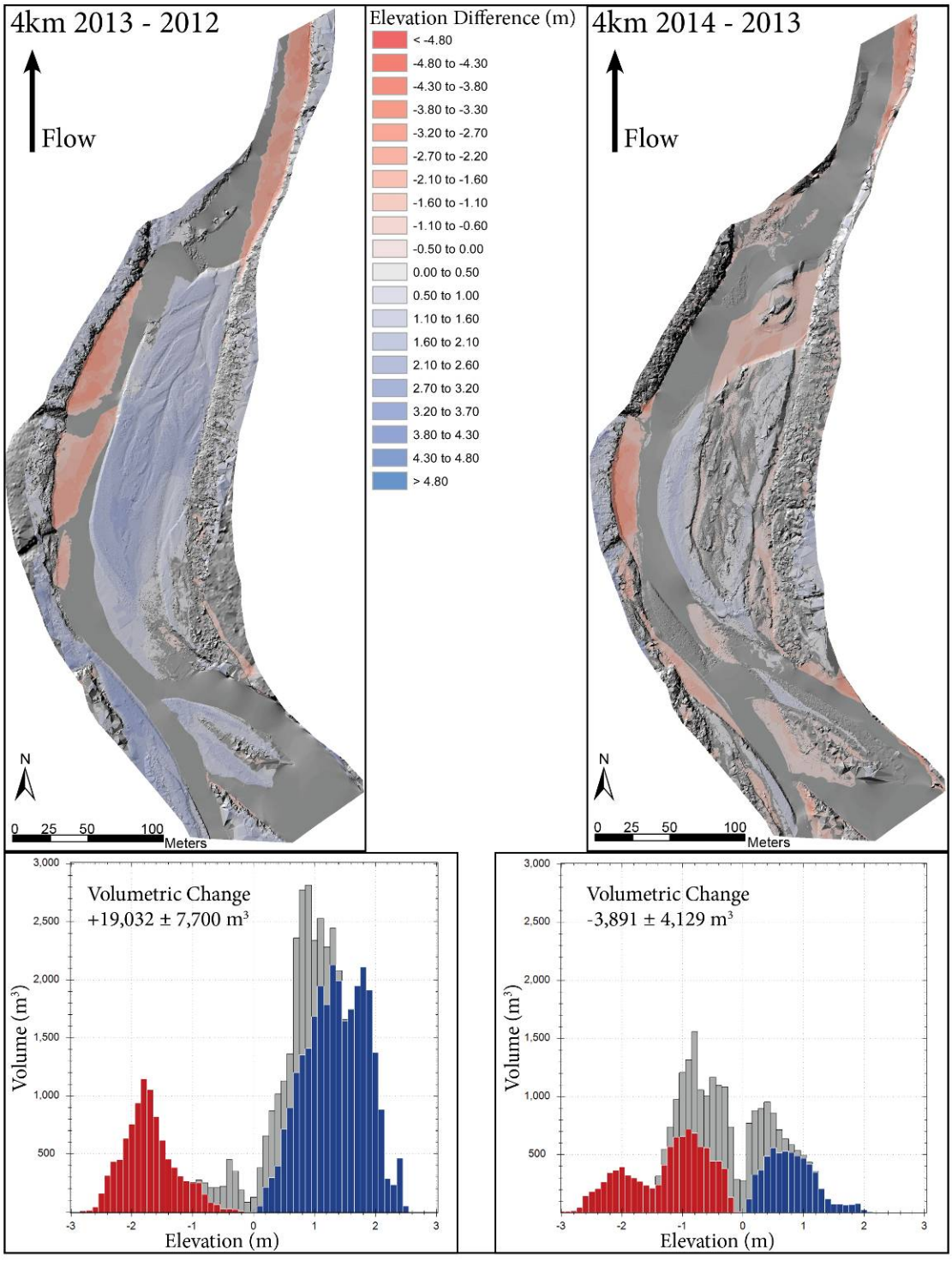

Elwha Figure 7b. DEM of Difference (DoD) at Elwha River Site 2. From B. Free (2015).

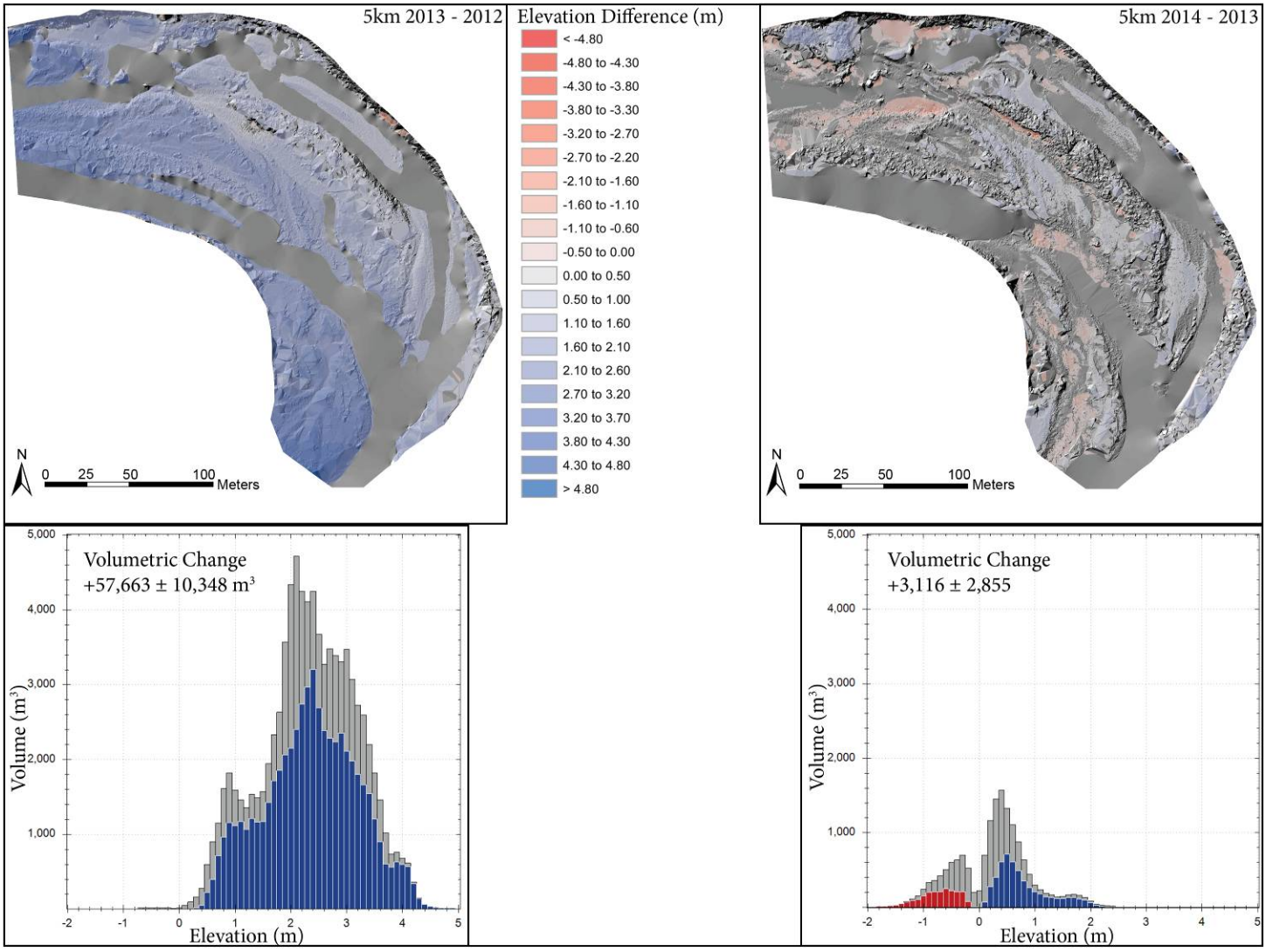

Elwha Figure 7c. DEM of Difference (DoD) at Elwha River Site 4 (River Bend). From B. Free, (2015).

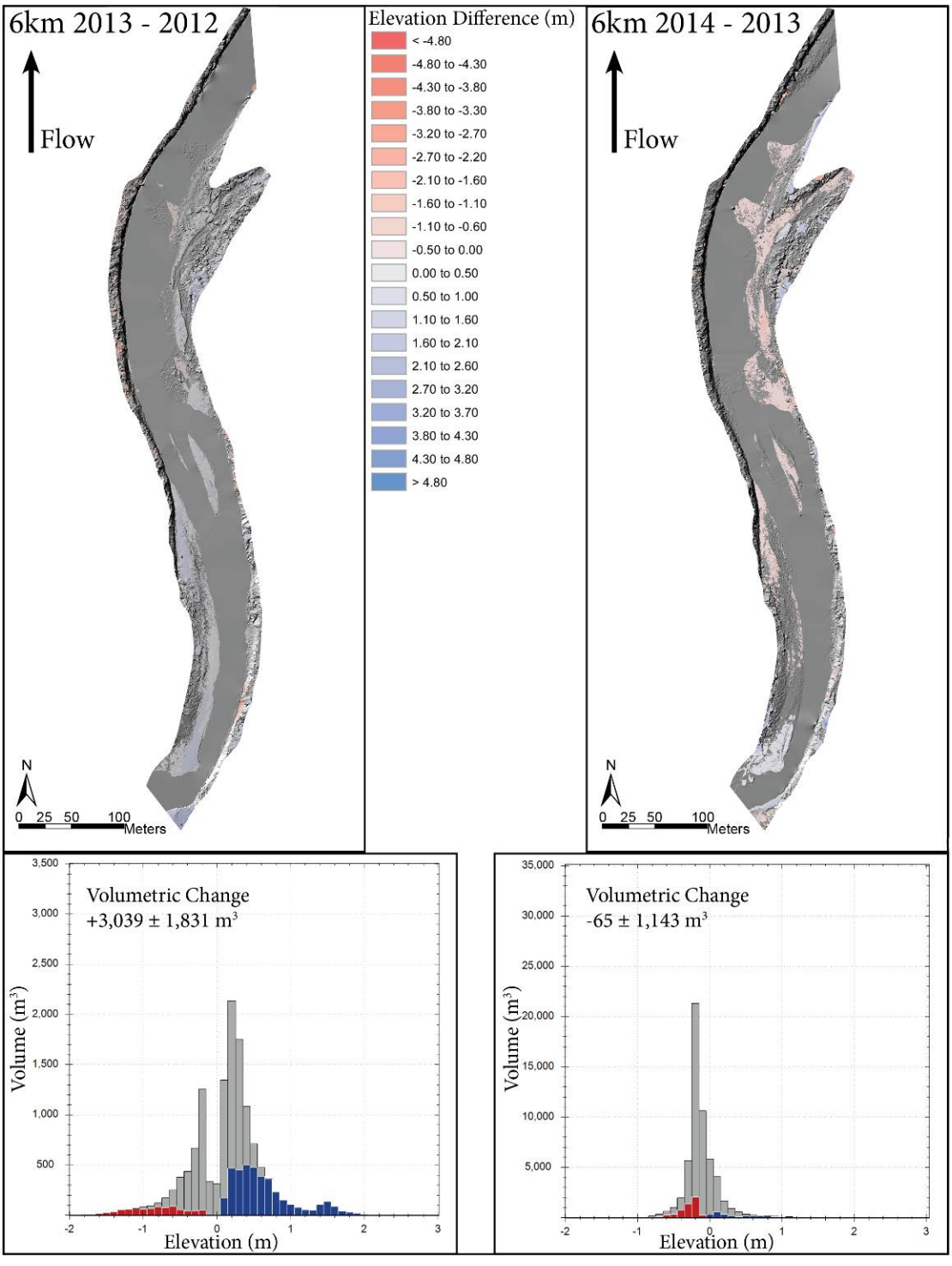

Elwha Figure 7d. DEM of Difference (DoD) at Site 4 (Madison Falls). From B. Free (2015).

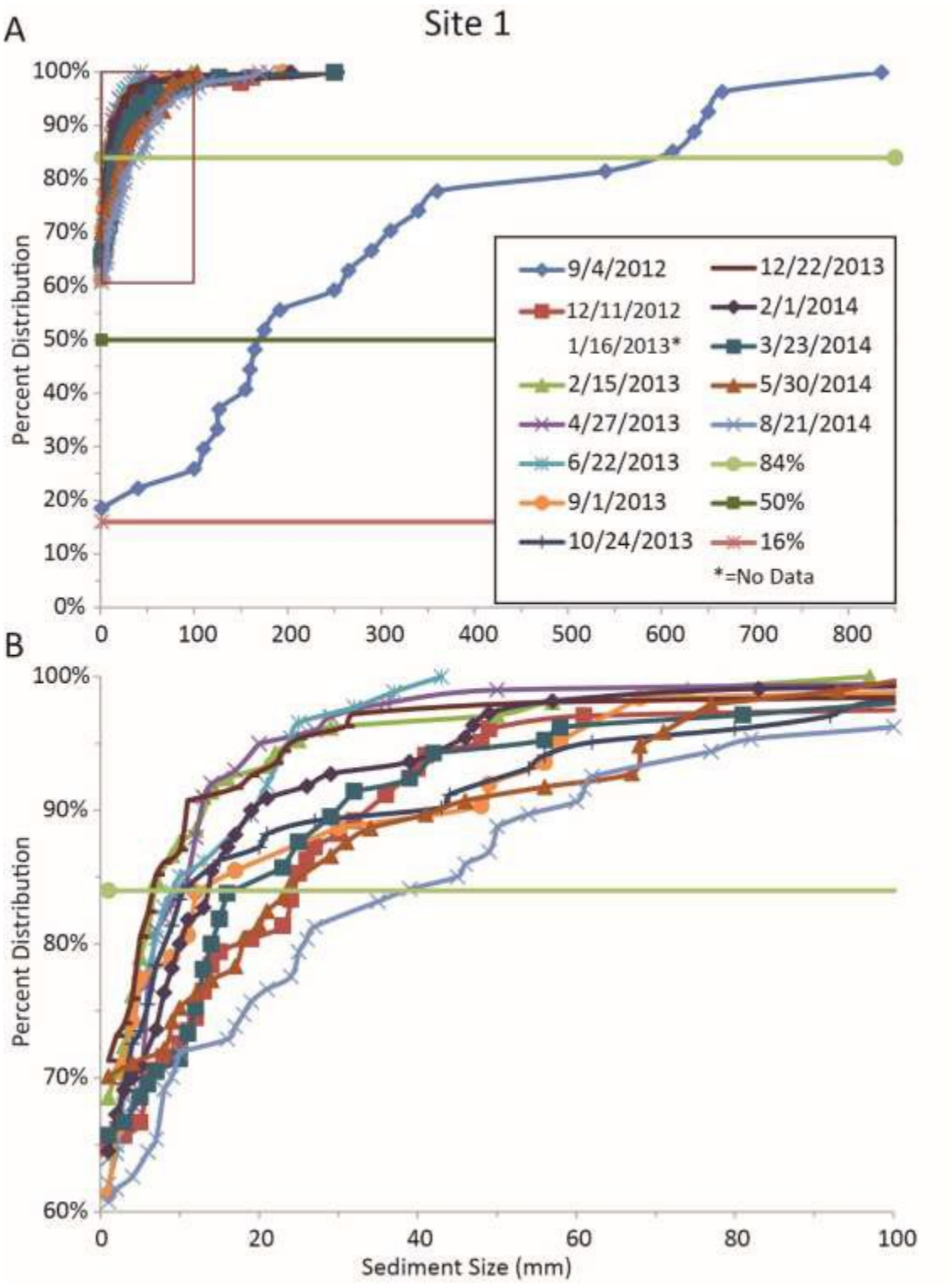

Elwha Figure 8. Site 1 (Altair Bridge). **A.** Surface distribution of sediment over the entire survey period. Notice the change from a primarily cobble system to a sand dominant system in the first 2 months following the coarse sediment release. Red box indicates the change in scale for Fig. 8b. **B.** Zoomed-in focus on the sand/fine gravel size component following the coarse sediment release. From B. Free (2015).

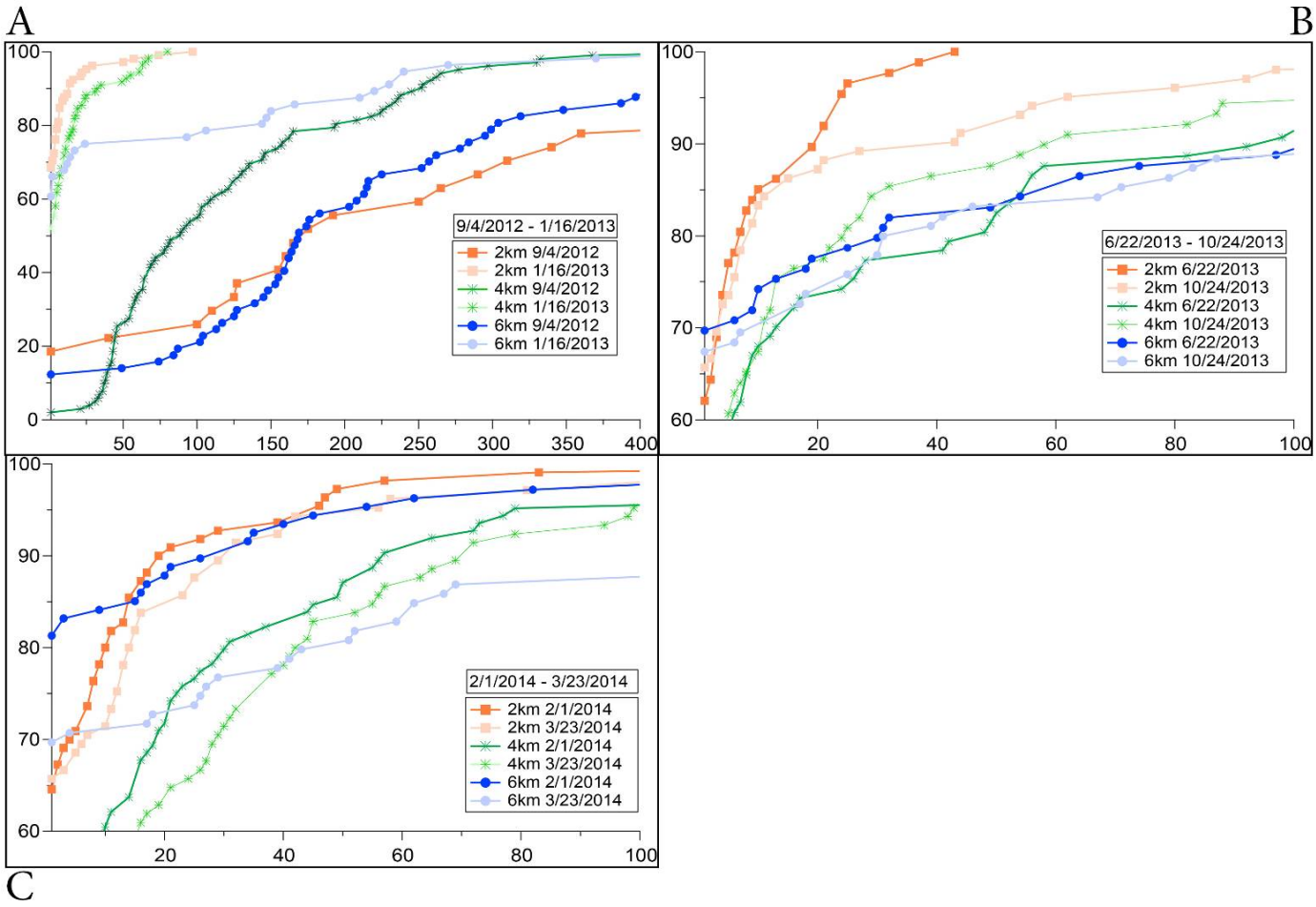

Elwha Figure 9. Summary of Fine Sediment-Size Distributions at Sites 1, 2 and 4. The initial accumulation of sediment was delayed at Site 4 compared to Sites 1 and 2. Site 4 is the farthest downstream and also the straightest reach with only a small point bar. From B. Free (2015).

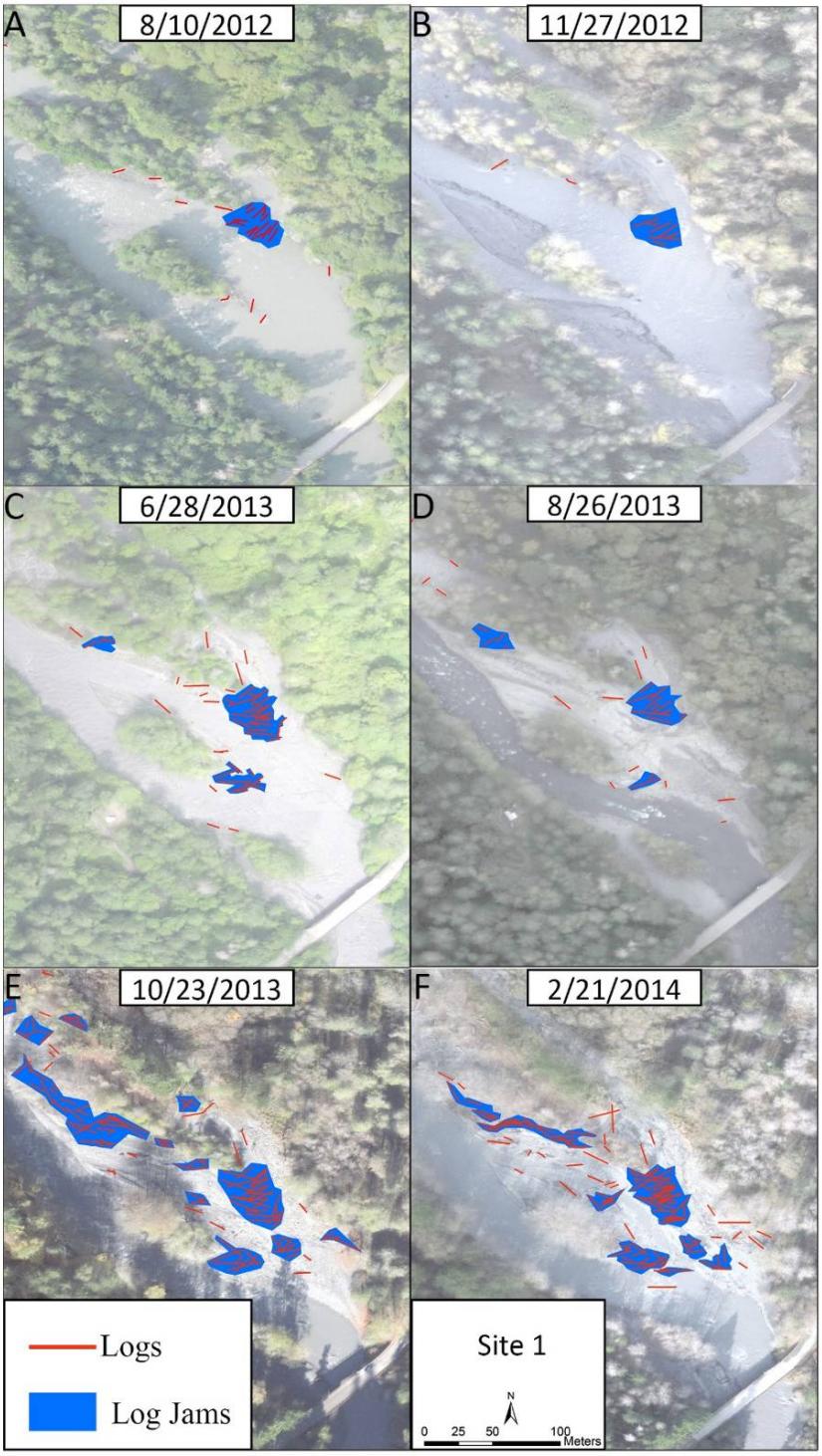

Elwha Figure 10: **Maps of woody debris at Site 1 (Altair Bridge, FOP Stop 11) on orthophotographs taken from August 2012-February 2014. Blue = Log Jam, Red = Individual logs >2 m in length. Aerial photographs acquired and mosaicked by Andy Ritchie, National Park Service. From B. Free (2015).**